

Alma Mater Studiorum – Università di Bologna

DOTTORATO DI RICERCA IN

Biologia Cellulare Molecolare e Industriale

Ciclo XXV

Settore Concorsuale di afferenza: 03/C1

Settore Scientifico disciplinare: CHIM/06

**ELECTROCHEMICAL SENSING STRATEGIES FOR
THE DETECTION OF INTERACTIONS BETWEEN
BIOLOGICAL MACROMOLECULES**

Presentata da: Manuele Onofri

Coordinatore Dottorato

Prof. Vincenzo Scarlato

Tutor

**Dott. Giampaolo Zuccheri
Prof. Bruno Samorì**

Esame finale anno 2013

Abstract

Key-words: electrochemical biosensor, DNA nanotechnology, model membrane, label-free strategy

The detection of very small amount of pathogens and the screening of pollutants, bacterial toxins in samples such as drinking water, are important goals for medical, biological and biotechnological applications.

Electrochemical detection is very useful to achieve the development of cheap, small, portable and simple devices, that allow multiplex and real-time detection. Another aspect to take in account regards nanobiotechnological strategies, that are drastically revolutionizing the development of biosensors. In fact many biosensing techniques and transduction strategies exploit concepts developed in the field of nanobiotechnology, such as quantum dots, nanoparticle labels, magnetic particles, model membranes, DNA-based nanostructures etc.

The aim of this PhD work has been the development of electrochemical biosensors based on nanobiotechnological strategies for the detection of biological macromolecules.

Specifically, one project, carried out within the European project DINAMICS (Diagnostic Nanotech and Microtech Sensors, Sixth Framework Programs), was focused on the application of a DNA-based nanostructure called hybridization chain reaction (HCR) as an amplification strategy to enhance the hybridization signal in an electrochemical DNA biosensor.

HCR is a strategy that involves two different DNA molecules with hairpin structure. The hairpin conformation allows to store energy that will be released only after the addition of an initiator, triggering the supramolecular polymerization of the hairpin molecules. Specifically, if the target sequence has hybridized with the probe on the electrode surface, HCR determines the formation of products with high molecular weight that should be easier to detect, and therefore should provide an increase in the sensitivity of DNA biosensors, lowering the limit of detection.

The recognition of the HCR products on the surface were carried out using an electrochemical label-based technique (voltammetry with a redox marker), and two label-free techniques (SPR and capacitive measurements), and the effects on the sensitivity and specificity of the different DNA biosensors were evaluated.

We found that HCR can be implemented on a solid surface and used as a strategy for signal amplification in a voltammetric DNA biosensors. Employing HCR, a lower limit of detection of about 2 orders of magnitude was observed. Moreover HCR improves the biosensor ability to discriminate between perfect matched and mismatched DNA targets; in addition the particular

mechanism of HCR allows to discriminate the position of the mismatch in the target sequence. Through SPR experiments and capacitive measurements we observed that the HCR is a label-free approach that is able to specifically amplify DNA binding signals, and that it is promptly suitable for both commercial SPR and multiplexed SPRi detection systems.

Another project on which the research activity was focused concerns the development of an electrochemical biosensor based on a biological model membrane anchored to a solid surface, and used as the sensing element for the recognition of interactions between lipid membrane and different types of target molecules.

We prepared and characterized layers of synthetic lipids, in our case 2,3-di-*O*-phytanyl-*sn*-glycerol-1-tetraethylene glycol-D,L- α -lipoic acid ester (DPTL), diluted with β -mercaptoethanol (β ME), a smaller thiol. Phosphatidylcholines were used to complete the lipid bilayer, obtaining lipid membranes with an electrical resistance in the $M\Omega/cm^2$ range. To characterize these surfaces, we decided to use several approaches that exploit the presence of the solid surface (flat gold surfaces): atomic force microscopy (AFM), electrochemical impedance spectroscopy (EIS) and surface plasmon resonance (SPR).

These tethered bilayer lipid membranes were used to detect interactions between the lipid membrane and different types of target molecules, such as pollutants, toxins and amyloid proteins. In particular the possibility of monitoring in real time with impedance measurements the interactions between the lipid membrane and different kinds of target molecules (model pore-forming peptides, toxins, pollutants and amyloid proteins) was evaluated, and we observed that our model membrane is potentially capable of operating as sensing element for biosensor.

This particular type of biosensor is not specific to a particular target molecule, and therefore has the advantage of being able to detect the presence (obviously without being able to recognize them) of a wide range of molecules that can interact with the lipid membrane and then alter its electrical characteristics. For this reason this type of biosensor may be applied in the analysis of preliminary screening, for example in environmental monitoring.

In conclusion, nanobiotechnological strategies were applied with some success as amplification strategy in a DNA biosensors (HCR) and as the sensing element in a label-free electrochemical biosensor. However, further analysis and improvement are required, to confirm the obtained results, and also to enhance the quality of the measurements.

Contents

Abstract.....	III
Contents.....	V
Table of abbreviations.....	IX
Introduction.....	1
1.1 Biosensors.....	1
1.2 Electrochemical biosensors.....	2
1.2.1 Electrochemical detection techniques.....	3
1.3 Application of electrochemical biosensors.....	7
1.3.1 Biocatalytic devices.....	7
1.3.2 Affinity biosensors.....	10
Immunosensors.....	10
Nucleic acid biosensors.....	11
Aim of the project and outline of the following sections.....	15
Section I: HCR as signal amplification method.....	19
2.1 Introduction.....	19
2.1.1 HCR.....	19
2.1.2 Voltammetric analysis and Hoechst 33258.....	21
2.1.3 Surface plasmon resonance.....	22
2.1.4 Capacitive method.....	24
2.2 Materials and methods.....	27
Materials.....	27
DNA sequences.....	27
HCR in solution.....	27
Gold surfaces and functionalization.....	28
Electrochemical cell measurements.....	29
Voltammetric measurements.....	29
Capacitive measurements.....	30
SPR measurements.....	30
2.3 Results and discussions.....	32
2.3.1 Sequence design and HCR in solution.....	32
Sequence design.....	32
HCR in solution.....	33
2.3.2 Voltammetric experiments with SPR.....	34
HCR on the surface.....	34
Mismatch recognition.....	36
2.3.3 SPR experiments with HCR.....	39
2.3.4 Capacitive measurements.....	44
2.4 Conclusions and perspectives.....	45

Section II: preparation and characterization of tBLM.....	47
3.1 Introduction.....	49
3.1.1 Lipid membrane models.....	50
Black lipid membranes	50
Lipid vesicles	50
Supported bilayer lipid membranes.....	51
Tethered bilayer lipid membranes.....	52
3.1.2 tBLM preparation.....	52
Tethering molecules.....	53
DPTL monolayer formation.....	54
Diluted DPTL monolayer formation.....	54
3.1.3 Bilayer formation.....	55
Vesicles fusion method.....	55
Protocol involving detergent.....	56
Rapid solvent exchange.....	56
3.2 Materials and methods.....	57
SAM preparation.....	57
Vesicles preparation.....	57
Bilayer formation.....	57
Electrochemical impedance spectroscopy.....	57
Reductive stripping assay.....	58
AFM.....	58
Surface plasmon resonance.....	58
3.3 Results and discussions.....	60
3.3.1 EIS data analysis.....	60
Impedance spectra.....	60
Equivalent circuits.....	61
3.3.2 Formation and characterization of DPTL layers.....	63
EIS.....	63
Reductive stripping.....	64
AFM imaging.....	65
Characterization with SPR.....	66
3.3.3 tBLM formation on DPTL layer.....	67
Preparation and characterization of lipid vesicles.....	68
tBLM characterization with EIS.....	69
Experiments with SDS to remove lipid bilayer.....	70
Formation and characterization of tBLM with SPR.....	71
3.3.4 Formation of diluted DPTL monolayer.....	73
Choice of diluents.....	74
Dilution experiments.....	74
3.3.5 Formation of tBLM on diluted monolayer.....	77
3.3.6 Conclusions and perspectives.....	79
Section III: applications of biosensors based on lipid membranes.....	83
4.1 Introduction.....	85
4.1.1 Studies about biophysical properties of lipid bilayers.....	85

4.1.2 Interactions with drugs.....	87
4.1.3 Neurodegenerative diseases.....	88
4.1.4 Studies about bacterial toxins and pollutants.....	89
4.1.5 Biosensors based on model membranes.....	90
4.2 Materials and methods.....	92
Reagents	92
tBLM preparation.....	92
Electrochemical methods.....	92
Pore-forming peptides and pollutants.....	92
α -synuclein oligomers and fibers preparation.....	93
Sample preparation and AFM imaging.....	93
4.3 Results and discussion.....	94
4.3.1 Model pore-forming peptides and toxins.....	94
4.3.1.1 Gramicidin.....	94
Interaction of gramicidin with tBLM.....	95
Real-time detection of gramicidin.....	97
4.3.1.2 Melittin.....	98
Interaction of melittin with tBLM.....	100
Real-time detection.....	100
4.3.1.3 Conclusions.....	101
4.3.2 Pollutants molecules.....	102
4.3.2.1 Cyclohexane.....	102
Results and discussion.....	102
4.3.2.2 DNP.....	103
Results and discussion.....	105
4.3.2.3 Conclusions.....	106
4.3.3 α -synuclein.....	106
Preparation α -synuclein aggregates and AFM images.....	107
Electrochemical recognition of α -synuclein.....	109
Conclusions.....	114
4.3.4 Conclusions and perspective.....	115
Section IV: conclusions.....	117
5.1 Conclusions.....	119
Acknowledgments.....	123
Bibliography.....	125

Table of abbreviations

AC: Alternating current

AFM: Atomic Force Microscope

ATP: Adenosine Triphosphate

BLM: Bilayer Lipid Membrane

β -ME: β Mercaptohexanol

CCD: Charged-coupled device

COWP: *C. parvum* Wall Protein

CPE: Constant Phase Element

DNA: Deoxyribonucleic Acid

DNP: Dinitrophenol

DOPC: 1,2-Dioleoyl-*sn*-glycero-3-Phosphocholine

DPV: Differential Pulse Voltammetry

DPTL: 2,3-di-*O*-phytanyl-*sn*-glycerol-1-tetraethylene glycol-DL- α -lipoic acid ester

EIS: Electrochemical Impedance Spectroscopy

FRET: Fluorescence Resonance Energy Transfer

GMO: Genetic Modified Organism

GOx: Glucose Oxidase

GUV: Giant Unilamellar Vesicle

HCR: Hybridization Chain Reaction

HEPES: 4-(2-Hydroxyethyl)-1-Piperazineethanesulfonic acid

HEV: Hepatitis E Virus

ICS: Ion Channel Sensor

IPE: Ideal Polarizable Electrode

LSV: Linear Sweep Voltammetry

LUV: Large Unilamellar Vesicle

MCH: Mercaptohexanol

OEO: Oligo Ethylene Oxide

PAGE: Polyacrylamide Gel Electrophoresis

PBS: Phosphate Buffer Saline

PD: Parkinson Disease

PDMS: Polydimethylsiloxane
PEG: Polyethylene Glycol
POPC: 1-palmitoyl-2-oleoyl-*sn*-glycero-3-phosphocholine
POPG: 1-hexadecanoyl-2-(9Z-octadecenoyl)-*sn*-glycero-3-phospho-(1'-rac-glycerol)
QCM: Quartz Crystal Microbalance
RB: Running Buffer
RNA: Ribonucleic Acid
RU: Resonance Unit
SAM: Self Assembled Monolayer
sBLM: supported Bilayer Lipid Membrane
SDS: Sodium Dodecyl Sulphate
SLIC: Synthetic Ligand-gated Ion Channel
SNP: Single-Nucleotide Polymorphism
SPR: Surface Plasmon Resonance
SPRi: Surface Plasmon Resonance imaging
SUV: Small Unilamellar Vesicle
TBE: Tris/Borate/EDTA
tBLM: tethered Bilayer Lipid Membrane
TEGL: Tetraethylene Glycol-D,L-R-Lipoic acid ester
TSG: Template Stripped Gold

INTRODUCTION

1.1 Biosensors

Research on biosensors has experienced increasing growth over the past two decades. A biosensor is generally defined as an analytical device which converts a biological response into a quantified and analyzed signal^[1]. Figure 1.1 shows schematically the parts that compose a typical biosensor: a) the sensing element is represented by bioreceptors which specifically bind to the analyte; b) the bioreceptors are generally fixed on an interface in which the biological event of specific recognition takes place and gives rise to a signal, that is picked up by c) the transducer element. The transducer signal is then converted into an electronic signal and then sent to d) a software that convert the signal in a meaningful physical parameter that describes the process under investigation. Finally, the resulting quantity was shown through e) a software interface to the human operator.

The biosensors can be applied to a wide variety of samples: body fluids, food samples, cell cultures, and environmental samples.

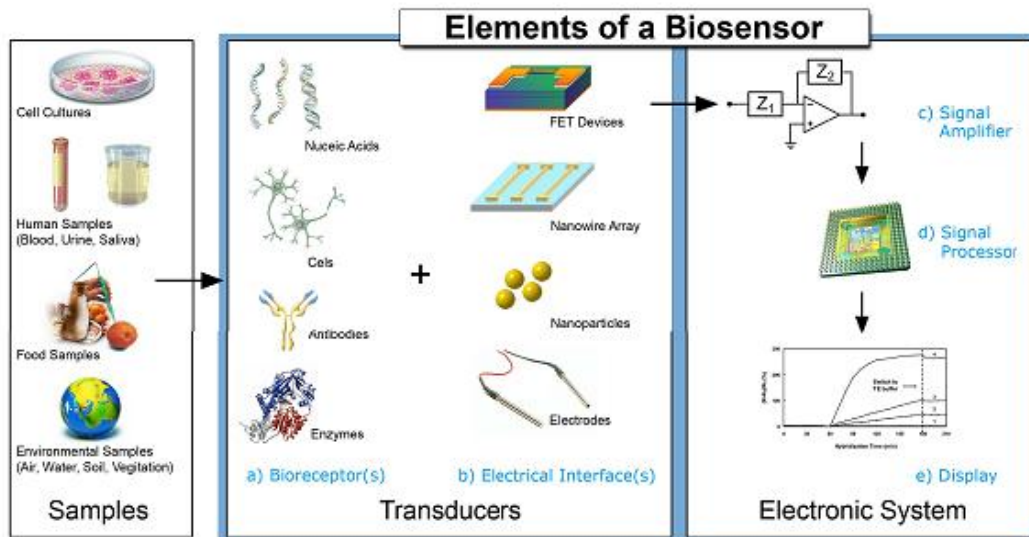


Figure 1.1: Elements and selected components of a typical biosensor. Figure reproduced from [2]

Over the years several characteristics that a biosensor should possess to exert their functions were proposed^[2]:

1. Bioreceptors should be highly specific for the analytes and show a low variation between assays.
2. The reaction should be independent of parameters such as stirring, and should tolerate wide variations in pH and temperature allowing the analysis of samples with minimal pre-treatment.
3. The response must be accurate, precise, reproducible and linear on the concentration range of interest.
4. In the case of invasive monitoring in clinical situations, the probe should be very small and biocompatible, and free from toxic or antigenic effects. Furthermore, the biosensor should not be prone to inactivation or proteolysis.
5. The biosensor should allow real-time analysis.
6. The biosensor should be cheap, small, portable and can be used by semi-skilled operators.

Biosensors are generally highly selective exploiting biological recognition through specific binding affinity between elements immobilized on the sensor with the target molecules^[3]. Recognition elements typically used in biosensors are enzymes, nucleic acids, antibodies, whole cells and receptors.

To fully exploit the specific interaction of the biosensors, the sensor surface must suppress any nonspecific interaction and in fact tremendous efforts has been made to find surface modifications that allow specific interactions over extended periods of time in biological fluids^[4].

1.2 Electrochemical biosensors

The electrochemical biosensors represent a subclass of chemical sensors that combine the sensitivity of electrochemical sensors with the high specificity of the recognition processes of biological molecules.

Other advantages include simple and low cost instrumentation and the possibility to develop miniaturized, multiplexing and portable devices, allowing *in situ* analysis of different compounds simultaneously^[5].

Nanobiotechnology is drastically revolutionizing the biosensors development. Many biosensing techniques and different transduction strategies exploit concepts developed in the field of nanobiotechnology: tailor-made biorecognition molecules, quantum dots and nanoparticle labels, carbon nanotubes, nanostructured supports, magnetic particles, flow-system analysis devices, microarrays, etc^[6]. Although they may appear sophisticated systems, the purpose of these innovative analysis devices is to simplify the analysis operations for operators and end users. These characteristics offer advantages in different aspects, for example higher specificity, higher sensitivity, higher operational stability, integrated sample treatments and shorter analysis time.

In the medical field, the electrochemical sensors have been reported for diagnosis of genetic diseases through the identification of SNPs^[7], the detection of pathogens^[8], forensic applications^[9] and drug response measurements^[10]. In food analysis electrochemical biosensors have been reported for analysis of foods and beverages^[11], for the detection of GMOs in food^[12] and for measuring the freshness of foods^[13]. Biosensors were applied also in the environmental monitoring area, especially in the evaluation of microbial cells in water and in the environment quality control^{[14],[15]}. In the area of biodefense, in the last 10 years, research projects finalize to the development of alarm systems against bioterrorism has been largely promoted and founded by European Governments^[16].

1.2.1 Electrochemical detection techniques

Since the electrochemical reactions are usually detected only in the vicinity of the surface of an electrode, electrodes play a crucial role in the functioning of electrochemical biosensors.

The electrode material, its modification of the surface or its size can significantly affect its ability in detection, depending on the function of a specific electrode.

Generally, electrochemical sensors are part of an electrochemical cell which is formed by three or two electrodes. A typical three-electrode electrochemical cell consists of a working electrode, usually a chemically stable and conductive material, such as platinum, gold, or graphite; a reference electrode, usually consisting of silver metal coated with a layer of silver chloride (Ag/AgCl); and an auxiliary electrode, for example a platinum wire (see figure 1.2). An advantage of this system is that the charge generated by electrolysis events passes through the auxiliary electrode rather than through the reference electrode, enabling the reference electrode to maintain its half-cell potential. A two-electrode cell has only the working electrode and the reference electrode. If the current density is quite low ($< \mu\text{A}/\text{cm}^2$), then the reference electrode can carry the charges with no adverse effects^[17].

Both of these systems, with two or three electrodes, are used in sensors. Despite their limitations, the cells with two electrodes are generally preferred for disposable biosensors since in this case the long-term stability of the reference electrode is not required and their cost is lower^[18].

The electrochemical reaction exploited in an electrochemical biosensor typically generates a measurable current (amperometric), a potential or accumulation of charge (potentiometric) or alters the conductive properties of a medium (conductometric) between two electrodes. Another approach applied in electrochemical biosensors is the electrochemical impedance spectroscopy (EIS), which allows monitoring the resistance and the capacitance of the working electrode interface^[2].

Amperometric and voltammetric techniques are characterized by the application of a potential to the working electrode *versus* a reference electrode and measuring the resulting current. Usually

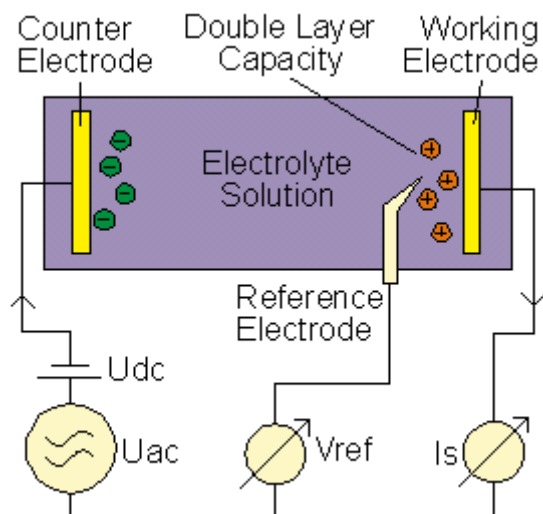


Figure 1.2: Principle set-up of a three electrode electrochemical cell. Picture modified from the original published in http://novocontrol.de/html/intro_eis.htm

the current is the result of a reduction or oxidation at the working electrode and is normally limited by the mass transport rate of the electroactive molecules to the electrode. Furthermore, the current peak measured over a linear potential range is directly proportional to the bulk concentration of the analyte.

Specifically voltammetry is a term used for those techniques in which the potential is scanned into a set potential range. In amperometry instead, changes in the current generated by oxidation or reduction are monitored as a function of time, while a constant potential is maintained between the working electrode and the reference electrode^[19]. Compared to voltammetric biosensors, amperometric biosensors have an additional selectivity since the oxidation or reduction potentials used for the detection are specific of the redox species in analysis. There are several version of voltammetry that differ in the waveform of the applied voltage and the phase of the waveform in which currents are measures. Among these, stripping voltammetry represents a particular case in which the potential necessary for oxidation (stripping) can be used to discriminate among multiple electroactive species, allowing multiplexed measurements of different analytes.

Conductometric biosensors monitor variations in the electrical conductivity of the solution, depending on changing in the composition of the solution or of the medium during the chemical reaction. Conductometric biosensors often involve enzymes that allow the production of charged molecules, so they can change the ionic strength of the solution, causing an increase of the conductivity.

Potentiometric devices measure the accumulation of charge on the working electrode *versus* the reference electrode in an electrochemical cell with zero or no significant current that flows between them. In other words, potentiometry provides information of the ionic activity in an

electrochemical reaction. Common examples are the ion-selective electrode for ions such as K^+ , Ca^{2+} , Na^+ , Cl^- ; these chemical sensors can be converted in biosensors by coating them with a biological element such as an enzyme catalyzing a reaction that produces the ion that the underlying electrode was designed to detect^[20].

Electrochemical impedance spectroscopy (EIS), described by Lorenz and Schulze in 1975, measures the resistive and capacitive properties of the working electrode by means of perturbation with a small amplitude sinusoidal excitation signal typically of 2-10 mV. The frequency is varied over a wide range to obtain the impedance spectrum. The in-phase and out-of-phase current response are then determined in order to obtain the resistive and capacitive components of the impedance, respectively^[21]. Impedance methods are powerful because they can sample electron transfer at high frequencies and mass transfer at low frequencies.

The basic concept of electrical resistance is the ability of circuit elements to resist the flow of electric current. Ohm's law defines the resistance (R), in terms of voltage (E), and current (I), through the relationship:

$$R = \frac{E}{I}$$

As the resistance, the impedance is a measure of the ability of a circuit to resist the flow of electric current. Impedance then generalized Ohm's law to circuits operating in the sinusoidal steady state.

The impedance is normally measured by applying a sinusoidal potential to an electrochemical cell and measuring the resulting current, a sine wave at the same frequency but out of phase. Through the resistance measured by impedance spectroscopy in alternating current, information about conductivity can be obtained.

The input signal or excitation, expressed as a function of time is:

$$E(t) = E_0 \cos(\omega t)$$

where E(t) is the potential at time t, E_0 is the amplitude of the input signal and ω is the radial frequency. The output signal I(t) has an amplitude I and shifted phase:

$$I(t) = I_0 \cos(\omega t - \varphi)$$

An expression analogous to Ohm's law allows us to calculate the impedance of the system:

$$Z = \frac{E(t)}{I(t)} = \frac{E_0 \cos(\omega t)}{I_0 \cos(\omega t - \varphi)} = Z_0 \frac{\cos(\omega t)}{\cos(\omega t - \varphi)}$$

The impedance is therefore expressed in terms of a magnitude, Z_0 , and a phase shift, φ . Using Euler's relationship, the impedance is then represented as a complex number:

$$\begin{aligned} Z &= \frac{E(t)}{I(t)} = \frac{E_0 \exp(j\omega t)}{I_0 \exp(j\omega t - j\varphi)} = Z_0 \exp(j\varphi) \\ &= Z_0 (\cos \varphi + j \sin \varphi) \end{aligned}$$

Impedance vector, $|Z|$, in the complex plane is described by two components, real (Z'), and imaginary (Z'').

The real part of Z is in the direction of the axis X, and the imaginary part is represented on the vertical axis Y. The absolute value of impedance can then be represented on a plane, as shown in figure 1.3.

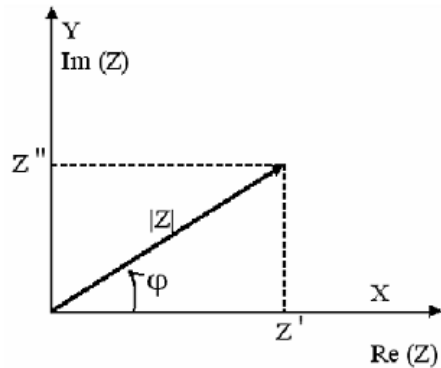


Figure 1.3: The impedance Z plotted as a planar vector using rectangular and polar coordinates. Reproduced from [21].

The coordinates of the rectangle are given by:

$$\begin{aligned} \text{Re}(Z) &= Z' = |Z| \cdot \cos \varphi \\ \text{Im}(Z) &= Z'' = |Z| \cdot \sin \varphi \end{aligned}$$

with phase angle:

$$\varphi = \tan^{-1}(Z'' / Z')$$

The impedance may be calculated from the vector of length $|Z|$

$$|Z| = \sqrt{(Z')^2 + (Z'')^2}$$

1.3 Application of electrochemical biosensors

There are two main approaches for electrochemical biosensors: label-free and label-based methods. In label-based approaches, an electroactive molecule selectively interacts with the target analyte previously recognized by the bioreceptors, producing a detectable signal. Labels used for the detection of an oligonucleotide or a protein can be intercalators or groove-binders, electroactive markers or nanoparticles. Label-free approaches instead, are based on changes in the electrical properties of the interface, on the intrinsic electroactive properties of the analyte or on the change in capacitance or resistance after the interaction with the analyte.

The electrochemical biosensors can be also divided according to the nature of the biological recognition: biocatalytic devices and affinity devices. Biocatalytic devices, that include enzymes, whole cells or slices of tissues, recognize the target analyte and as result produce electroactive species. Instead the affinity sensors rely on a selective binding interactions between the analyte and a biological component such as nucleic acids and antibodies.

1.3.1 Biocatalytic devices

Enzyme-based electrochemical biosensors exploit the selectivity of enzymes and their catalytic activity to generate the electroactive product which will be detected through electrochemical techniques^[22].

These biosensors can be classified historically in three generations. The first-generation biosensors were oxygen-based, while the second generation was mediator-based. The third-generation enzyme-based biosensors are also defined “directly coupled enzyme electrodes”.

The most popular and widespread application of enzyme-based biosensors is represented by the glucose sensor, that was introduced in 1962 and over the years has undergone many improvements (generations). Generally, the first generation biosensors had oxidase enzymes immobilized behind a semi-permeable membrane on the surface of the electrode, for example platinum (figure 1.4). In the case of glucose sensor, electrodes coated with glucose oxidase (GOx) has been widely used for the detection of glucose in blood sample^[23].

For the detection of glucose, these biosensors are based on the following reactions:

- a) $\beta\text{-D-Glucose} + \text{GOx-FAD} \longrightarrow \text{GOx-FADH}_2 + \delta\text{-D-gluconolactone}$
- b) $\text{GOx-FADH}_2 + \text{O}_2 \longrightarrow \text{GOx-FAD} + \text{H}_2\text{O}_2$
- c) $\text{H}_2\text{O}_2 \longrightarrow 2\text{e}^- + \text{O}_2 + 2\text{H}^+$

To work best, the first generation of these biosensors required a large and constant presence of oxygen as a co-substrate of the enzyme. Unfortunately, the oxygen is not very soluble in aqueous solutions and therefore may limit the production of current in the presence of analyte.

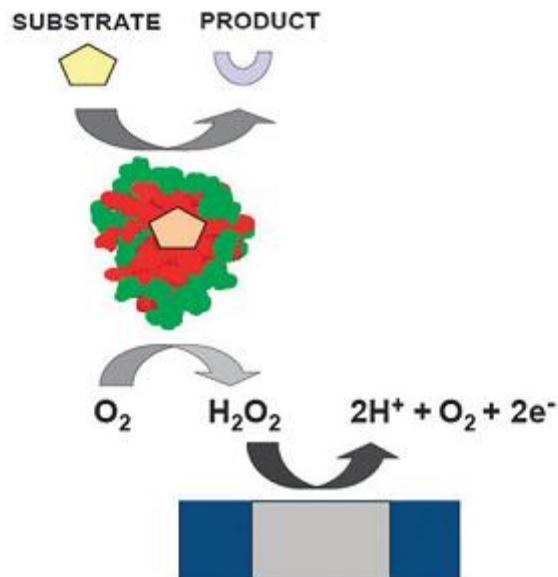
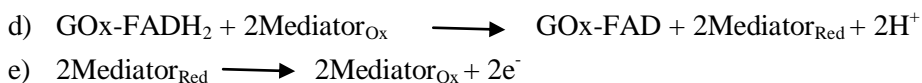


Figure 1.4: Oxygen-dependent first-generation biosensor with amperometric detection. Figure taken from [18].

In order to enhance efficiency of these sensors, the second generation biosensors have replaced oxygen as a co-substrate of the enzyme with artificial redox mediators. These are small soluble molecules capable to undergo rapid and reversible redox reactions, allowing the transfer of electrons between the active site of the enzyme and the electrode surface. Organometallic compounds are the most common redox enzyme mediators. In the case of second generation glucose sensors, a redox mediator replaces oxygen as the electron shuttle:



The wide variety of redox mediators allows the detection of the analyte in a potential range carefully selected by the operator, in which the interference is minimized due to possible events of oxidation or reduction of other components present in solution^[17].

Another step forward has been made with the third generation biosensors, where both the enzyme and the mediator are co-immobilized on the electrode surface, usually as a conducting polymer (figure 1.5). In this way the mediators cannot diffuse away from the surface of the biosensor, allowing the generation of high current density. In addition, this generation of enzyme-based biosensors are very useful for repeated measurements^[24].

Besides the sensor for glucose, which has been widely applied in health care, other enzyme-based sensors have been developed.

An example is represented by xanthine sensors; other existing methods for detecting xanthine such as anion-exchange chromatography, thin layer chromatography, precipitation and capillary

electrophoresis are complicated and very time-consuming. Xanthine is an intermediate of purine metabolism and is produced following the decomposition of adenosine triphosphate (ATP). This biosensor relay on xanthine oxydase that catalyzes the oxidation of xanthine to uric acid, and it is widely used in food industries to determine the freshness of fish^[25].

Another enzyme-based biosensor is represented by lactate sensors, used especially in the context of sport medicine, even if the concentration of lactate in blood is also a sensitive measure of oxygen deprivation from ischemia, trauma, and hemorrhage, which can lead to life-threatening shock, and its measurement has therefore become a vital component in medical monitoring^[26]. This biosensor is used to detect the presence of lactate in blood samples, a fermentation product which is produced under conditions of anaerobic metabolism^[27]. Four different enzymes have been used as the sensing component in lactate biosensors: lactate dehydrogenase, lactate oxidase, lactate monooxidase, and cytochrome b₂. Some of the electrochemical lactate sensors include mediators such as NAD⁺/NADH and ferricyanide.

Despite the clear advantages associated with the selectivity and catalytic activity of enzymes, it is also true that the number of the available enzymes is much lower than the number of potential analytes. Moreover the layer of enzymes on the surface of the sensor must be replaced periodically as it tends to lose activity. Another drawback is that enzymes require particular chemical and physical conditions to work properly.

Some biocatalytic sensors incorporate whole cells or tissue slices, as they are in some cases better sources of enzymatic activity compared to isolated enzymes, which often are very expensive or not commercially available^[5].

Also live microorganisms were immobilized on electrodes to monitor processes such as brewing, food manufacturing, waste-water treatment and pharmaceutical synthesis^{[5],[28]}.

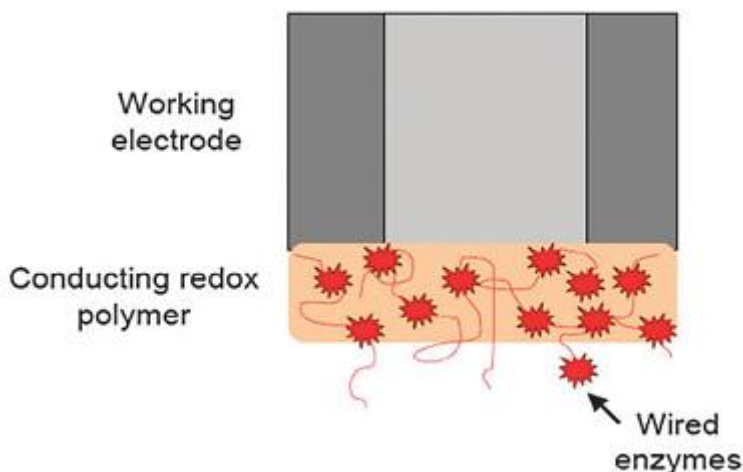


Figure 1.5: Third-generation catalytic biosensor containing enzymes wired to the electrode through a conducting redox polymer. Figure reproduced from [18].

Some drawbacks of these sensors include slower response and therefore longer recovery times following the exposure to the analyte and possible loss of selectivity due to the presence of many types of enzymes^[28].

1.3.2 Affinity biosensors

Affinity sensors are based on the ability of certain biomolecules such as antibodies, oligonucleotides and membrane receptors to form strong and selective bonds with a specific analyte, producing a measurable signal. Often, this signal must be amplified, since in these cases is not present the typical catalytic activity of enzymes. In the case of the electrochemical affinity biosensors, the amplification of the signal is carried out using enzymes, metal nanoparticles^[29], quantum dots^[30], redox intercalators or groove binder molecules^[31].

Immunosensors

The advantages of immunosensors reside in the high specificity of the antibodies for their respective antigens, no sample preparation and ease of automation, making them a viable alternative to more conventional analytical methods such as chromatography and mass spectroscopy^[32]. Many immunosensors were developed for biomedical applications and for several applications in environmental, agricultural, processed food and beverage areas^[18].

Most of the immunosensors employ a sandwich immunoassay approach, in which the surface of the biosensor is functionalized with capture antibodies (Ab1). After the addition of the sample and a subsequent washing, a tracer antibody (Ab2) is added to bind to the analyte captured by Ab1. Tracer antibodies in electrochemical immunosensors usually are labeled with enzymes producing electroactive products, or with metal nanoparticles. These labels can be detected and quantified using various form of voltammetry and amperometry techniques.

Moreover, the coupling of electrochemical devices with nanomaterials, such as gold nanoparticles, carbon nanotubes, magnetic particles, and quantum dots, offers multiplexing capability for simultaneous measurements of multiple analytes.

The first examples of immunosensors used radioactive labels to show the formation of the antigen-antibody complex^[33]. In 1971 enzyme immunoassay were introduced, which proved to be a safer, selective and less expensive alternative, although with less sensitivity and with a greater complexity. In these immunosensors the enzyme label produces an electroactive product which is then recognized by electrochemical techniques, in particular with voltammetry or amperometry. The enzyme labels most commonly used are alkaline phosphatase, β -galactosidase, horseradish peroxidase and glucose oxidase^[33].

Nanoparticles are a valid alternative to enzymes. Nanoparticles have physical and chemical properties different from the bulk form of the same material. In addition, the nanoparticles possess a large surface area-to-volume ratios, and therefore a high binding efficiency that makes them very useful for biomedical applications. Nanoparticles can be used as direct labels in electrochemical immunoassays, as descibe by Dequaire et al.^[34]; in this case nanoparticles are

conjugated with Ab2, and after the nanoparticle-antibody complex is bound to the captured analyte, the nanoparticles were dissolve in an acidic solution to form a large number of electroactive metal ions, that are detected using anodic stripping voltammetry.

Another strategy involves the accumulation of gold nanoparticles on the surface, used in a second step to catalyze the precipitation of silver to produce high concentration of electrochemically detectable metal ions^[35], or to bridge a gap between two electrodes, leading to a measurable change in conductivity^[36].

Another approach used in electrochemical immunosensors regards the electrochemiluminescence, that is a process in which light emissions have start from a redox reaction that occurs on the surface of the electrode. The electrochemiluminescence signal is proportional to the concentration of analyte, and is measured by a charged-coupled device (CCD) or a photomultiplier tube (PMT)^[37]. This system has been used to detect various cancer biomarkers, such as P53 protein^[38], PSA^[39], α -fetoprotein^[40], and others.

Nucleic acids biosensors

DNA sequence recognition has played an important role in detection of genetic diseases, medicine development, epidemic prevention and environmental monitoring.

Electrochemical DNA biosensors attract attention because they have advantages of being simple, cheap, sensitive, selective and compatible with array systems.

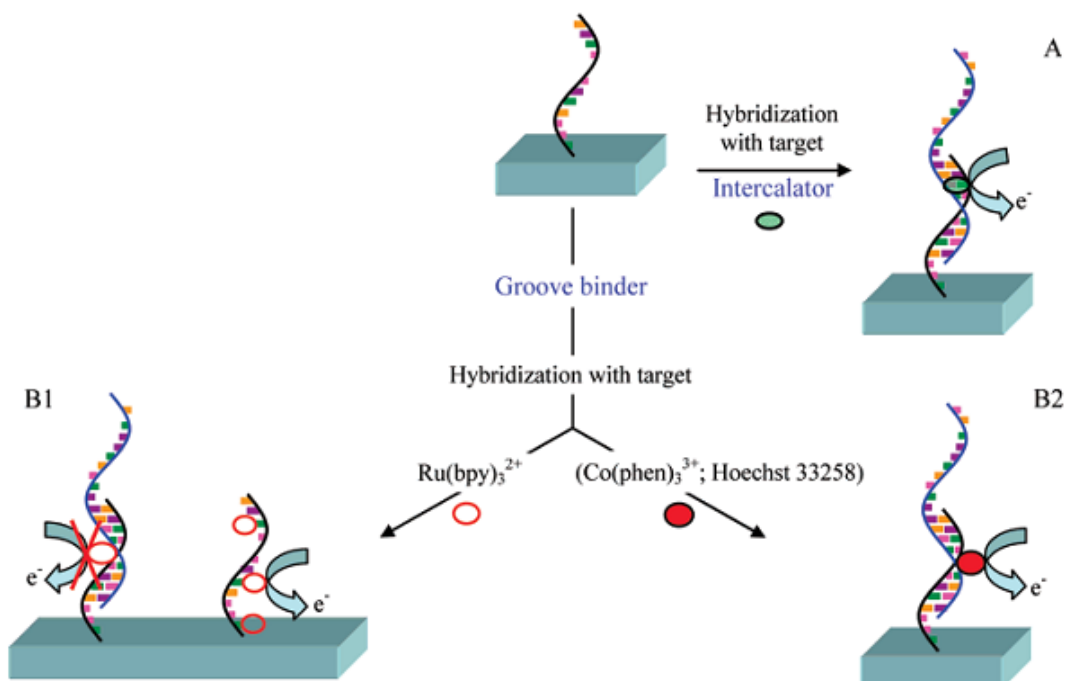


Figure 1.6: Several strategies for the development of redox-indicator-based electrochemical DNA biosensors. (A) Intercalator interacts with the DNA duplex. (B1) $\text{Ru}(\text{bpy})_3^{2+}$ interacts with guanines (green bases) of ssDNA whereas the formation of the double helix precludes the interaction of $\text{Ru}(\text{bpy})_3^{2+}$ with guanine bases. (B2) $\text{Co}(\text{phen})_3^{3+}$ or Hoechst 33258 interact with the DNA duplex, thus allowing DNA detection. Picture reproduced from [41]

Electrochemical detection of hybridization events can be effected by direct methods (label-free) and indirect methods (label-based); in both cases massive efforts have been made to recognize the selected target sequences and to distinguish the presence of single mismatch.

Direct methods are based on the electrochemical oxidation of guanine bases^[42], on variations in interfacial properties of electrode such as capacitance, conductivity or impedance^[43] and in the change in flexibility from ss-DNA to the rigid ds-DNA^[44]. The former is the most popular label-free method, because of its simplicity and its versatility. However, non-specific binding of the target DNA could be an issue, because it increases background signals.

Direct methods can be extended using EIS^[43]. Using redox species the change in the Faradaic impedance is measured before and after the hybridization event; owing to the repulsion of the redox species by the negatively charge DNA-duplex, an increase in charge transfer resistance is measured.

Label methods use electroactive labels that can be covalently bound to a nucleic acid sequence, or that can intercalate in the double-stranded DNA or can interact with major or minor grooves of ds-DNA. There have also been a number of reported strategies where the labels are enzymes^[45], nanoparticles^[46] or liposomes^[47].

Using enzymes as DNA label is also a very sensitive method for hybridization detection^[48]; however the enzymatic activity is easily lost during the preparation of the enzyme-DNA conjugation, and moreover it is more expensive than other methods.

Ferrocene (Fc) can be used to label single stranded DNA thanks to its good stability. In many cases oligonucleotides labeled with ferrocene were employed in sandwich-type assays^[49]. The electrode surface functionalized with probe sequences was exposed to unlabeled targets; afterwards a signaling oligonucleotide modified with ferrocene, was hybridized in a region of the target adjacent to the capture probe binding site. At the redox potential of ferrocene, the current peak is proportional to the number of Fc moieties on the surface; in other words the peak was proportional to the number of targets on the surface.

Some researchers proposed to exploit physical changes of DNA from the flexible ss-DNA to the rigid rod-like ds-DNA both with labeled and label-free detection methods, for example by attaching a ferrocene tag to the end of the immobilised probe^[50]. Upon hybridization, the rigid DNA duplex stands normal to the electrode surface, increasing the electron transfer distance from the electrode to the ferrocene, where any appreciable electron transfer can be observed.

Nanoparticles, especially silver or gold nanoparticles, are widely used for signal hybridization in several DNA assays.

A popular method provides direct detection of gold nanoparticles on the electrode surface: thus, the specific target sequences were directly detected by anodic analysis of gold colloids^[51]. In another approach signal of gold nanoparticles can be measured after dissolving them with particular treatments, such as HBr/Br₂, and then detected using stripping techniques^[52]. An electrochemical detection method based on the catalytic precipitation of silver onto the gold

nanoparticle label was also reported^[53]; with this approach hybridization was monitored by DPV or with conductivity measurements.

However the most common electrochemical strategies for detecting DNA hybridization rely on electroactive substances such as groove binders or intercalating organic compounds (that interact in different ways with ssDNA or dsDNA), because the target DNA does not required chemical modification with electroactive indicator, and because there are many more ways in which transduction can be configured with high sensitivity and selectivity.

Intercalators such as methylene blue or daunomycin were used in strategies based on the ability of ds-DNA to act as a conduit for charge transfer over distances of 40 Å or more^[54], an ability that ss-DNA does not possess. Thus, when a DNA duplex is formed, the intercalators can be oxidized through charge transfer. This technique also allows to recognize the presence of mismatches in the target sequence^[55].

Instead the groove binders use their ability to fit in the minor groove present in ds-DNA, but which is absent in ss-DNA. Cobalt complexes such as $\text{Co}(\text{bpy})_3^{3+}$ and $\text{Co}(\text{phen})_3^{3+}$ can bind electrostatically in the minor groove of the DNA helix and they can be detected voltammetrically^[56]. Another molecule used as electroactive hybridization indicator is Hoechst 33258 (see pag 18 for further informations). Hoechst 33258 is a DNA minor groove binder that recognizes adenine/thymine-rich sequences of DNA within the helix. Usually target sequence detection was monitored using LSV or DPV in the presence of Hoechst 33258, with the anodic current that increased with the quantity of the hybridized target on the surface^{[57],[58]}.

Aim of the project and outline of the following sections

Electrochemical biosensors provide an attractive means to analyze the content of a biological sample due to the direct conversion of a biological event to an electronic signal, enabling the development of cheap, small, portable and simple devices, that allow multiplex and real-time detection.

The aim of this PhD work has been the development of electrochemical biosensors based on nanobiotechnological strategies for the detection of biological macromolecules.

Specifically, one project was focused on the application of a DNA nanotechnology called hybridization chain reaction (HCR), to amplify the hybridization signal in an electrochemical DNA biosensor. Another project on which the research activity was focused concerns the development of an electrochemical biosensor based on a biological model membrane anchored to a solid surface (tBLM), for the recognition of interactions between the lipid membrane and different types of target molecules.

This thesis has been divided in three parts. In the first part, the results obtained for the DNA biosensor and HCR as signal amplification method have been described. The second part has been reserved for the preparation and characterization of the lipid membrane-based biosensors, while the third part has been reserved to the application of this biosensors. For each method, a general introduction, the descriptions of the experimental procedures and the detailed results have been reported. Finally the last chapter has been devoted to the general conclusions of the work.

Section I:
HCR as signal amplification
method

HCR as signal amplification method

2.1 Introduction

The aim of the project is to evaluate the possibility of using a strategy called hybridization chain reaction (HCR) on electrochemical DNA biosensors as an amplification method for the hybridization signal. This work was carried out within the European project Dynamics (Diagnostic Nanotech and Microtech Sensors, Sixth Framework Programs), with the aim of developing a lab-on-a-chip device for detection of pathogens in water using on-the-spot recognition and detection based on the nanotechnological assembly of unlabelled DNA.

In this case, if the target sequence has hybridized with the probe on the electrode surface, HCR determines the formation of products with high molecular weight that should be easier to detect, and therefore should provide an increase in the sensitivity of DNA biosensor, lowering the limit of detection.

The recognition of HCR products on the surface were carried out with different techniques, both electrochemical and optical, and the effect on the sensitivity and specificity of the different DNA biosensors was evaluated.

In the following paragraphs, a description will be given of the molecular mechanism underlying HCR and its applications that have been described in the literature. Furthermore the signal transduction techniques described in the following paragraphs will be treated, especially regarding the electrochemical measurements (voltammetry and capacitive measures), and the SPR assays.

2.1.1 HCR

Dirks and Pierce^[59] developed the concept of hybridization chain reaction (HCR), in which two different single-stranded DNA oligonucleotides were triggered to polymerize into a long double stranded structure when a third oligonucleotide was added in solution. HCR is an isothermal approach and does not involve enzymes, with the advantage of not requiring a careful control of temperature.

Hybridization chain reaction is a strategy that involves two different DNA molecules with hairpin structure (H1 and H2). In contrast to molecular beacons, where the DNA hairpin presents a very broad loop and one short stem, in HCR is the contrary: there are in fact very short loops protected by long stem. These structures stabilize H1 and H2 in the hairpin conformation and at the same time allows to store energy that will be released only after the addition of an initiator (I). The

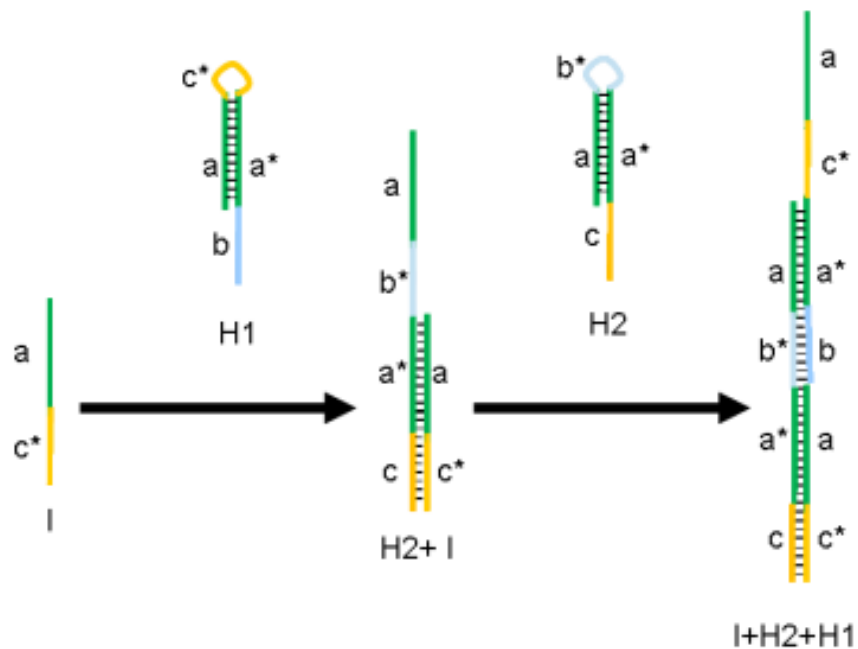


Figure 2.1: Scheme for the first round of HCR in solution. Hairpins with a protrusive end are added to an initiator (the target) and opened one after the other. A copolymer of nicked dsDNA with repetitive sequence results from the spontaneous repeated additions.

initiator hybridizes with the single-stranded end of H1, bringing its opening with the consequent exposure of a new single stranded end (figure 2.1).

The latter hybridizes with the free end of H2, opening the hairpin and showing a new free end that is identical to the initiator sequence. So each copy of initiator triggers a series of hybridization events between H1 and H2, leading to the formation of a long double-stranded sequence, thus amplifying the first recognition event between the initiator and H1 (figure 2.1).

The polymerization reaction ends only when H1 or H2 are exhausted, and the molecular weight of the polymer is inversely related to the concentration of initiator in solution.

Recently, Niu and colleagues combine HCR with enzyme amplification to improve fluorescence detection on magnetic beads, using biotin-modified hairpins and horseradish peroxidase labeled with avidin, thus allowing to detect 0.8 fM of target^[60]. Huang and co-workers have used dual-labeled hairpins with pyrene; HCR determines the formation of excimer pyrene, and due to their long lifetime fluorescence emissions they can detect the presence of nucleic acids in biological fluids complexes^[61]. Moreover, HCR was used also in a immunosensor assay by Choi and colleagues^[62], while Dirks and Pierce suggest an aptamer HCR system, in which the reaction is triggered by the molecular recognition event^[59].

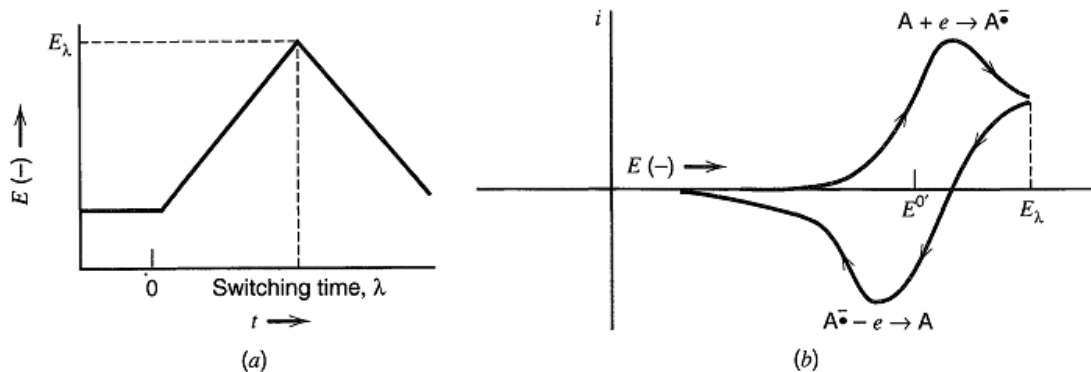


Figure 2.2: Cyclic potential sweep (a), and the resulting cyclic voltammogram (b). Picture modified from [21].

2.1.2 Voltammetric analysis and Hoechst 33258

Voltammetric techniques are very useful for detecting nucleic acids, because of the intrinsic electronegativity of nitrogen bases, especially guanine, and also because oligonucleotide can easily interact with electroactive molecules, either by covalent bonds, as for example in the case of ferrocene, or by weak interactions. In the latter case it mainly exploits the ability of these molecules to fit into the minor groove of double-stranded DNA (such as Hoechst 33258 or cobalt complexes), or to intercalate between the nucleobases (daunomycin, methylene blue).

Voltammetry is the easiest and fastest way to detect these electroactive molecules that interact with nucleic acids.

Among all the available redox molecules, intercalators and groove-binders are the most frequently used in this type of measurements, because they have the advantage of not requiring the modification of the target oligonucleotide (or an indicator oligonucleotide) through the formations of covalent bonds.

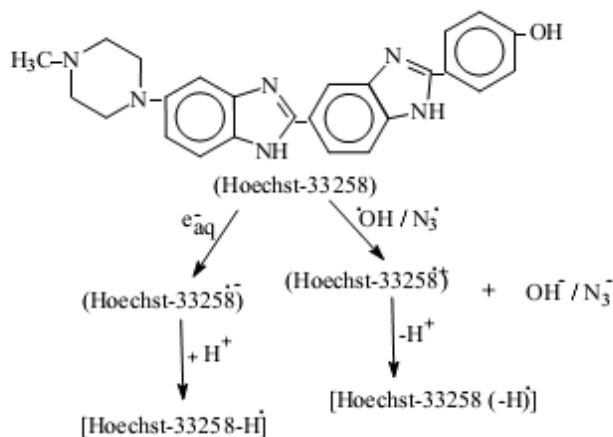


Figure 2.3: chemical structure of Hoechst 33258 and reactions of Hoechst-33258 with transient species. Picture reproduced from [63].

Another advantage is that the minor groove is present only in double stranded DNA, so there should be a very low nonspecific signal.

A groove-binder described in several papers in the literature is a bisbenzimidazole dye called Hoechst 33258. Hoechst 33258 has been known as a DNA minor groove binder (figure 2.4) which recognizes adenine-thymine-rich sequences of DNA^[64], and one molecule can interact with a maximum of five bases of the ds-DNA. It was irreversibly oxidized on the gold electrode at a low potential (550 mV) with a high current density (1.4 mA/cm² at 100 pmol/L).

Previous exploitations of Hoechst 33258 in DNA analysis and sensing were performed using several techniques. Hashimoto and colleagues suggest that the primary oxidation site of Hoechst 33258 is N-3 of the benzimidazole ring^[31] (figure 2.3) and used it to detect 1 pg/mL of a 20-mer oligonucleotide target. Choi et al. showed that Hoechst 33258 can be used to recognize the presence of DNA single-nucleotide polymorphisms and to detect DNA oligonucleotides with a concentration down to 1-10 nM^[58]. Toshiba Corp. developed an electrochemical DNA chip called Genelyzer and based on Hoechst 33258 that is able to analyze SNPs and common DNA sequence variations^[65].

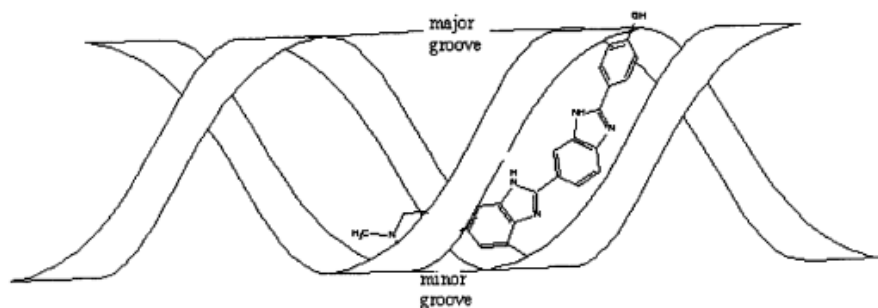


Figure 2.4: The binding of Hoechst 33258 to DNA. Picture reproduced from [66].

2.1.3 Surface plasmon resonance

Surface plasmon resonance (SPR) is an optical phenomenon that can be exploited for the characterization of adsorption of materials such as proteins, nucleic acids, lipids and small molecules on surfaces or for the detection of alterations that occur in the dielectric medium close to the surface. This technique allows label-free and real time measurements with high sensitivity; moreover, small amounts (often in the order of nanomoles) of sample are required in the experiments and kinetic parameters of association and dissociation can be determined.

The basic SPR-based analytical technique characterizes the average binding kinetics on a small surface area with respect to that of a reference cell. A development of the basic SPR technique is represented by SPR imaging (SPRi), in which measurements are taken by imaging the change of reflectivity (dependent on SPR) of the whole sensor surface during or after the binding of analytes to the interface. This allows for direct realization of array measurements.

SPR occurs in thin layers of conducting metals, usually gold, placed between two media of different refractive indices. A polarized laser light is directed through a medium with high

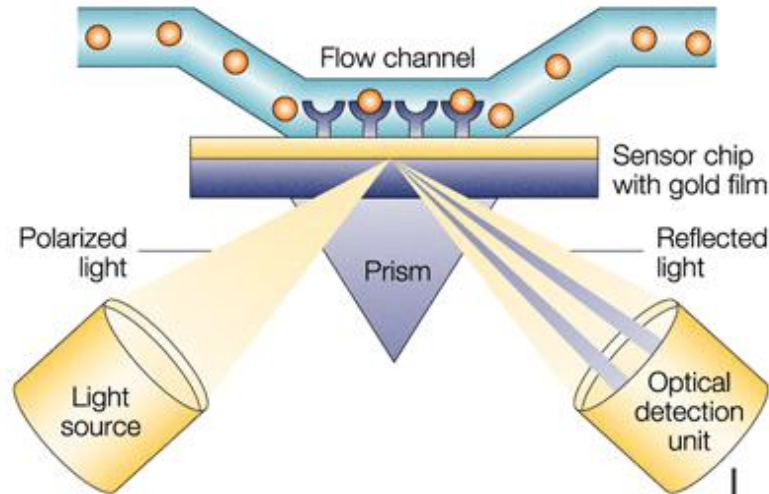


Figure 2.5: Surface plasmon resonance principle.

refractive index to the back of the sensor chip under condition of total internal reflection. A component of the energy carried by photons, the evanescent wave, is transferred through the gold layer to the medium with low refractive index. At a critical angle of incident light, the evanescent wave generates surface plasmons in the gold layer. This phenomena adsorbs light and determines a drop in the intensity of the reflected light. The critical angle at which surface plasmons are generated is called SPR angle and depends on the mass present in the sensor chip surface.

A change of mass within a hundred nanometers from the surface, for instance due to a binding event, changes the refractive index and thus the SPR angle. An optical detection unit measures and records this shift (**Errore. L'origine riferimento non è stata trovata.2.5**).

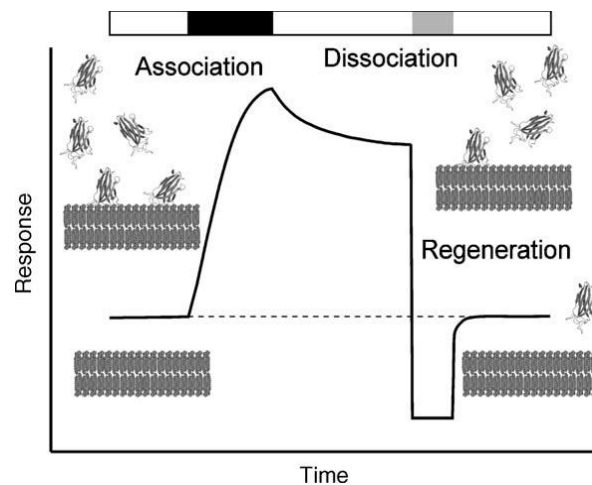


Figure 2.6: Schematic representation of the sensorgram. The sensor chip is equilibrated with buffer (white bar). The analyte is injected over the chip (black bar) for a certain period; the concentration of the analyte near the surface increases due to binding with the ligand. In the dissociation phase the buffer is injected (white bar) to equilibrate the binding. The regeneration of the surface is usually performed with an injection of high salt concentration or high pH solutions (grey bar). Figure taken from [67].

The response is measured in resonance units (RU) per time. One RU corresponds to a shift of 0.0001° of the SPR angle and is proportional to the mass bound to the surface. The RU response versus time is usually plotted in a graph called sensorgram (figure 2.6).

Two major information can be evaluated from a sensorgram: the binding level, which provides information on affinity constants at equilibrium, and the rate of interaction from which it is possible to extract kinetics constants.

In a typical SPR experiment probe molecules is immobilized onto the surface of the sensor chip and a solution with the other interacting molecules is flushed over the surface. The immobilized probe molecule is usually called ligand, while the injected molecule is called analyte. Generally the injection of the analyte solution is performed in a controlled fashion with a microfluidic system.

In DNA sensors, the refractive index of the sensing layer, which is in intimate contact with the sensor surface, changes depending on the amount of label-free complementary strand hybridized. SPR system is particularly useful for the analysis of binding and dissociation kinetics and real-time hybridization monitoring.

Other SPR advantages are no target labeling, rapidity of the hybridization reaction (within a few minutes), and probe reutilization.

However, a significant drawback is the somewhat low sensitivity, requiring up to the nanomolar concentration.

Lower limits of detection can be achieved using metal nanoparticles, especially Au nanoparticles, taking advantage on the increased surface mass, on the high dielectric constant of Au particles and on the electromagnetic coupling between Au nanoparticles and the Au film^[68].

Another approach that can greatly reduce the limit of detection involves the use of enzymes. RNase H was employed by Goodrich and colleagues on RNA microarray to detect DNA oligonucleotides with a 10^6 enhancement in sensitivity^[69]. The presence of complementary ssDNA sequences leads to the formation of RNA-DNA heteroduplexes; RNase H will then specifically hydrolyze only the RNA strand in the heteroduplex, triggering a cyclic process in which a very small number of DNA molecules can initiate the hydrolysis of many RNA molecules from the surface. To avoid the use of RNA probes, ExoIII can be used for the detection of DNA target using DNA arrays^[70], even if this system ensures a lower increase in sensitivity.

2.1.4 Capacitive method

An electrode without charge transfer across the electrode-solution interface regardless the applied potential is called ideal polarizable electrode (IPE). Although this kind of electrodes does not exist, some systems may behave as IPE within certain potential range. An example is represented by gold surfaces on which SAMs of alkanethiols were formed.

In these conditions the systems described above can be represented by the equivalent circuit consisting of a resistance and a capacitance placed in series (figure 2.7).

When a step potential (E) was applied on a IPE, a non-faradic current transient (i) was obtained, due to a variation of the ionic distribution at the interface (figure 2.8).

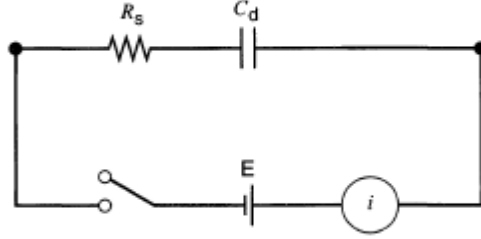


Figure 2.7: RC circuit used in potentiostatic step experiments. Picture reproduced from [21]

The behavior of this current as a function of time (t) is described by the following equation:

$$i = E/R_s e^{-t/R_s C_d} \quad \text{Equation 1}$$

where R_s and C_d correspond to the resistance and capacitance of the system.

Equation 1 can be obtained from the relationship between the charge (q) in a capacitance (C_d), and the potential applied on it (E_c):

$$q = C_d E_c \quad \text{Equation 2}$$

At any time the sum of the potential E_R and E_C , respectively through the resistance and the capacitance, must equal the whole potential applied to the circuit:

$$E = E_R + E_C = iR_s + q/C_d \quad \text{Equation 3}$$

Knowing that $i = dq/dt$, it is obtained that:

$$dq/dt = [(-q/(R_s C_d)) + (E/R_s)] \quad \text{Equation 4}$$

So, if we assume that the capacitor is initially uncharged ($q = 0$ when $t = 0$), then equation 4 above can be written:

$$q = E C_d (1 - e^{-t/R_s C_d}) \quad \text{Equation 5}$$

Making the necessary substitutions, Equation 1 is obtained again, which can be used to calculate the values of resistance and capacitance of the interface. In fact calculating the logarithm of the current as a function of time from Equation 1 we obtain:

$$\log(i) = \log(E/R_s) - t/(2.303 * R_s C_d) \quad \text{Equation 6}$$

Thus from the value of intercept obtained experimentally it is possible to determine R_s , while the capacitance value can be obtained from the slope of the linear regression.

This method was developed by researchers at the University of Lund as detection technique for biosensors. Berggren and coworkers have applied this strategy for the detection of antigens^[71] and for the detection of DNA^[72]. The system involves the use of a fast potentiostat and a relatively low concentration of electrolyte, and requires the detection of the initial part of the current dissipation curve.

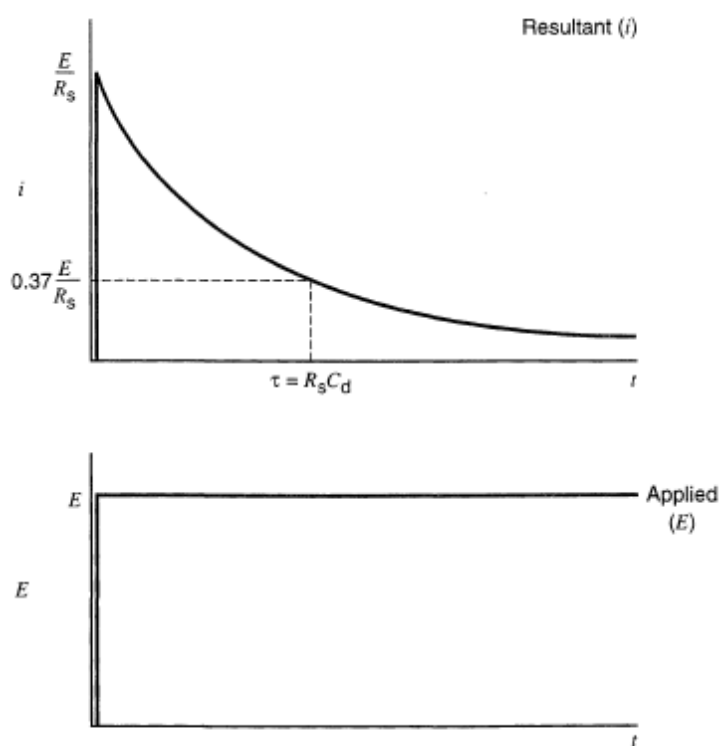


Figure 2.8: transient current generated during a potential step experiment. Picture reproduced from [21].

2.2 Materials and methods

Materials

All reagents are from Sigma-Aldrich unless noted otherwise, and have been used as such without further purification.

DNA sequences

Table 2.1 Oligonucleotide sequences were purchased from Eurofins MWG and Sigma-Genosys.

Probe_Parvum	CCTTGTA AAAATGAAATTTT-SH
T_Parvum	ATTCATTTTACAAGGCCTCCAATGTATACAAACTAGTTC
H1_Parvum	ATGTATACAAACTAGTTCACGGCGGAACTAGTTTGTATACATTGGAGG
H2_Parvum	AGTCTAGGATTCGGCGTGGGTTAACACGCCGAATCCTAGACTACTTTG
Probe_HEV	CTGCGGCCACAGCCGCTTTT-SH
T_HEV	GCGGCTGTGGCCGAGCAAAGGCATCCATGGTGTGTTGAGA
H1_HEV	CATCCATGGTGTGTTGAGATCGCGCTCTCAAACACCATGGATGCCTTTG
H2_HEV	GCGCGATCTCAAACACCATGGATGCAAAGGCATCCATGGTGTGTTGAGA
Probe_Giardia	CGTACATCTTCTTCTTTT-SH
T_Gia	AGGAAGAAGATGTACGACCAGCTCAACGAGAAGGTTCGCAG
H1_Gia	TCAACGAGAAGGTTCGCAGTAAGTCTCGACCTTCTCGTTGAGCTGGT
H2_Gia	GACTTACTGCGACCTTCTCGTTGAACCAGCTCAACGAGAAGGTTCGCAG
Probe 2	HS-GGTTCCGAAAGTTGGAA
Target 2	TTCCAAC TTTTCGGAACC
Probe 3	HS-ATGCATGCATTAGCATGCTA
Target 3	TGGAGAACTGATCGACACAGTTTTTTTTTTTAGCATGCTAATGCATGCAT
TGia_C8_mp	AGGAAGACGATGTACGACCAGCTCAACGAGAAGGTTCGCAG
TGia_C8A19_mph	AGGAAGACGATGTACGACAGCTCAACGAGAAGGTTCGCAG
TGia_A19_mh	AGGAAGAAGATGTACGACAGCTCAACGAGAAGGTTCGCAG

HCR in solution

Hairpins samples were heated to 95°C for 2 minutes and then allowed to cool to 20° C for 1 hour before use. Native polyacrylamide gel was a 10% gel made with TBE 1x. The gel was run at 8 V/cm for 60 minutes, stained with Sybr Gold, and viewed with a Gel Doc 1000 (Biorad). For the HCR reactions, stock solutions of target (T), hairpin 1 (H1) and hairpin 2 (H2) were diluted in running buffer (0.5 M NaCl, 50 mM Na₂HPO₄, pH 6.8) to 15 µM, 30 µM and 30 µM respectively. Then 9 µL of each solution was combined to allow hybridization chain reaction for 1 hour at room temperature.

Gold surfaces and functionalization

Capacitive measures were performed using gold surfaces commonly referred to as 'template stripped gold' (TSG). Briefly, a 200 nm layer of ultrapure gold (Electron Microscopy Sciences, 99.99 % purity) was evaporated in vacuum onto freshly cleaved muscovite mica which had been previously left at about 300 °C overnight in a vacuum of 10^{-6} Torr or less (we used resistive heating of the metal in an Edwards high-vacuum evaporator with a resistively heated specimen stage). After cooling, round glass cover slides (12 mm in diameter) were glued on the evaporated gold with EpoTek 377 (Epoxy Technology Inc., Billerica, MA, U.S.A.). At the moment of use, the glass cover slides with the glued gold layer are separated from the templating mica chip exposing an ultra-flat and ultra-clean gold surface (figure 2.9).

Gold electrodes for voltammetric measures are prepared with the following protocol. Briefly, a 200 nm layer of ultrapure gold (Electron Microscopy Sciences, 99.99 % purity) was evaporated in vacuum onto cleaned glass disk which had been previously left at about 300 °C overnight in a vacuum of 10^{-6} Torr or less. These surfaces have 4 gold sites with a surface area of 1 mm² (figure 2.9).

Commercial gold surfaces (Sensor chip Au or SIA kit Au, from GE Healthcare) were used for SPR experiments.

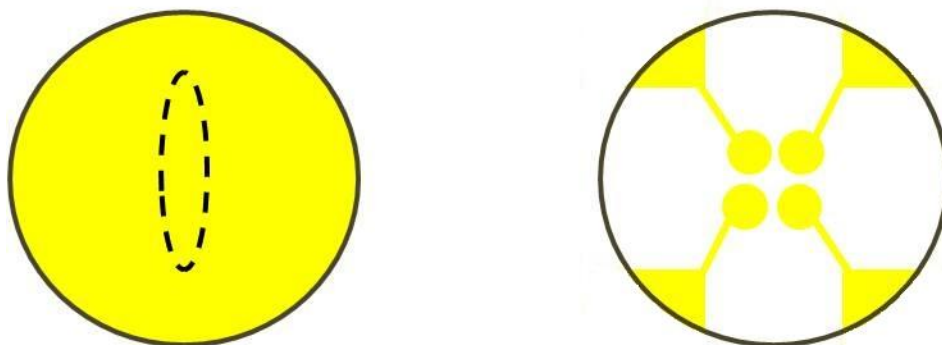


Figure 2.9: Gold surfaces used for capacitive measurements (on the left) and for voltammetric experiments (on the right).

Gold surfaces for voltammetric experiments have been derivatized with oligonucleotides according to the following protocol. A 3 μ M solution of thiol-modified 'probe' oligonucleotide is prepared in 50 mM Na₂HPO₄, 500 mM NaCl (pH 6.8). Approximately 10 μ L of oligonucleotide solution is layered on the surface of a freshly-exposed gold electrode disc, covered with a Hybrislip™ and left overnight at room temperature in a humid chamber. The surface is then rinsed with 2 mL of buffer added drop by drop and dried with a gentle stream of nitrogen gas.

For voltammetric measures a 3-electrodes electrochemical cell was used, consisting of a single room that covers all 4 gold sites (see figure 2.9). The cell has a volume of 6 μ l and has an inlet and an outlet to make the flow cell.

For capacitive and SPR experiments gold surfaces were functionalized with an overnight incubation of thiolated oligonucleotides 3 μM in PBS buffer. Subsequently the whole surface was passivated with 6-mercapto-1-hexanol (MCH) 1 mM for 30 minutes at room temperature, in order to reduce unspecific binding of DNA on the gold surface.

For SPRi measurements, gold surfaces were functionalized with an overnight incubation of thiolated oligonucleotides 3 μM . Then the surface was docked in the flow cell and MCH 1 mM was injected in each channel for 20 minutes to passivate the surface. The running buffer was injected for 10 minutes at 5 $\mu\text{l}/\text{min}$ after every hybridization and HCR steps (20 minutes at 5 $\mu\text{l}/\text{min}$) to obtain a baseline after every hybridization and HCR steps.

Electrochemical cell measurement

All measurements were carried out using an electrochemical cell designed and built in our laboratory (Figure 2.10). This is a cell in polydimethylsiloxane (PDMS), a polymeric non-toxic and transparent material, which behaves as an excellent electrical insulator. The cell is also equipped with a microfluidic system designed for the passage of solutions in the measuring cell, characterized by a volume of 20 μL and approximately a working area of 15 mm^2 .

The auxiliary electrode consists of a platinum wire; the reference, instead, consists of a silver wire on which is deposited a layer of at least 1 μm of AgCl electrochemically. In general a galvanostatic oxidation is carried out with a current of about 190 μA immersing the electrodes in a solution 0.1 M KCl. A two-electrode cell was used, in which the anode is represented by the silver wire, while the cathode consists of a platinum wire. Once you have the electrode, it should be inserted into the electrochemical cell of PDMS.

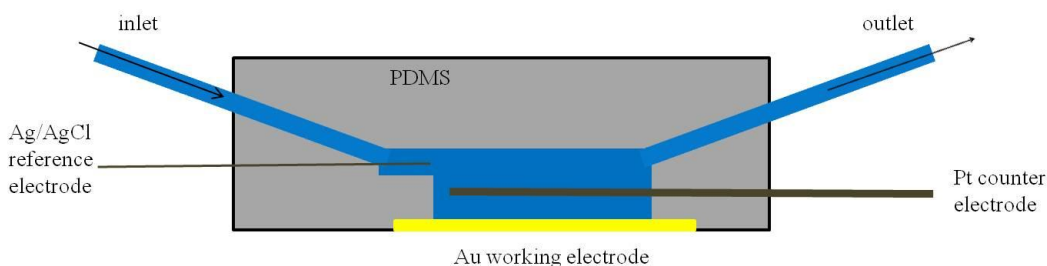


Figure 2.10: section of the electrochemical cell used for electrochemical analysis.

Voltammetric measures

10 μl of “target” oligonucleotide at different concentrations were prepared in 30 mM sodium citrate, 300 mM NaCl (pH 7). These solutions were added to the gold surfaces for 1 hour. The surfaces were then rinsed with 2 ml of buffer added drop by drop and dried with a gentle stream of nitrogen gas.

Then 10 μl of hairpin 1 and hairpin 2 (1 μM) in 50 mM Na_2HPO_4 , 500 mM NaCl (pH 6.8) were added to the surfaces and left on them for 1 hour. The surfaces were then rinsed with 2 ml of buffer added drop by drop and dried with a gentle stream of nitrogen gas.

Staining with Hoechst 33258 is performed flowing 200 μl of a 100 μM solution of dye in 10 mM Na_2HPO_4 , 100 mM NaCl (pH 7) at 50 $\mu\text{l}/\text{min}$; after that the solution was left inside the cell for one minute and then the cell was flushed with 200 μl of buffer at 50 $\mu\text{l}/\text{min}$. The same buffer was used for the following measurements.

Three-electrode linear sweep voltammetry measurements have been performed on a $\mu\text{Autolab}$ electrochemical workstation (Metrohm Autolab B.V., Utrecht, The Netherlands), using the manufacturer's software. For three-electrode measurements, potential scan was between 0.3 and 0.7 V vs. Ag/AgCl (NaCl 100 mM) with the usual connections.

Capacitive measurements

Capacitive measures were performed applying the method described by Berggren and colleagues^[73]. All the measures were performed in a three electrodes cell, using the following solution as measuring buffer: 10 mM NaCl, 197 μM KCl, 291 μM Na_2HPO_4 , 131 μM KH_2PO_4 , pH 7.4. A potential step of 50 mV was applied to the working electrode and the resulting current decay was sampled at 20 kHz. The measure was performed every minute before the injection of the target, until a stable capacitance was reached. After the hybridization occurs, the measurement was repeated, and the capacitance variation after the hybridization event was calculated.

Surface plasmon resonance measurements

SPR experiments were performed on a commercial SPR device from Biacore, the Biacore X100 (see figure 2.11). Once the functionalized chip (Biacore, GE Healthcare) was docked into the Biacore X100, the hybridization protocol was performed by cycles of subsequent injections starting by an injection of running buffer (0.5 M NaCl, 50 mM Na_2HPO_4 , pH 6.8) for 1080 s at



Figura 2.11: Biacore X100.

5 $\mu\text{l}/\text{min}$ to obtain a baseline, and then several injections of oligonucleotides (1 μM of the target sequence and H1 and H2 both 0.5 μM), for 1080 s at 5 $\mu\text{l}/\text{min}$, followed by an injection of running buffer for 300 s at 5 $\mu\text{l}/\text{min}$. After each cycle the surface was regenerated by DNA denaturation with an injection of urea 7 M, followed by a stabilization period.

HCR control and multi-detection measurements were performed using a custom-built SPR imaging instrument (see figure 2.12) with a Kretschmann optical configuration with a 680 nm superluminescent light source and a 1 MP CCD camera with 25° range of incident angle. In this configuration the position of the light source and the camera is fixed, only the prism holder platform could be rotated to scan and find the inflexion point of the SPR peak in order to maximize sensitivity. There are no moving parts during the measurements. The experiments were done in a custom PDMS flow cell designed and fabricated specifically for our SPRi instrument. The flow cell has four parallel channels and their assignment during the HCR control and multi-detection measurements are discussed in the respective chapters.

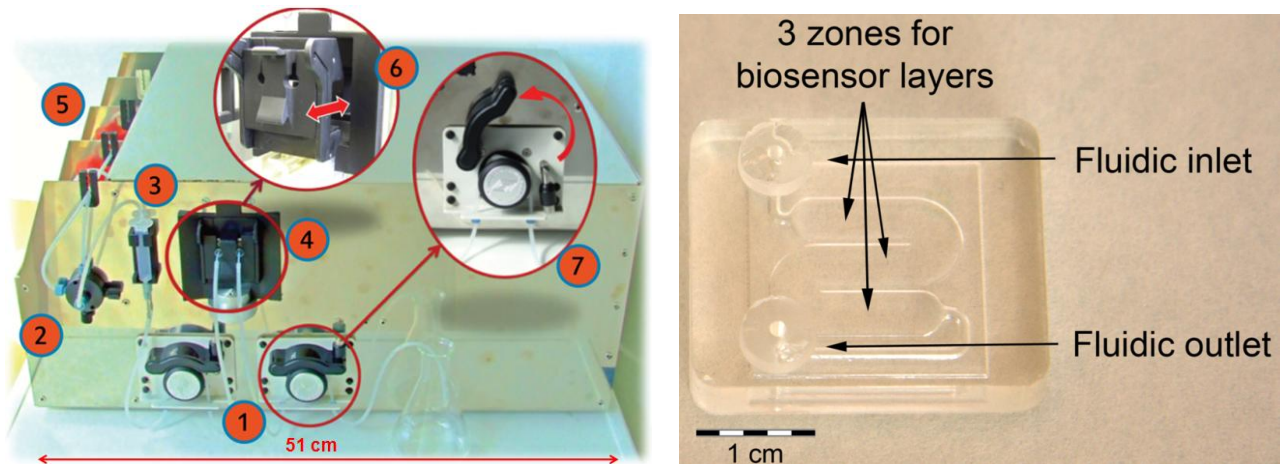


Figure 2.12. On the left, components of SPRi instrument: 1) peristaltic pumps, 2) 5-port manifold, 3) syringe, 4) removable prism and flow cell holder platform, 5) bottle holders, 6) attachment of the prism holder platform to the rotator platform, 7) opening mechanism of the peristaltic pumps. On the right: PDMS flow cell applied in the SPRi instrument.

2.3 Results and discussion

2.3.1 Sequence design and HCR in solution

Sequences design

The sequence design for the probes and hairpins towards real pathogen sequences was done starting from GenBank sequences of characteristic genes that had already been used before for detection of such pathogens. The sequence of the selected gene (for example the COWP gene in *Cryptosporidium parvum*, GenBank AF248743), was analyzed with a custom-made script (written in MATLAB) that calculated the thermodynamic stability of the secondary structure of a portion of sequence, if taken alone (thus limited to short-range interactions only, for example suitable for model target oligonucleotides, partially denatured DNA, fragmented or PCR amplified tracts).

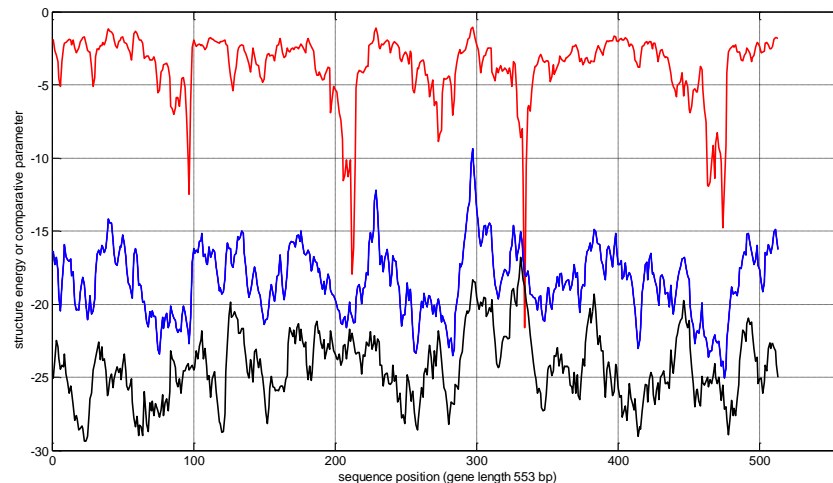


Figure 2.13: example of sequence structure analysis for the COWP gene in *Cryptosporidium parvum*. A search window of 40 nt was passed along the sequence, calculating the secondary structure stability (black trace), the stability of the structure bound with a 16 nt probe (blue trace) and a comparative parameter which tries to evaluate the penalty of high secondary structure with respect to strong binding. The red trace shows the result of binding energy / (structure energy – binding energy). The regions of minimum have been evaluated manually for probe and hairpin candidates. Alternative formula using binding energy and secondary structure energy for the evaluation of candidate regions gave similar results. Manual checking of candidates is always suggested.

Subsequently the binding energy of a 16 nt probe oligo perfectly matched with the target sequence was calculated. Energy calculations were performed with Matlab calling Vienna package's *RNAcofold* program, ver. 1.80^[74] set for DNA and called on a sliding portion of sequence along the characteristic gene sequence. For each position along the gene sequence, a penalty parameter was calculated proportional to the energy of the secondary structure of the target, its possible self-binding stability and the amount of secondary structure upon binding the target (as it would hinder the binding) and inversely proportional to the probe-target binding energy (figure 2.13).

HCR hairpin design was done using Nanev^[75] forcing the selected gene target sequence tract in the recognition portion of the probe and hairpin and letting the software guess the rest. Several probe, target, hairpins candidates located in the regions of minimal penalty along the sequence (low secondary structure, plausibly unhindered binding) were then checked manually using the Vienna package and NUPACK^[76] testing for probe-target and probe-hairpin binding.

Sequences from the pathogens *Cryptosporidium parvum* (the gene COWP for the *Cryptosporidium* oocyst wall protein^[77]), *Giardia lamblia* (the β -giardin gene^[78]) and Hepatitis E virus (HEV, the DNA version of a portion of the polyprotein gene^[79]) were used to design sets of oligonucleotides listed in table SD1 for the following HCR experiments.

C. parvum and *G. lamblia* are unicellular protozoa with known ability to contaminate drinking water sources, and they appear to be responsible for severe forms of enteritis, even if taken in small amounts. HEV is a RNA virus transmitted mainly via fecal-oral routes among humans either through contaminated foods or water contaminated with feces.

HCR in solution

In the present work three sets of DNA oligonucleotides were designed, starting from the genomic sequences of three pathogens (*C. parvum*, *G. lamblia* and HEV), in order to trigger an hybridization chain reaction in the presence of the pathogen DNA (figure 2.14).

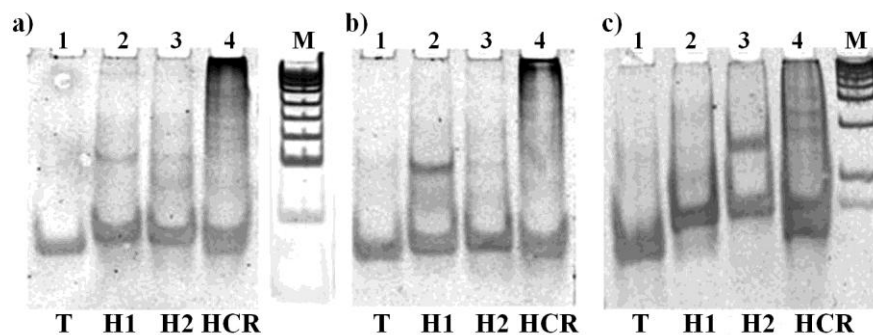


Figure 2.14: HCR in solution generates high molecular weight dsDNA molecules. 10% polyacrylamide gels stained with Sybr Gold, loaded with all the three sets of target and hairpins. a) Hepatitis E virus, b) *G. lamblia* and c) *C. parvum*. In all three panels lane 1 was loaded with the reaction when only Target oligonucleotide is added, lane 2 with the reaction of Target and Hairpin 1, lane 3 with the reaction of Target and Hairpin 2, while lane 4 was loaded with the reaction of Target, hairpin1 and Hairpin2.

After one hour of reaction the formation of high molecular weight products as a result of HCR can be observed only in the presence of the initiator and the two hairpins, even if the reaction does not seem to exhaust all available hairpins.

So electrophoresis data confirm the proposed mechanism about HCR and that the DNA oligonucleotides can carry on HCR in solution.

2.3.2 Voltammetric experiments with HCR

HCR on the surface

Since HCR determines an increase of dsDNA amounts in response to hybridization events, the feasibility of HCR in an electrochemical DNA biosensor using Hoechst 33258 was checked.

Recently, Zheng and coworkers^[80] used a surface-initiated assembly chain reaction described by Lubrich and colleagues^[81] as a strategy for amplifying the signal for an electrochemical DNA biosensor. They used $[\text{Ru}(\text{NH}_3)_6]^{3+}$ as redox-active compound, and after at least 6 hours of polymerization process they obtained a limit of detection of 4.9 pM.

The voltammetric measurements were performed using working electrodes consisting of a gold surface functionalized with thiolated probe.

The hybridization with target oligonucleotides was detected by Hoechst 33258, a minor groove binder with some preference for AT-rich regions of the DNA double-helix, which oxidizes irreversibly to a potential of about 470 mV vs Ag/AgCl (in 100 mM NaCl)^[82].

First, gold surfaces (working area of about 1 mm²) were functionalized with 3 μM of thiolated probe in incubation buffer (50 mM Na₂HPO₄, 500 mM NaCl, pH 6.8) with over-night incubation

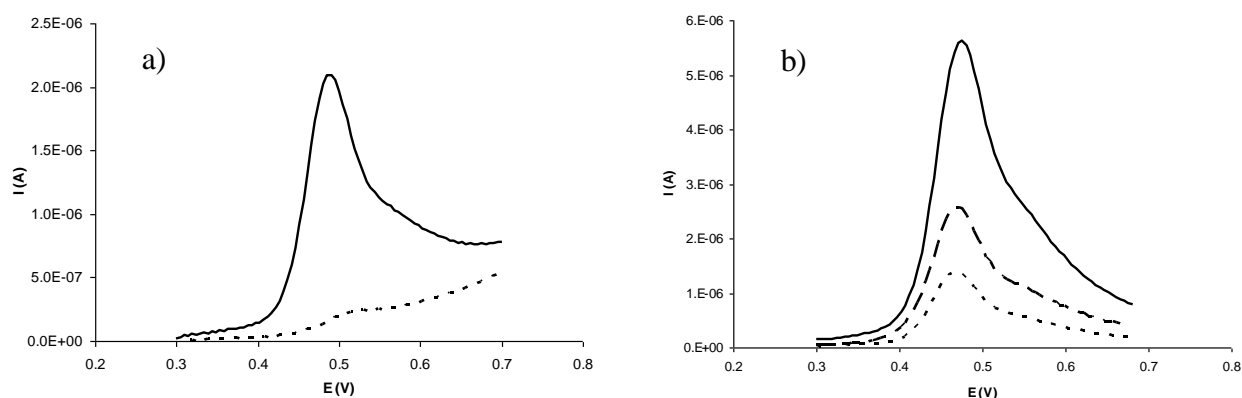


Figure 2.15: (a) Black curve: first LSV scan with an oxidation peak after 1 hour of hybridization of target 10 nM and 5 minutes of staining with Hoechst 33258 100 μM . Dotted curve: second LSV scan; this scan has been used as background signal and subtracted from the first LSV scan. (b) Dotted curve: signal of probe-modified electrode; dashed curve: after hybridization with 10 nM target; continuous curve: amplified signal after HCR. Hoechst 33258 was used in a concentration of 100 μM in 100 mM NaCl and 10 mM phosphate buffer. Potential scan rate was 0.1 V/s.

at room temperature. Then the surfaces were washed with 1 mL of the incubation buffer, and dried with a gentle nitrogen flow. Gold surfaces were then inserted in the electrochemical cell; a first set of measures has been carried out to measure the background signal, so 200 μl of Hoechst 33258 100 μM in 10 mM Na_2HPO_4 , 100 mM NaCl (pH 7) at 50 $\mu\text{l}/\text{min}$ were injected in the measuring cell. During an incubation time of 5 minutes, Hoechst 33258 accumulates on the surface and it is easily detected with linear sweep voltammetry. As a result, an oxidation peak with the height proportional to the amount of Hoechst 33258 present on the surface is obtained (see figure 2.15). A second potential scan does not show any oxidation peak, so it was used as experimental background to be subtracted from the oxidation peak obtained in the first scan.

Unfortunately, a certain amount of Hoechst 33258 binds to the ssDNA on the surface, and also to the gold surface, as observed in other experiments performed on bare gold surfaces (data not shown). Moreover, the binding of Hoechst 33258 is irreversible, thus just one measure per electrode is possible and then the measurements with only target and those with target and HCR were conducted on different electrodes.

To investigate the possibility to amplify the hybridization signals with HCR, calibration curves were obtained working with a series of target concentrations (more precisely 1 μM , 100 nM, 10 nM, 1 nM and 100 pM).

So in another set of measurements, gold surfaces functionalized with thiolated probes were incubated with 10 μL of target solution (in 30 mM sodium citrate, 300 mM NaCl, pH 7) for an hour and then washed with the same buffer. After that the surfaces were incubate with Hoechst 33258 as described before, and LSV measurements were performed.

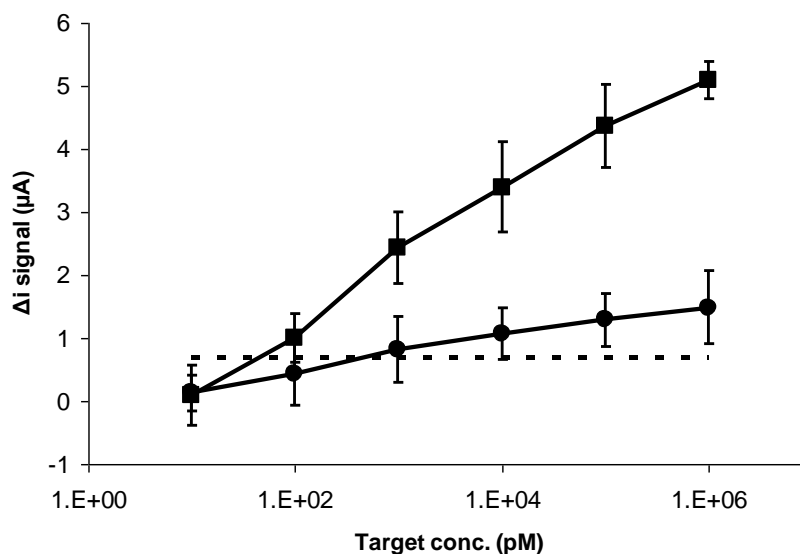


Figure 2.16: Calibration curves of an electrochemical DNA sensor without HCR amplification (circle markers) and after HCR amplification (square markers). Background signals, obtained from experiments carried out in absence of target DNA, were subtracted for each value. Error bars represented to standard deviation based on at least three independent measures, while the dashed line correspond to 3 times the standard deviation of the background.

Finally, another set of measurements were made, in which the incubation with target oligonucleotides was followed by an incubation with a solution containing H1 and H2 (both 1 μ M) in 50 mM Na_2HPO_4 , 500 mM NaCl (pH 6.8), for an hour. Then the gold surfaces were washed with the same buffer and incubated with Hoechst 33258 as described before, in order to perform, at the end, LSV measurements.

Figure 2.16 show the results obtained in these sets of experiments; in this plot, each data point were obtained from at least 3 independent experiments. In this biosensor HCR leads to an increase of the signal of approximately 5-fold compared to the not-amplified hybridization signal. This increased signal is much lower than the amplification ratio obtained in experiments on the surface with HCR hairpins labeled with fluorophores^[60] (up to 20-fold). This discrepancy could be due to possible limitations in the electron exchange of Hoechst 33258 with the surface, especially regarding Hoechst 33258 molecules that are at a certain distance from the surface. However, even if the signal enhancement factor is not very high, after 1 hour of reaction HCR can lowers the limit of detection of the biosensor (corresponding to a signal/noise ratio of 3 or, in other words, 3σ of blank experiments) of about 2 orders of magnitude.

Mismatch recognition

To test the selectivity of this electrochemical assays, target oligonucleotides with different mismatch were designed (see table 2.1 in Materials and methods).

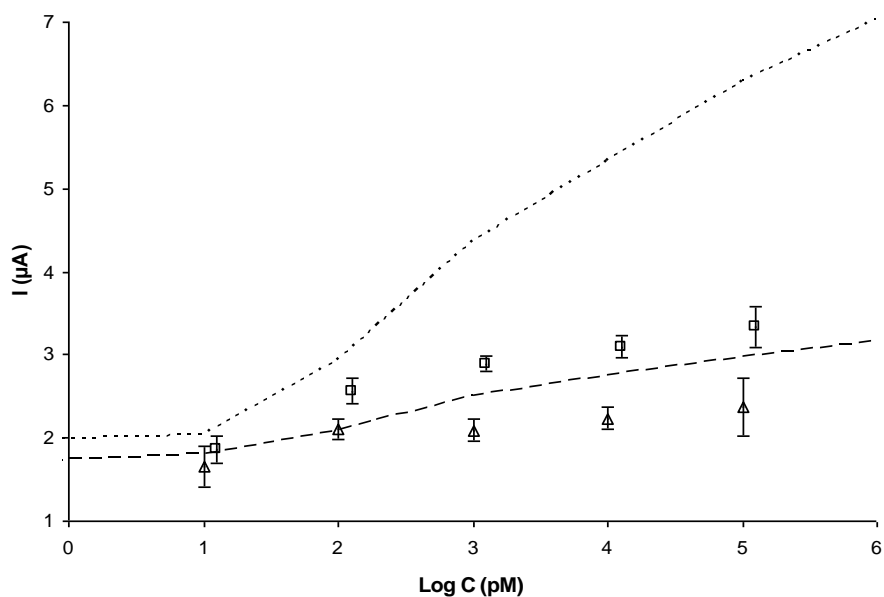


Figure 2.17: Mismatched target with a single mutation in the portion complementary to probe. Triangle markers correspond to target hybridization, while square markers correspond to HCR experiments. Dashed line represent biosensor response to perfect matched target, while dotted line correspond to HCR experiments performed after hybridization with matched target. Error bars represent standard deviations calculated on three independent measurements.

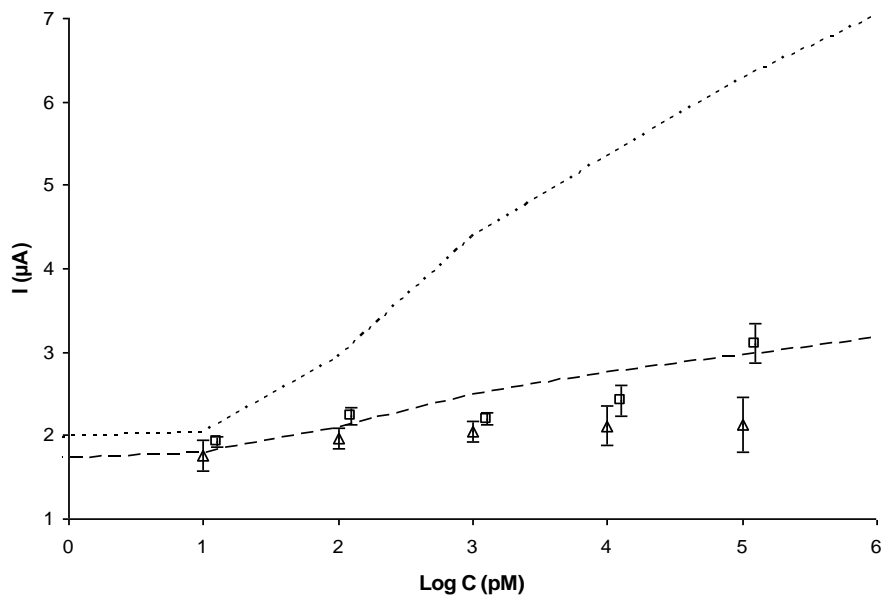


Figure 2.18: Mismatched target with 2 mutations, one for probe sequence and one for HCR. Triangle markers correspond to target hybridization, while square markers correspond to HCR experiments. Dashed line represent biosensor response to perfect matched target, while dotted line correspond to HCR experiments performed after hybridization with matched target. Error bars represent standard deviations calculated on three independent measurements.

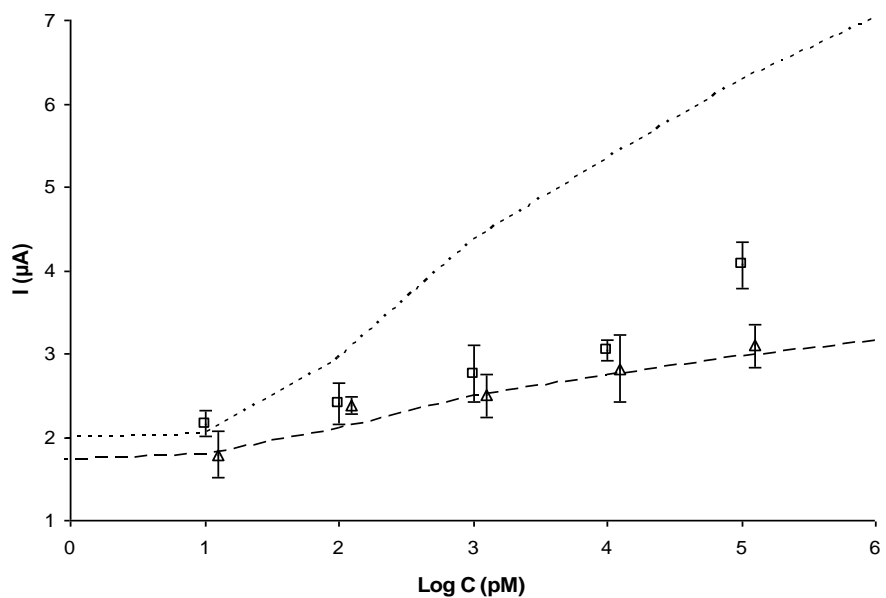


Figure 2.19: Mismatched target with a single mutation in HCR-trigger portion. Triangle markers correspond to target hybridization, while square markers correspond to HCR experiments. Dashed line represent biosensor response to perfect matched target, while dotted line correspond to HCR experiments performed after hybridization with matched target. Error bars represent standard deviations calculated on three independent measurements.

In the experimental set-up applied in these experiments, target molecules undergo two different recognition events, first with the probe and then with H1. For this reason, two different mismatch were used. Specifically, in the first sequence the mismatch is in the portion complementary to the probe (TGia_mp, figure 2.17), while in the second sequence the mismatch is in the portion that can trigger HCR (TGia_mh, figure 2.19). Finally, a third target sequence was designed with both the mismatch (TGia_mph, figure 2.18).

The same experimental procedure reported previously was repeated for each non-complementary target. Specifically, also in this case one set of measurements were performed only with the non-complementary targets, and the another set of measurements were made with the non-complementary targets, followed by HCR, as described before. The results obtained in this experiments were compared with the results obtained using complementary targets (figure 2.16 and dashed lines in figure 2.17, 2.18 and 2.19).

When the mismatch is placed in the portion complementary to the probe (TGia_mp), a decrease in the current signals occurs, while no difference in signals appear when the mismatch is in the portion complementary to H1 (TGia_mh and TGia_mph). Instead target with this mutation failed to trigger HCR (TGia_mh+HCR), as we expected considering that the target portion that promotes the opening of H1 is formed by just 6 bases. Actually also the mutation in the portion complementary to the probe determines a lower signal after HCR (TGia_mp+HCR). This effect may be due to the fact that the mutation causes a decrease in the amount of target after hybridization step, thus slowing the following HCR. Finally, the effects of the two mutations appear to add up on HCR when they are on the same target sequence (TGia_mph+HCR).

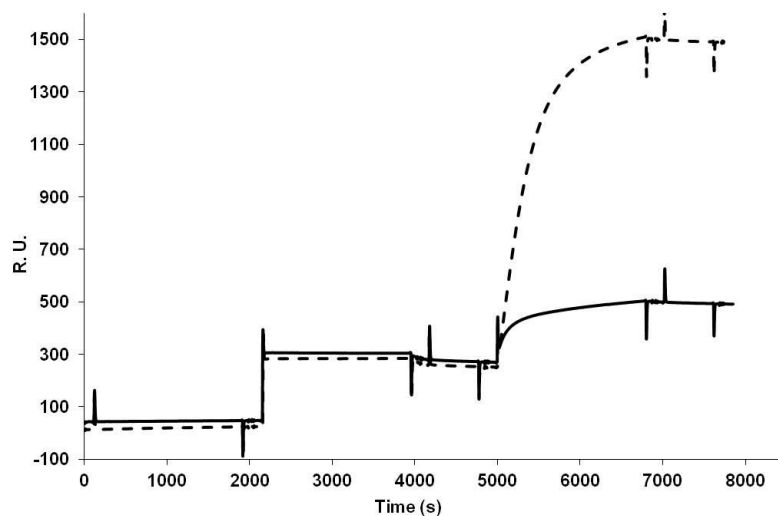


Figure 2.20: HCR-generated signal is visible in real-time with a commercial SPR system. SPR curves depicting the response after the consecutive injections of running buffer, T_Gia (1 μ M) and H1_Gia (1 μ M, solid line) or of running buffer, T_Gia (1 μ M) and H1_Gia/H2_Gia mix (0.5 μ M each, dotted line). The sensorgrams represent the response of the working cell (functionalized with the probe P_Gia) minus the response recorded in the reference cell (functionalized with a control oligonucleotide).

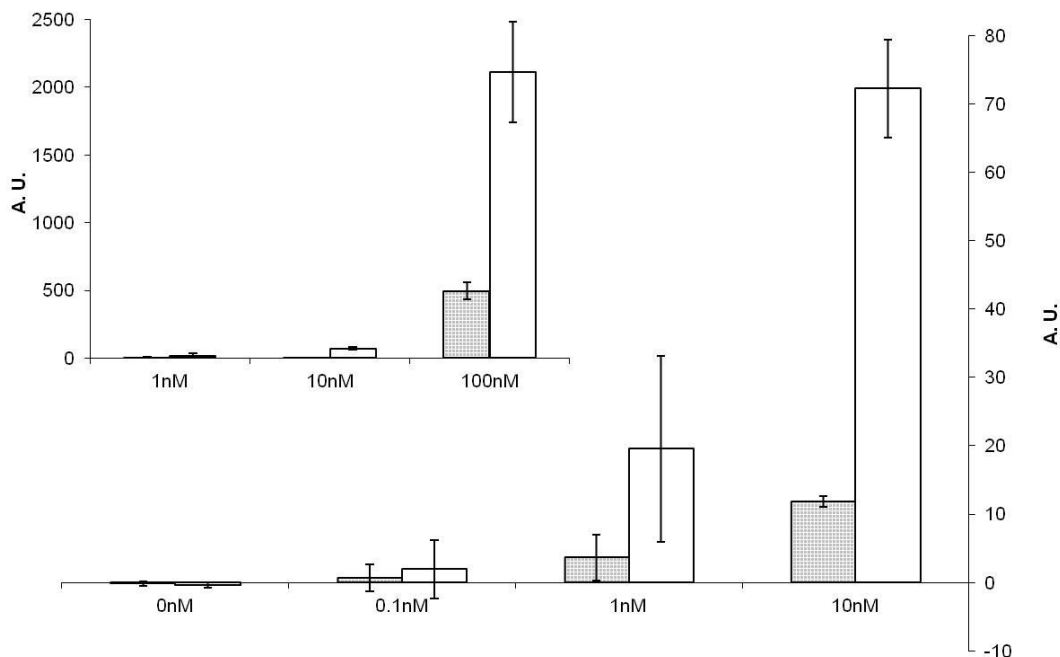


Figure 2.21: HCR is able to reveal Target T_Gia binding on the surface at concentrations below the direct-detection limit. Response values after the injection of different concentrations of the target T_Gia (grey bars) and the following HCR (white bars). The inset shows the higher signals measured with 100 nM target, compared with lower signals of 10 and 1 nM. Error bars represent the SD of multiple experiments.

Thus HCR seems to improve the capability of this biosensor to distinguish perfectly complementary target from a target with one or more mismatches.

2.3.3 SPR experiments with HCR

To evaluate the ability to perform HCR on a solid surface, thiolated probe oligonucleotides (specifically Pro_Giardia, see table 2.1 in Materials and methods) complementary to a portion of the initiator sequence were immobilized on a commercially available SPR gold chips (Biacore, GE Healthcare) that was then passivated with MCH. A commercial SPR instrument (Biacore SPR X100) was used to detect HCR products and to define the amplification factor (figure 2.20). All the SPR measurements were performed at EPFL in Lausanne, at the Laboratory of Life Science Electronics.

The first injection of running buffer gives no visible signal and serves as baseline. The following injection of the target oligonucleotides (T_Gia) produces a clear peak due to the DNA binding on the surface, which quickly reaches a plateau toward the end due possibly because of surface saturation. The next injection of H1_Gia (1 μ M), performed after T_Gia injection, produces a binding signal similar in amplitude to the target, albeit with a slower kinetic. On the same surface, regenerated with urea 7 M, another target injection gives a signal identical to the first cycle.

However, the following injection of H1_Gia and H2_Gia (both 0.5 μM , so 1 μM in oligonucleotides) clearly determines a peak of higher magnitude, indicating the formation of HCR products on the surface. The HCR signal is 4 times bigger than the signal from the T_Gia alone or the signal of H1_Gia alone (over T_Gia).

So HCR visibly amplifies the target-binding signal of about 4 to 5 times (furthermore, T_Gia 10 nM yield to a 7 times bigger signal upon HCR with respect to T_Gia alone, see figure 2.21). The signal increase is correlated to the formation of HCR products on the surface, formed only in the presence of both hairpins and the target hybridized on the surface.

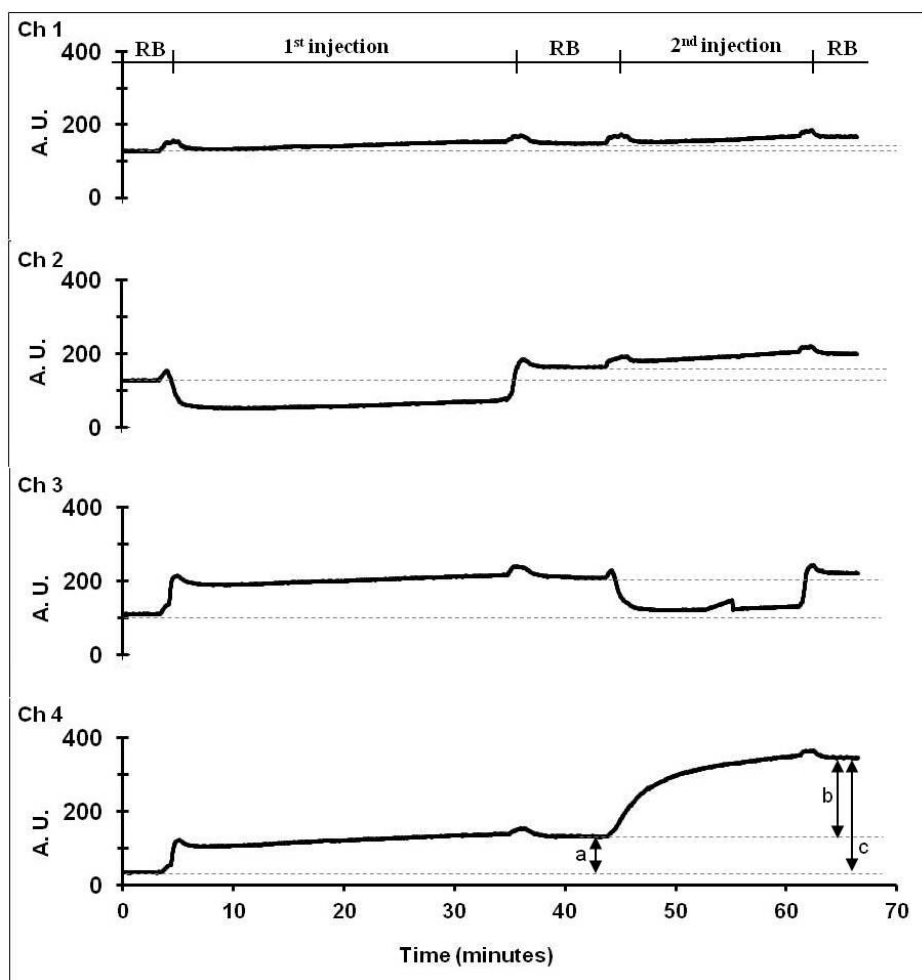


Figure 2.22: Comparison of SPRi response obtained in four parallel channels. [Ch1]: only buffer; [Ch2]: non-complementary target + HCR; [Ch3]: complementary target + non-complementary target; [Ch4]: complementary target + HCR. It can be seen that the introduction of a new sample into a channel is marked by a small transient peak which is caused by the handling of the silicone tubing; practically these small peaks help us to identify the different steps. In channel 1 the minor signal drift measured on the running buffer was used to compensate the other results.

Note that the addition of the non-complementary DNA in channel 2 and in channel 3 resulted in an abrupt drop of the signal. This is due to a buffer effect, since the 10 μM stock solution of the non-complementary DNA used for the measurements was stored in 10 mM PBS instead of the running buffer, which was used for the dilution of the other DNA solutions.

In fact, the injection of the hairpin H1_Gia alone determines a signal increase that is comparable to the one of the target DNA alone. In addition it is possible to observe that the signal peaks due to the HCR and to H1_Gia alone show a slower kinetic than the target alone, possibly due to the time needed to open the DNA hairpins.

In order to test the possibility of using the HCR signal to amplify the label-free binding of the target, the effect of HCR on the limit of detection of target sequences was hence evaluated using different target concentration (figure 2.19). Consecutive cycles of injections were performed as in the previous experiment; at the end of every cycle, the surface was regenerated with urea 7 M. T_Gia injection at different concentrations was performed, followed by a second injection of H1_Gia/H2_Gia mix (both 1 μ M) for the HCR. As shown in figure 2.21, for low T_Gia concentrations of 0.1 nM and 1 nM, the bound level remains very close to the value for the running buffer alone (set to 0 nM). The following HCR determines a signal increase with a T_Gia concentration of 1 nM, and even higher signals were obtained with a T_Gia concentration of 10 nM and 100 nM, although HCR also seems to increase the noise of the measurement. T_Gia 1 nM is practically not distinguishable from the lower concentrations of 0.1 nM or from the negative control (without target). Instead the corresponding HCR amplifies the hybridization signal and, despite an apparent increase of the signal dispersion, it allows an increase of the hybridization signal, enabling its detection. Finally at a lower concentration (0.1 nM) the hybridization is not detectable even after the HCR. So at the T_Gia concentrations of 1nM and 10nM the HCR effect allows the detection, especially for the 10nM injection.

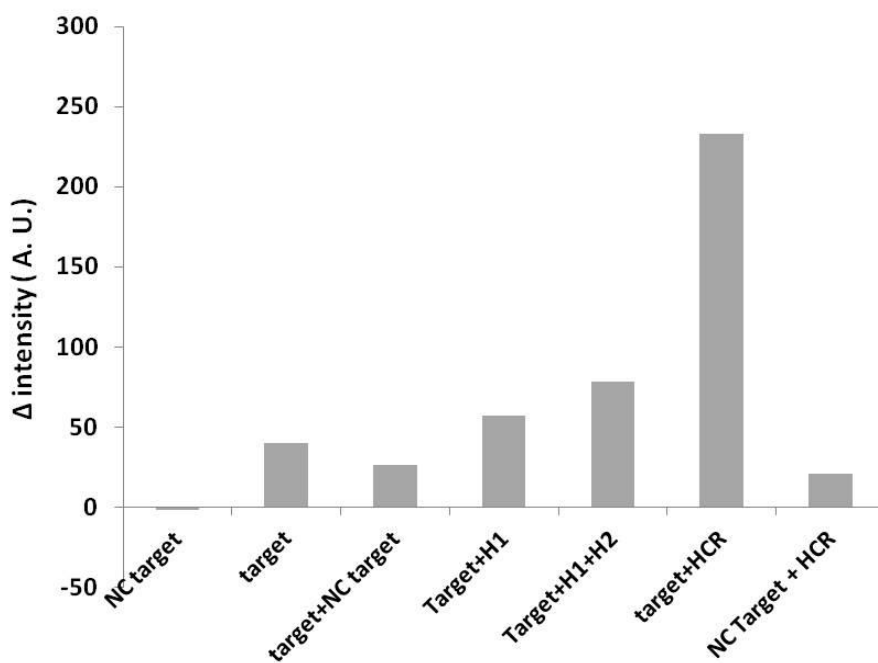


Figure 2.23: signal increments measured in experiments performed with SPR imaging show in figure 2.22. Control experiments were performed with non-complementary target. Target concentration was 1 μ M.

Nevertheless, due to the higher experimental variability observed in the HCR, the detection limit is decreased of only about one order of magnitude.

Therefore this data demonstrate that the HCR-generated signal can increase the detection limit for the bound target T_Gia oligonucleotide.

HCR on the surface was then tested also with a custom-built SPR imaging instrument. All SPR imaging measurements were performed in Budapest (Hungary), at Budapest University of Technology and Economics (BME).

Figure 2.22 and 2.23 show the intensity variations after the injection of T_Gia and the HCR hairpins.

The injection of T_Gia determines a clear signal increase, while the next injection of H1_Gia/H2_Gia mix yielded a significantly higher signal, consistent with the formation of HCR products on the surface.

These measures confirm the data observed using the commercial SPR; in fact it can be seen that all of the negative control steps, including the ones with the non-complementary target and the

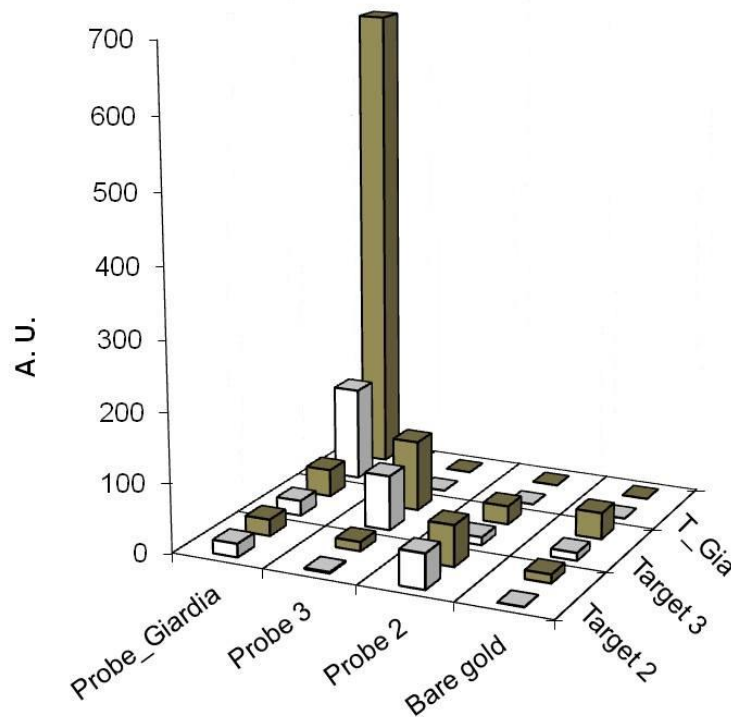


Figure 2.24: SPR imaging data showing the specificity of HCR amplification. A three-component array (Probe_HCR, Probe 2 and Probe 3) was created on a gold surface. After the injection of the target sequences (Target_HCR, Target 2 and Target 3) the resulting signals were collected (white bars). Then HCR was performed in each channels (grey bars).

hairpins without initiator, resulted in nearly zero signal, compared to the complementary target and HCR signals.

Several control experiments were performed. First, after the injection of T_Gia, an addition of H1_Gia (Target+H1 in figure 2.23) was performed. After this step a signal increase was observed, corresponding to an increase of material on the surface, even if lower than what observed for T_Gia alone. A further signal increase of similar magnitude is produced after the subsequent injection of H2_Gia (Target+H1+H2).

This data confirm the molecular mechanism underlying the HCR on the sensor surface.

Then the specificity of the HCR for the target was assessed by performing two different experiments. First a non-complementary target (Target 2, see table 2.1) was injected producing no signal variation. The following injection of H1_Gia/H2_Gia mix (NC target+HCR), determines only a slight non-specific signal, suggesting that no reactions occurs on the surface without the specific target oligonucleotide. In the second experiment the injection of target was followed by the injection of non complementary target (Target+NC target). This results in a signal decrease, therefore indicating that the accumulation of DNA on the surface occurs only with HCR.

The advantage of the custom SPRi system over the commercial SPR is that it allows multiplexed detection. The same experimental setup was indeed used to demonstrate that HCR could be effectively applied in a multi-receptor array to amplify interactions selectively. For this purpose a three-component array was prepared on gold surface.

The *in-situ* probe immobilization took place in the four channels of the PDMS microfluidic cell, using the following probe sequences: Probe 2, Probe_Giardia, Probe 3 and without any DNA (running buffer only). After the overnight immobilization the chip was rotated of 90 degrees with respect to the microfluidic, leading to the formation of a 4x4 array where each channel feeds a portion of the four surface areas, and all the sensor surface was then passivated with MCH.

In the next step in each of the four channels the following solutions were injected: Target 2, T_Gia, Target 3 and RB, respectively, for 30 minutes (figure 2.21). It can be seen that the hybridization signal is visible only in the areas where the matching combination of probe/target is present, indicating that each target sequences (1 μ M) hybridized with the corresponding probes, instead of nonspecifically adsorbing to the surface. After a washing step with running buffer, all the channels were injected with the H1_Gia/H2_Gia mix (both 1 μ M). Although three surface areas showed Target hybridization, only the area where the specific T_Gia oligonucleotide is bound reacts with the hairpins and hence generates the HCR signal. Only a slight signal increase was observed in the other spots, indicating the specificity of HCR.

Accordingly with the data on the commercial SPR system, the HCR reaction on SPRi amplifies the specific-Target signal of a nearly 5 factor. Taken together, these data demonstrate that the HCR is a label-free approach that is able to specifically amplify the DNA binding signal, and that it is promptly suitable for both commercial SPR and multiplexed SPRi detection systems.

2.3.4 Capacitive measure with HCR

It was determined that the HCR is a suitable approach for real-time SPR based biosensors, we investigated whether the HCR can be used in a simpler and more miniaturizable detection system based on a label-free detection. Therefore, we set up an experiment to measure HCR on a label-free electrochemical DNA biosensor.

The measurements were performed in a three electrode cell, where the working electrode was functionalized with the thiolated sequence Probe_Parvum (3 μM for 15-16 hours) and passivated with MCH. Subsequently, the biosensor cell was incubated for 1 hour with different concentrations of the target DNA (T_Parvum) in order to allow the hybridization on Probe_Parvum.

The hybridization was detected using the potentiostatic step method described by Berggren and colleagues^[73]. In order to apply this method, a buffer of low ionic strength (typically 10 mM) is required; this allows to slow down the current decay, thus allowing facile sampling of the discharge current, in particular at the beginning of the pulse.

In these experiments a sampling frequency of 20 kHz was applied. The subsequent analysis to calculate the capacitance has been performed on the first 10 points of the current, and then fit with the RC model (linear regression greater than 0.99).

The capacitance at the electrode-solution interface was monitored before and after the hybridization events and also after HCR, and then the capacitance variations due to the hybridization and the HCR were calculated.

To investigate the possibility to amplify the hybridization signals with HCR, calibration curves were obtained working with a series of target concentrations (figure 2.22).

The results obtained with the capacitive biosensor show that the hybridization of the Target DNA T_Parvum on the electrode surface produces a signal that is somehow proportional to the concentration of Target DNA (Figure 2.22). However, due to the experimental error, only at T_Parvum concentration of 1 μM the signal falls above the detection limit (3 times the standard deviation) and can therefore be considered as detectable. When the HCR was performed on the electrode surface, the capacitive signals are increased, while still being somehow proportional to the Target concentration. Nevertheless, although the standard deviation of the HCR signal is bigger than the one of the Target, the HCR allows the detection of the Target already at 0.5 μM , hence improving the detection limit of DNA hybridization on the sensor surface.

While further efforts are necessary to improve the measurement system and therefore to increase the sensitivity of the sensor, already in these preliminary measurements HCR shows the ability to amplify the signal of hybridization, and that it can therefore be exploited to improve the limit of detection of potentially simple and miniaturizable detectors.

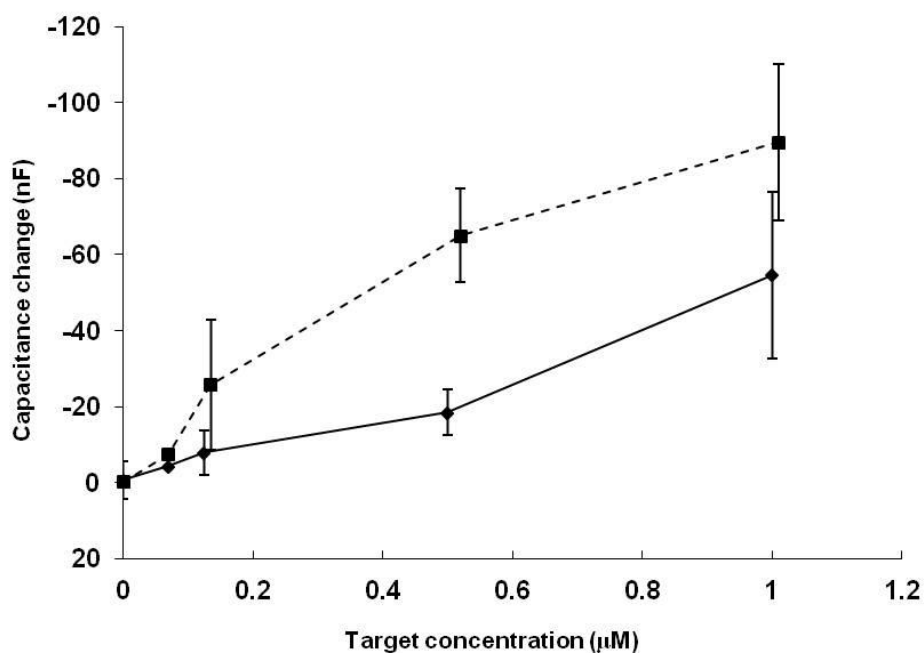


Figure 2.25: Calibration curves of a capacitive DNA sensor before HCR amplification (diamond markers) and after HCR amplification (square markers).

2.4 Conclusion and perspective

In the experiments discussed in this chapter, we evaluated the possibility of using HCR to amplify hybridization signals in different types of biosensors.

First of all, probes and hairpins designed from real pathogen sequences can trigger HCR in solution, but also on the surface of biosensors, as shown by SPR experiments conducted with oligonucleotides designed from the β -giardin gene of *G. lamblia* and by capacitive experiments, performed using oligonucleotides designed from the gene COWP of *C. parvum*.

The detection of the high molecular weight products of HCR with electrochemical label-based biosensor was also performed, in order to evaluate its effect on the limit of detection.

We found that HCR can be implemented on a solid surface and used as a strategy for signal amplification in a voltammetric DNA biosensor. Employing HCR, a lower limit of detection by about 2 orders of magnitude is observed ($\sim 10^{-10}$ M). In addition, HCR seems to improve the ability of the biosensor to discriminate between perfect matched and mismatched DNA targets; in addition the particular mechanism of HCR allows to discriminate the position of the mismatch in the target sequence.

Then application of HCR as a label-free strategy to amplify the hybridization signal was evaluated. HCR has proved capable to amplify the hybridization signal, even though low amplification factors were observed. Specifically, the maximum amplification factor measured in these experiments was approximately 5-fold and a decreasing in the limit of detection by about

one order of magnitude is observed in SPR experiments. Moreover SPR results have confirmed the molecular mechanism proposed for the HCR and in particular HCR results particularly promising for multiplexed detections on array systems.

The preliminary results obtained with the capacitive sensor also indicate the possibility of applying HCR to parallelized, automated and point-of-care biosensors.

The signal enhancing after HCR is substantially low (with amplification factor of 5-7) which looks far from what could be sufficient for biosensing applications. For instance the signal enhancing is much lower than the amplification ratio obtained in experiments performed on magnetic beads with HCR hairpin labeled with fluorophores^[60] (up to 20-fold). This discrepancy could be due to possible limitations in the electron exchange of Hoechst 33258 with the surface, especially regarding Hoechst 33258 molecules that are at a certain distance from the surface.

The detection limit of 100 pM obtained with HCR is higher than other signal amplification strategies for electrochemical DNA sensors (usually in the order of magnitude of 10^{-12} M or lower). For example a strategy similar to HCR, described recently by Zheng and coworkers^[80] and based on a surface-initiated assembly chain reaction for amplifying the hybridization signal in an electrochemical DNA biosensor shows a limit of detection of 4.9 pM.

In conclusion, some optimization steps are surely required in order to improve the overall yield. As mentioned before, it is possible that the electroactive molecules that have interacted with the ds-DNA but are too far from the surface are not recognized, resulting in the low amplification ratio. A possible variation is suggested by Shimron and colleagues: they used two hairpin structures that include three-fourths and one-fourth of a G-quadruplex. In the presence of the analyte DNA one of the hairpins is opened and this triggers the chain reaction between the hairpins, with the formation of several G-quadruplex. Hemin/G-quadruplex complex has catalytic properties; for example, it can convert a substrate into an electroactive product free to diffuse in solution, and thus probably easier to detect, allowing to improve the sensitivity of this strategy.

Section II:
preparation and characterization of
tethered bilayer lipid membrane

Tethered bilayer lipid membranes

3.1 Introduction

Biological lipid membranes define the boundaries of cells and provide a platform for important biological processes. The main function of biomembranes is to form a highly selective barrier between the inside and the outside of living cells or between particular cell compartments and the rest of the cell. They are highly insulating to inorganic ions, so large electrochemical potentials can be maintained across them.

The permeability and other structural properties of biological membranes depend on the chemical nature of the membrane components and are sensitive to events that occur at the interface or within the bilayer. For example, biomembranes provide the environmental matrix for proteins which specifically transport certain ions and other molecules, for receptor proteins and for signal transduction molecules.

Due to the structural and functional complexity of cell membranes, it is clear that any alterations in the integrity and functionality of the membrane can determine negative effects at the cellular level and, in some cases, also for the whole organism. For example, the interactions between oligomeric forms of amyloidogenic proteins and cell membranes appear to be correlated with numerous neurodegenerative diseases^[83]. Moreover, cell membranes constitute a target for many bacterial toxins; in fact, many pathogens produce soluble proteins that interact with cell membrane either to permeabilize the cells or to enter into the cytosol to express their enzymatic activity^[84]. In addition, increasing evidence indicates the cell membrane as a common target for many pollutants widely used in industry^[85] and for many drugs^[86].

For the above mentioned reasons, it is important to detect interactions that involve the cell membrane, but the complexity of biological membranes makes direct investigations difficult. It would also be advantageous to detect these interactions with a fast, parallelizable and automated approach, and that is not necessarily bound to operate within a laboratory.

For this reason, in recent years several model membranes were developed, whose main characteristic is to mimic, at least structurally, the cellular membranes. Consequently, model membranes are much simpler, without many of the components that might interfere with the experimental results and their interpretation.

In the following paragraphs the main types of model membranes and their applications will be described.

3.1.1 Lipid membrane models

Black membranes

The first successfully employed model membrane was simply called “black lipid membrane” (BLM). It consists of a lipid bilayer that occludes a small hole, about 1 mm in diameter, in a teflon septum which separates two aqueous solutions. The bilayer is formed spontaneously by placing a drop of lipids in a suitable solvent, e.g. decane, on the hole. With BLMs researchers can recreate physiological condition, in which both sides of the membrane are in contact with an aqueous solution, so they provide a friendly environment to integral proteins. Moreover BLMs resulted very useful for electrochemical measurements and to evaluate the lateral mobility of the lipid molecules in the membrane^[87].

At the same time there are several drawbacks. In fact the hydrocarbon tail region could incorporate an appreciable amount of the solvent molecules. Other important drawbacks are their fragility and their high sensitivity toward vibrations and mechanical shocks. Moreover, they show a low resistance to electric fields, so they hardly last more than 8 hours and collapse for transmembrane potential differences greater than 100–150 mV between the solutions that bathe the two sides of the BLM.

Finally, BLMs do not allow investigations with surface-sensitive techniques, such as AFM and SPR^[88].

Lipid vesicles

The simplest model membranes are represented by liposomes. They are lipid vesicles composed of phospholipids that, in an aqueous environment, organized themselves in spherical structures.

Usually liposomes can be classified according to the number of lipid bilayers that they possess: in fact they can be divided as unilamellar or multilamellar. Multilamellar vesicles are characterized by multiple double layers, while unilamellar vesicles have a single double layer, and for this reason they are the most use vesicles.

Moreover, according to their dimensions they can be classified in three categories: vesicles with a diameter higher than 1 μm are called giant unilamellar vesicles (GUV), the ones with diameters between 0.2 e 1 μm are defined large unilamellar vesicles (LUV), and finally vesicles with diameters lower than 0.2 μm are called small unilamellar vesicles (SUV)^[89].

Lipid vesicles have been very useful for studies about thermodynamic stability and for general characterization of the lipid membranes. As model membrane they were used in leakage experiments to study the permeabilization of the lipid bilayer induced by different kinds of molecules, such as amyloid proteins^[83].

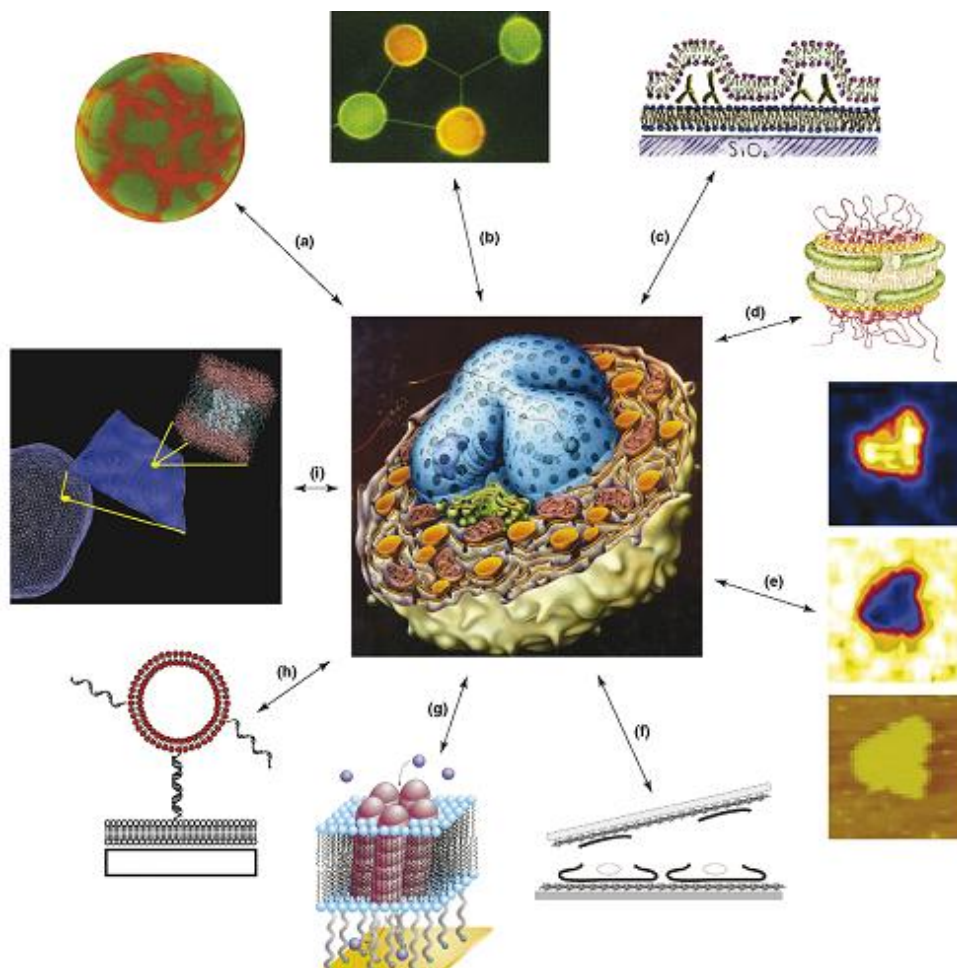


Figure 3.1: The cell membrane, in the centre, and its model systems. In particular: (a) giant unilamellar vesicles; (b) networks of giant vesicles connected by lipid microtubules; (c) ruptured GUV's on solid supported bilayers; (d) membrane nanodiscs containing transmembrane proteins; (e) supported lipid bilayers analyzed by NanoSIMS; (f) ruptured cell membranes on solid supports; (g) bilayers tethered to a solid support containing ion channels; (h) vesicles tethered to a supported lipid bilayer by DNA; (i) visual representation of multi-scale simulations. Figure reproduced from [87].

Supported bilayer lipid membranes

To overcome the drawbacks of conventional BLMs and lipid vesicles, supported bilayer lipid membranes (sBLMs) have been developed. Usually they are obtained by self-organization, which can be driven exclusively by non-covalent, hydrophobic interactions or with the additional contribution of covalent linkages.

sBLMs can be used to investigate the behavior of the polar heads in the film-forming lipids with varying pH, and the behavior of small lipophilic biomolecules incorporated in the lipid film or about peripheral redox proteins adsorbed on the film surface^[88].

However, they are not suitable to study the function of integral proteins. Quite often, these proteins have hydrophilic sections protruding by over 60 Å outside the lipid bilayer. To avoid their denaturation, the incorporation of integral proteins into biomembrane models must therefore

ensure that their protruding hydrophilic sections are accommodated in a hydrophilic medium on both sides of the lipid bilayer.

To overcome this issue several kinds of model membranes, characterized by the presence of a physical separation between the solid support and the surface, were developed.

One of the first solutions involves polymeric cushions as supports on which rest the lipid bilayer, separating it from the surface^[90]. These supports can be of different types, for example can be constituted by gel rich in water or they can be “spacer” molecules that bind covalently the membrane and the solid support separating themselves. This kind of structure has been proposed by Kiessling and Tamm and consists of a polymeric molecule called polyethylene glycol (PEG), which with one end binds the solid surface, while the other one binds with the distant lipid membrane^[91].

This structures were developed in order to combine the advantages of black lipid membrane with the stability and the mechanical strength of membranes directly supported on the surface. So the applicability of different characterization strategy was guaranteed, as well as the possibility of incorporating proteins. Model membranes supported on polymeric structures have, however, low impedance values, and this characteristic limits their application for biosensing purposes.

Tethered bilayer lipid membrane

To overcome this problem another kind of model system known as tethered lipid bilayer membrane (tBLM) has been developed. This kind of model membranes are characterized by a hydrated space between the surface and the lipid membrane, in order to create an environment more similar to the physiological conditions^[92].

The membrane can be physically separated from the surface using a particular kind of molecules, known as tethering molecules, which with one end can anchor themselves to the surface, while with the opposite end they inserted themselves within the lipid bilayer^[93].

An advantage of these model membranes is that they can contain integral membrane proteins, thanks to the submembrane space between the lipid bilayer and the surface. At the same time, the anchoring to the solid surface makes them particularly resistant and stable and therefore it is possible to apply on them numerous surface-sensitive techniques, such as SPR, AFM, etc..

3.1.2 tBLM preparation

tBLMs are usually prepared with a 2-step procedure: in the first step a SAM of tethering molecules is formed, while in the second step the tBLM is completed by the addition of lipids on the surface.

Other authors have suggested another approach, in which they use lipid vesicles formed by phospholipids and tethering molecules; in this way the binding of tethering molecules to the surface and the formation of the lipid bilayer occur in a single step^[94]. Obviously the main

drawback of this approach is related to the fact that in the resulting tBLM the outer leaflet exhibit tethering molecules that can interfere with following measures on these membranes.

Tethering molecules

Usually the tethering molecules consist in synthetic lipids that show a common design:

[chemical linker to surface]–[hydrophilic polymer tether]–[lipid backbone]–[lipid tails]

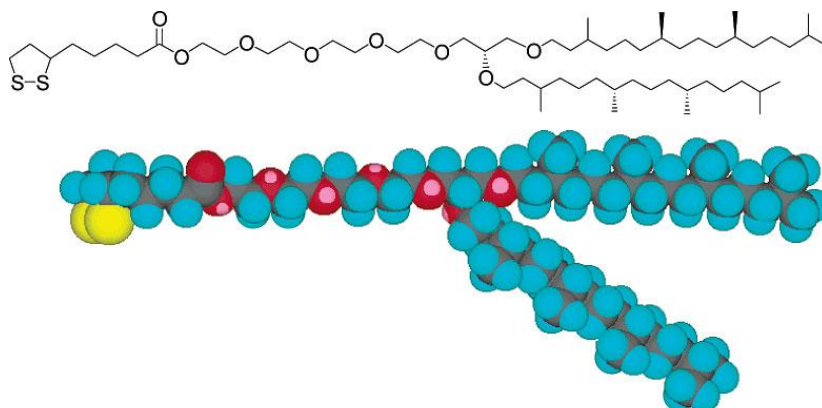


Figure 3.2: Representation of the formula (above) and the space-filling model (below) of the 2,3-di-O-phytanyl-*sn*-glycerol-1-tetraethylene glycol-DL- α -lipoic acid ester (DPTL). Picture reproduced from [93].

For gold surface the best chemical linker is the thiol group, that allows the formation of reproducible and stable SAMs.

Often the hydrophilic polymer tether used in the synthetic lipids is an oligo ethylene oxide (OEO) segment. It provides a physical separation of the lipid bilayer from the surface and allows the formation of an aqueous reservoir between the lipid bilayer and the surface. The reservoir has two advantages:

- ♦ as said before, the inner surface of the membrane is maintained in a hydrated biological state, very similar to the condition in the cytosolic environment.
- ♦ it provides a space that allows the insertion of transmembrane proteins into the lipid bilayer.

Anchor lipids with different spacer and anchor groups have been synthesized, and the resulting membrane structures have been investigated using several techniques^[95].

One particular kind of tethering molecules is represented by DPTL, formed by lipoic acid for the binding with the surface, a tetraethylene glycol spacer and 2,3-di-O-phytanyl-*sn*-glycerol as lipid tails. The phytanyl chains in DPTL are known for their high thermodynamic stability (liquid crystallinity ranging from -80°C to 120°C)^[96], their low phase-transition temperature and their influence on the density and stability of biological membrane^[97]. DPTL contains two hydrophobic chains, because it's known that a single hydrophobic chain does not guarantee a stable insertion of tethering molecules into the lipid membrane^[97]. A very low roughness of the gold surface is

required to obtain the perfect supramolecular alignment of the functional units, with a perfect arrangements of the monolayer^[97].

In the following pages will be treated the main protocols regarding the formation of tBLMs that use DPTL as tethering molecules, since it is the molecule used in the experiments described in the experimental section.

DPTL monolayer formation

DPTL monolayer formation seems to follow a first-order kinetics (described well by Langmuir isotherm, based on physisorption where molecules can adsorb and desorb reversibly).

Typically this is done in ethanol, since the DPTL is practically insoluble in water. Vockenroth proposed a simple 2-step process to describe the formation of DPTL monolayers:

- ♦ fast adsorption of the molecules to the surface;
- ♦ slow organization and rearrangements of the monolayer (they suggested that probably forces between adsorbed and free molecules hinder the completion of defect in the layer).

However, tBLMs formed on these DPTL monolayers are effective only for the incorporation of small ion carriers; larger peptides typically adsorb to the surface of these tBLMs if solid surfaces are used as support. In fact a particular case is represented by tBLMs formed on mercury surfaces^[98]: in this case the fluidity of the surface compensates for the high density of DPTL molecules in the submembrane layer. So, working on solid surfaces, the tethering molecules in the SAM must be spatially diluted to allow the incorporation of larger peptides into a bilayer^[99].

Diluted DPTL monolayer formation

Some authors reported difficulties to dilute monolayers of thiolipids with short hydrophilic thiols (such as β ME or lipoic acid), resulted in bilayers with poor electrically properties^[99]. However, there are several other articles describing procedures that allow the preparation of mixed SAM where the thiolated lipids were diluted using β ME^[100-102]. Generally the mixed SAMs were prepared by exposing gold surfaces to solution of thiolated lipids and β ME using different molar ratio, with a final concentration of 0.2 mM. The incubation usually last from 12 to 24 hours.

Hong and colleagues used a different approach to dilute the thiolated lipid layer for SPR experiments: first they form a β ME layer not particularly dense, and then they add the thiolated lipids in water with a detergent to complete the mixed SAM^[103].

He^[99] used a particular molecule called tetraethylene glycol-D,L-R-lipoic acid ester (TEGL) to dilute DPTL monolayer. This molecule is identical to the hydrophilic portion of DPTL, while the hydrophobic portion is absent; so specifically TEGL allows the dilution only of the hydrophobic region of DPTL. With AFM He and colleagues observed a uniform distribution of these two molecules on the surface.

3.1.3 Bilayer formation

There are different procedures that allow the formation of lipid bilayers on pure or diluted DPTL layers. However, the choice of the lipid to be used for preparing the lipid bilayer must be performed. In fact, according to the type of the polar head of the selected lipid or the type of lipid tails, the resulting lipid membrane will have particular physical and chemical characteristics, with important consequences in allowing interactions with different kinds of molecules^[100].

Vesicles fusion method

Darvel and colleagues^[96] suggest the following deposition pathway for tBLM formation: first vesicles diffuse through the solution and then eventually they contact the preformed DPTL monolayer. When the critical coverage point is reached, the vesicles on DPTL monolayer rupture into bilayer islands, where they fuse on the DPTL layer; after the initial rupture point, vesicles continue to adsorb to the DPTL layer and fuse to form a tBLM.

Actually the formation of a lipid bilayer from vesicles in aqueous solution depends on the chemical and physical parameters used during the process, such as the pH and the ionic strength of the solution, the concentration of vesicles and their composition and the temperature at which the formation of the lipid bilayer was performed^[104].

Lei et al.^[105] prepared tethered or supported bilayers using a unilamellar vesicle suspension (0.3 mM) onto the substrate and incubating at 60°C for 2 hours; afterwards the sample was cooled to room temperature at ambient conditions and then rinsed with mQ water at least 20 times. Vockenroth and colleagues^[92] prepared lipid bilayers on DPTL by addition of SUV on DPTL layer (0.02 mg/mL final concentration in NaCl 0.1 M) for 24 hours. Naumann^[93] and Schiller^[97] carried out the vesicles fusion at 30°C (0.02 mg/mL final concentration in NaCl 0.1 M), but they didn't report how long is the incubation.

There are three different procedures to prepare vesicles in aqueous solution:

- ♦ the most common involves the extrusion of the lipid dispersion through nucleopore filters (usually 100-200 nm size) to obtain large or small unilamellar vesicles^[92, 93, 96, 106, 107];
- ♦ an alternative procedure involves the sonication of an aqueous lipid suspension for several minutes (about 15-30 minutes), in order to obtain small unilamellar vesicles with diameters that ranges from 30 nm to 100 nm. The most common instrumentation for the preparation of sonicated particles are bath and probe tip sonicators. Bath sonicators are the most widely used instrumentation for preparation of SUV. Mean size and distribution is influenced by composition and concentration, temperature, sonication time and power, volume, and sonicator tuning. Since it is nearly impossible to reproduce the conditions of sonication, size variation between batches produced at different times and with different instruments is not uncommon. Terrettaz and colleagues^[108] perform the sonication at 10°C in an eppendorf vial to obtain SUVs with a mean diameter of 30 nm. A similar protocol was described by other authors^[105, 109, 110];
- ♦ another procedure was described by Wiegang et al.^[111]: after the preparation of lipid solution, they performed 5 cycles of freezing (with liquid nitrogen) and thawing (water bath at

50°C. Immediately before the injection into the measuring cell, the vesicle suspension was sonicated for 10 min.

He and colleagues suggest to use liposomes prepared in water to take advantage of the osmotic shock caused by the relatively high ionic strength electrolyte used during the vesicles fusion. Vockenroth et al.^[92] and He et al.^[99] also suggest that the lipid composition of the vesicles should have an effect on the assembly kinetics.

Some authors add in the lipid vesicles also cholesterol; in fact it is known that cholesterol can influence the function of membrane proteins both by binding directly to the proteins and by changing biophysical properties of the lipid membrane^[99].

Protocol involving detergent

In this procedure an aqueous solution of lipids in detergent (for instance octyl glucoside) is prepared, then the next dilution of the detergent below the critical micellar concentration leads to the formation of a stable lipid layer on the hydrophobic alkanethiol surface. The solution containing lipids and detergent is placed in the cell, and after 5 min, 30% of the total aqueous phase was exchanged with pure buffer and the cell content were mixed. This procedure was repeated until no further change of the optical and electrical properties of the self-assembled lipid layer was observed^[108, 112].

Rapid solvent exchange:

According to McGillivray and colleagues^[101], rapid solvent exchange technique has three advantages:

- ♦ the bilayer formation completed more reproducibly;
- ♦ it allows the formation of bilayers on SAMs of relatively low hydrophobicity (as in the case when a significant proportion of the hydrophilic backfiller β ME is used);
- ♦ the bilayer phase state of the lipid used for completion was found to be largely irrelevant, because the lipid is applied to the surface in organic solution.

The usual procedure involves a brief incubation of the SAM-covered surface in a solution of lipid in absolute ethanol (10-20 mM) for 5-10 min at room temperature (actually Yaron^[113] extends the lipid incubation for 1 hour). Then it was rapidly (within 5-7 sec) displaced by a large excess of aqueous buffer solution, taking care to avoid the formation of air bubbles at the surface that could disturb the SAM^[100-102, 114, 115].

According to them the lipid molecules, that are insoluble in water, during the exchange step complete the bilayer rather than to mix with water and get washed away.

3.2 Materials and methods

SAM preparation

For the realization of SAM formed by DPTL (Diverchim), each gold surface (TSG) was incubated with 30 μ L of thiolipid solution with a concentration of 1 mg/mL. The incubation took place in an ethanol-saturated chamber, at a temperature of 4°C. The DPTL is stored at -20°C in ethanol and, before being used, was sonicated for 10 minutes.

Mixed SAM were carried out by incubating each TSG with 30 μ L of a mixture of DPTL and β ME (Sigma) to a final concentration of 1 μ M in ethanol for 18-19 hours at a temperature of 4°C. Several mixed SAMs were obtained using different molar ratios of the two components of the mixture.

Each TSG during the incubation has been covered with a HybriSlip (Sigma) so that the solution was uniformly distributed on the surface. After the incubation the samples were washed with a slow addition of 1 mL of ethanol, dried with nitrogen and placed very quickly inside the electrochemical cell.

Vesicles preparation

Lipid vesicles were obtained from 1,2-Dioleoyl-sn-glycero-3-phosphocholine (DOPC) or 1-palmitoyl-2-oleoyl-sn-glycero-3-phosphocholine (POPC) from Sigma at a concentration of 1 mg/mL. First, 2 mg of lipids were dissolved in chloroform, then the solvent was evaporated. The pellet obtained in this process was hydrated by the addition of 2 mL of buffer (10 mM HEPES and 50 mM CaCl₂, pH 7.2), thus obtaining multilamellar lipid vesicles. To obtain unilamellar vesicles the solution was sonicated in an ultrasonic bath for about 20-30 minutes, until a clear solution was obtained.

Bilayer formation

Lipid membranes anchored to the surface were carried out incubating a solution of unilamellar lipid vesicles (1 mg/mL) in an aqueous buffer (10 mM HEPES and 50 mM CaCl₂, pH 7.2) on functionalized gold surfaces with DPTL or DPTL + β ME for at least 4 -5 hours at room temperature.

Electrochemical impedance spectroscopy

Electrochemical impedance spectroscopy measurements were performed with μ Autolab Type III/FRA2. The data analysis was performed using the software FRA (Frequency Response Analyzer System), provided by the manufacturer of the instrument, and Zview (Scribner

Associated Inc.). All the impedance experiments were performed in the three-electrode cell described at pag. 27.

EIS measurements were conducted in the frequencies ranges 1 MHz-5 mHz or 1 MHz-1 Hz with an excitation amplitude of 10 mV and a bias potential of 0 V vs. Ag/AgCl reference electrode.

Reductive stripping assay

The experiments of reductive stripping were performed with μ Autolab Type III/FRA2. The data analysis was performed using the software GPES (General Purpose Electrochemical System), provided by the manufacturer of the instrument. All the reductive stripping assays were performed in the three-electrode cell described at pag. 27.

The potential range applied is between -0.7 V and -1.4 V, with a scan rate 0.1 V/sec, in 0.1 NaOH.

AFM

All the images were obtained by Multimode AFM facility (Nanoscope III, Veeco/Digital Instruments, Santa Barbara, CA) with scanner 2795E in a contact mode. Slandered etched silicon cantilevers (Ultra sharp NSC15/AIBS silicon probes with tip apex radius of \sim 10 nm, resonant frequency range of AFM cantilever 325 Hz, and number of pixels 512 \times 512) were used for imaging in liquid. All the images were taken at room temperature (\sim 25 $^{\circ}$ C).

Surface plasmon resonance

The SPR instrument used for the experiments is a Biacore X100 by GE Healthcare. It consists of two microfluidic cells; one of the two is usually used as a reference cell in order to subtract the bulk effect. Each flow cell is 0.5 mm wide, 2.1 mm long and 50 μ m tall. The total contact area is 1.05 mm². In all the experiments a sensor chip with a gold surface (Sensor chip Au or SIA kit Au, from GE Healthcare) was employed. For data analyses, the Evaluation Software available with the Biacore X100 was used.

Injections consist of a two phases: an association phase in which a solution of the determined molecule is injected; and a dissociation phase, or stabilization period, in which the running buffer (in this case PBS 0.1 M KCl) flows inside the flow cell. The maximum single-injection volume in the Biacore X100 is 90 μ l. Ten successive injections of DPTL 0.4 mg/ml in an aqueous 1% poly-(ethylene glycol)-octyl ether (octyl-POE) solution were performed for 200 seconds at 2 μ l/min over the gold surface of the chip. With a final injection of SDS 0.5% we removed any molecules non-specifically bound to the surface.

After the formation of the monolayer, an injection of SUVs would form a complete lipid bilayer. DOPC 1 mg/ml in PBS 0.1 M KCl was injected for 40 min at 2 μ l/min followed by a dissociation phase of 600 seconds. Then 10 consecutive 1 min-injections of ultrapure water at 10 μ l/min with a stabilization period of 480 seconds for each injection and a fast injection of PBS 0.1 M KCl

(30 seconds at 100 $\mu\text{l}/\text{min}$). Also in this experiment with a final injection of SDS 0.5% we removed any molecules non-specifically bound to the surface.

3.3 Results and discussions

3.3.1 EIS data analysis

Impedance spectra

Data from impedance measurements can be expressed using different kinds of plots. The impedance (Z) and the admittance (Y) are usually described by complex numbers, whose real and imaginary parts represent their components for a phase delay of 0° and 90° , respectively. The impedance data obtained in our experiments were displayed using two different representations, the Bode plot and the complex admittance plot.

Bode-Plot: Bode plot is a very common representation for impedance data, and contains two different information: a graph of the absolute magnitude of impedance is plotted against the logarithm of frequency, whereas a graph of phase angle versus the logarithm of frequency gives a Bode phase plot (figure 3.3a).

Complex Admittance (frequency normalized): the advantage to analyze AC circuit in terms of the admittance (Y), which is the inverse impedance ($Y=1/Z$), is that admittance represents a kind of conductance (figure 3.3b).

The complex admittance and impedance hold the relation:

$$Y = \frac{1}{Z} = Y' + jY'' = G + G_a + j\omega C$$

where G is the conductance and G_a is the conductance of electrolyte. The real part and the imaginary part of the admittance can be obtained from:

$$Y' = \frac{Z'}{(Z')^2 + (Z'')^2}$$
$$Y'' = \frac{-Z''}{(Z')^2 + (Z'')^2}$$

Variation of the AC frequency, $\omega(f)$, results in different figure in complex plane corresponding to changes in the ratio between real and imaginary components of the admittance. In this representation the diameter of the semicircle on the Y axis corresponds to the capacitance of the layer on the surface (figure 3.3b).

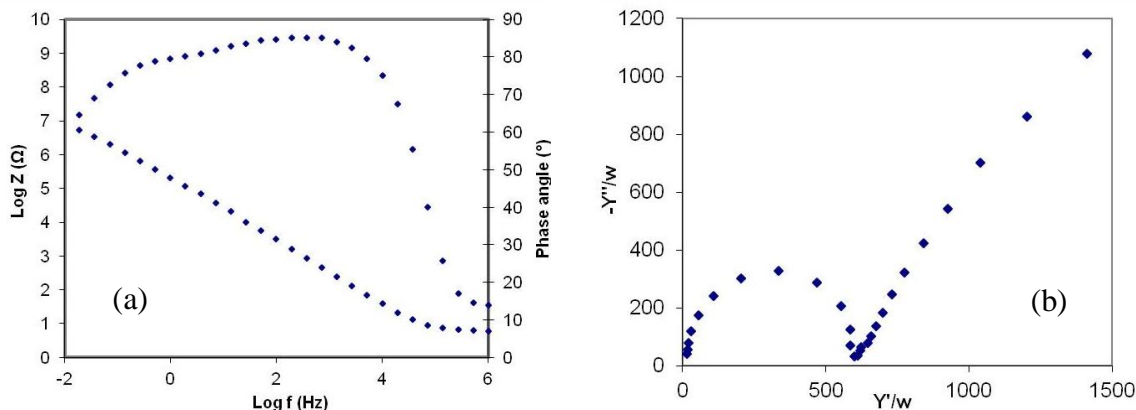


Figure 3.3: (a) Bode plot; (b) complex admittance plot.

Equivalent circuit

A simple equivalent circuit commonly employed to interpret impedance spectra of tethered lipid bilayers is shown in figure 3.4, where R_{Ω} is the resistance of the aqueous electrolyte, R_m and C_m are the resistance and the capacitance of the lipid bilayer respectively, and C_s is the capacitance of the hydrophilic spacer. For simplicity, this equivalent circuit can be expressed with the following nomenclature: $R_{\Omega}(R_m C_m)C_s$ that will be used in the following sections.

Figure 3.5 shows a plot of $\log |Z|$ versus $\log f$ (Bode plot), where $|Z|$ is the magnitude of the impedance and f is the frequency.

It is known that the impedance of circuit elements in series is determined by the element with the highest impedance; conversely, the impedance of circuit elements in parallel is determined by the element with the lowest impedance.

Therefore, at the highest frequencies, $|Z|$ is determined by the resistance R_{Ω} , because the impedance of the C_s element $[1/(2\pi f C_s)]$, is lower than R_{Ω} , and the same is true for the impedance of the $R_m C_m$ mesh, which is determined by the lowest impedance of these two elements in parallel.

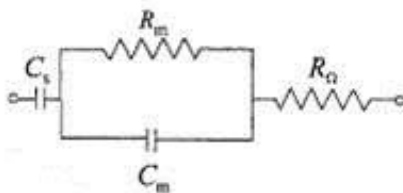


Figure 3.4: equivalent circuit. Figure modified from [90].

R_{Ω} is independent of frequency, therefore the slope of the Bode plot becomes equal to zero (portion a in figure 3.4).

Decreasing the frequency, C_m becomes greater than R_{Ω} , while still remaining lower than R_m , and it is also higher than C_s , because $C_s > C_m$. Hence, in this frequency range, $|Z|$ coincides with C_m ,

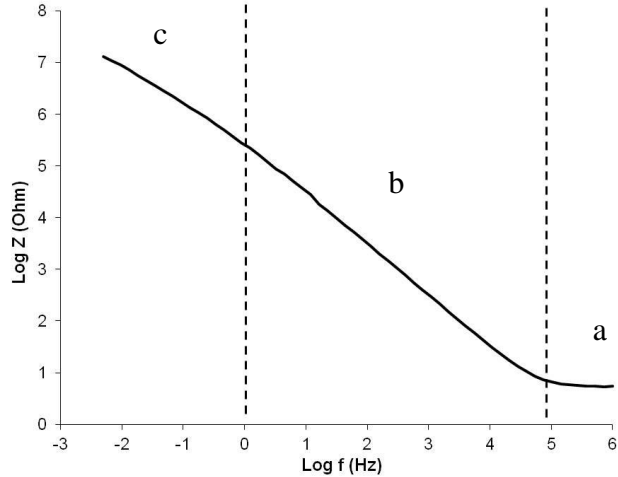


Figure 3.5: a plot of $\log |Z|$ versus $\log f$.

and the $\log |Z|$ versus $\log f$ plot has a slope equal to -1 (portion b in figure 3.5).

With a further decrease in frequency, C_m becomes comparable with R_m , and the slope of the Bode plot increases with respect to -1 , tending to attain the zero value, which would correspond to complete control by R_m . Before this can occur, however, the further decrease in frequency makes C_s higher than R_m , causing $|Z|$ to coincide with C_s . Hence, the slope of the Bode plot once again becomes equal to -1 (portion c in figure 3.5).

If a ion channel is assembled in the lipid bilayer, ions from the aqueous phase are shuttled to the hydrophilic spacer and vice versa across the lipid bilayer, with a resulting decrease in the resistance R_m . In this case, C_m becomes comparable with R_m at higher frequencies, as appears from figure 3.6. This means that in this example R_m starts to bypass the capacitance C_m for $f=100$ Hz, so the current starts to flow preferentially along the resistance R_m . Then, for $f=10$ Hz, $|Z|$ practically coincides with C_s and the Bode plot has the same sigmoidal shape as in figure 3.6.

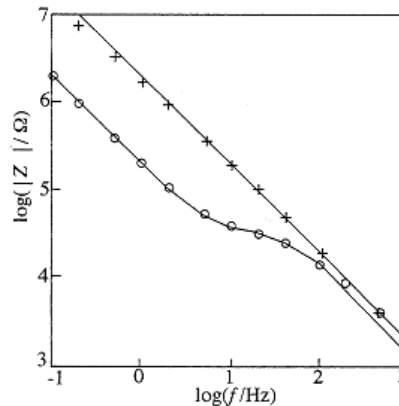


Figure 3.6: Bode plots of a tethered lipid bilayer with (o) and without (+) pore-forming peptide. Figure reproduced from [90].

3.3.2 Formation and characterization of DPTL layers

Electrochemical impedance spectroscopy

Self-assembled DPTL layers can be easily obtained incubating a small amount of DPTL in ethanol at a concentration of 1 mg/mL on a gold surface. The incubation is performed for about 24 hours in an ethanol saturated chamber at 4° C. After the incubation the functionalized surface is washed with a large amount of ethanol and dried with a stream of nitrogen. This procedure allows the formation of a single compact layer of DPTL with the molecules bound to the surface through the disolphur groups and the lipid tails pointing to the solution.

These layers were characterized with electrochemical impedance spectroscopic measures. The resulting spectra were fitted with the equivalent circuit reported in figure 3.4, as suggested from Naumann^[93] and Schiller^[97]. Actually to describe the capacitance C_m in this case is better to use a constant phase element (CPE or Q) rather than an ideal capacitance.

CPE is an electrical circuit component that models the behavior of an imperfect capacitor.

CPE admittance is: $Y_{CPE} = Q_0(\omega i)^n$, where Q_0 and n ($0 < n < 1$) are frequency independent. The constant phase is always $-(90 \cdot n)^\circ$, also with n from 0 to 1. The case $n = 1$ describes an ideal capacitor while the case $n = 0$ describes a pure resistor.

CPE is useful because it takes in greater account the heterogeneity of the layer due to the particular DPTL structure and the roughness of the gold surface. Because of this, in fact, the layer present on the surface deviates substantially from an ideal capacitor. However, as can be seen from the table 3.1, the n values of CPE for DPTL layers are very close to 1, and then the values of

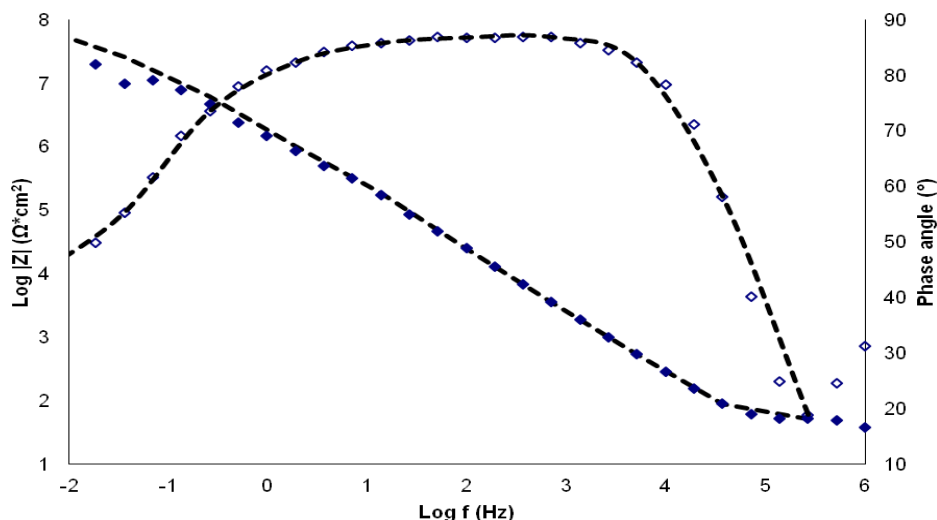


Figure 3.7: impedance spectrum relative to a DPTL layer on gold surface obtained by an incubation of 24 hours in DPTL 1mg/mL in ethanol. The impedance spectrum was obtained in 100 mM NaCl and 10 mM phosphate buffer, pH 7, by applying sinusoidal potential of 10 mV, with a range of frequencies from 1 MHz to 5 MHz, and a bias potential of 0 V. The red dashed lines correspond to the fitting of the data with the equivalent circuit $R_\Omega(R_m Q_m)C_s$.

CPE can be assimilated to an ideal capacitance.

In figure 3.7 is shown an impedance spectrum corresponding to a DPTL layer with the corresponding fitting; the quality of the fit is quite good indicating that the model used to describe what is present on the surface of the working electrode is correct.

In table 3.1, resistance values of DPTL layers generally change from 1 to 2 $M\Omega \cdot cm^2$ while the capacitance is generally between 0.6 and 1 $\mu F/cm^2$.

The capacitance values are in agreement with those reported in literature, which suggests that during the incubation step, a single DPTL layer has been formed on the surface and not a

	R_{Ω}	R_m	Q_m	α	C_s
	$\Omega \cdot cm^2$	$M\Omega \cdot cm^2$	$\mu F/cm^2$		$\mu F/cm^2$
1	5.73	1.23	1.1	0.94	1.63
2	6.78	1.49	0.83	0.95	2.83
3	6.86	1.23	0.93	0.92	3.673
4	4	1.39	1.056	0.93	3
5	7.4	1.65	1.144	0.94	2.7
Mean	6.15	1.40	1.01	0.94	2.77
St. dev.	1.35	0.18	0.13	0.01	0.74

Table 3.1: resistance and capacitance values of DPTL layers, obtained by fitting the spectra of impedance relative to 5 different DPTL layers with the equivalent $R_{\Omega}(R_m Q_m)C_s$.

multilayer; another indication that support this conclusion is that the values obtained are substantially in agreement with the capacitance value calculated taking into account the theoretical dimensions of a DPTL molecule, that is 4.7 nm^[93].

Instead the resistance values tend to be lower than those indicated in several articles, where values up to 4-5 $M\Omega \cdot cm^2$ are reported^[93]. A probable explanation could be that the gold surfaces used in these experiments had a roughness greater than those used in literature. Interactions between DPTL molecules involve the hydrophobic portions of the molecule: if the surface is not perfectly flat, these interactions will be more difficult to form and the monolayer will be not very compact. This aspect can greatly affect the resistance values.

Reductive stripping

A further evidence about the formation of a single layer of DPTL was obtained performing the reductive stripping of these molecules from the surface applying a reductive potential as suggested by Naumann and colleagues^[93].

Sulphur-gold bonds can be described as an oxidative additions of thiols on the gold surface, so it's possible to break these interactions applying a reductive potential.

The voltammetry experiment was performed in an electrochemical cell with a larger working area than the one used in the previous measurements, of about 50 mm². Even in this case a TSG was functionalized with DPTL, and before being inserted in the measuring cell, it was washed with

ethanol, and then it was dried with a gentle stream of nitrogen. The potential range used in the stripping assay is between -0.4 V and -1.4 V in NaOH 0.1 M at a scan rate of 100 mV/sec, and the appearance of a peak at a potential of about -1 V was observed.

The potential at which the reduction peak appears is the one expected for the DPTL^[93], and calculating the integral of the peak (figure 3.8), it's possible to estimate how many charges pass through the working electrode during the stripping experiment. Knowing that the reduction of a sulfur-gold bond involves a single electron, and that there are two sulfur-gold bonds for each DPTL molecule on the surface, we can estimate how many DPTL molecules are present on the surface. The value obtained from this calculation is equal to 2×10^{14} molecules/cm², in agreement with the value reported by Naumann and his collaborators^[94].

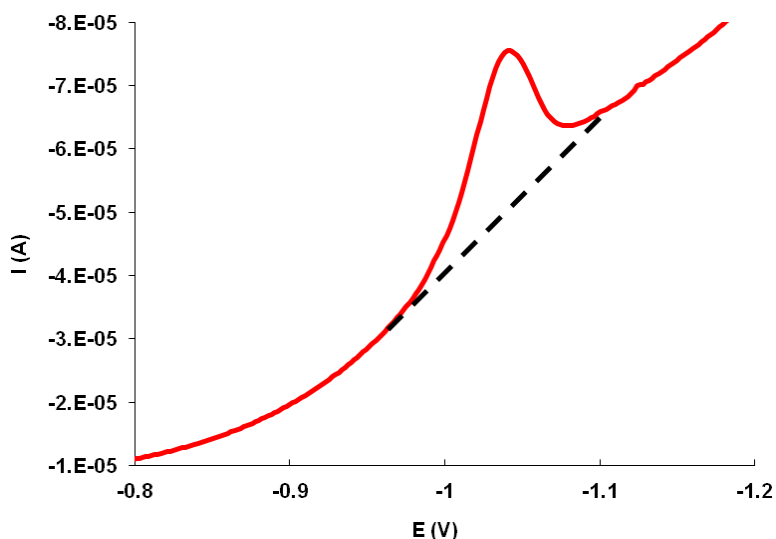


Figure 3.8: reductive stripping voltammetry of a DPTL layer on a gold electrode that was formed through a 24-hours incubation with DPTL 1mg/mL in ethanol. The assay was performed in NaOH 0.1 M, with a potential range from -0.4 V to -1.4 V and a scan rate of 100 mV/sec.

AFM imaging

Finally, DPTL monolayer was characterized performing AFM experiments. This technique allows to observe an high-resolution surface topography of a molecular monolayer.

In particular, a strategy called nanoshaving was performed (figure 3.9c), consisting in the removal of portions of monolayer from the surface, in order to estimate the thickness of the monolayer^[105].

Figure 3.9a shows an AFM image, in which the DPTL monolayer covers almost entirely the gold surface except for three rectangular areas where the DPTL has been removed.

Within these zones can be observe the gold surface below, that appears darker because it is located at a greater depth compared to the DPTL surface. These tests were carried out keeping the surface immersed in an aqueous buffer, and this could be the cause of the accumulation of DPTL at the edges of the holes, considering that DPTL is substantially insoluble in water.

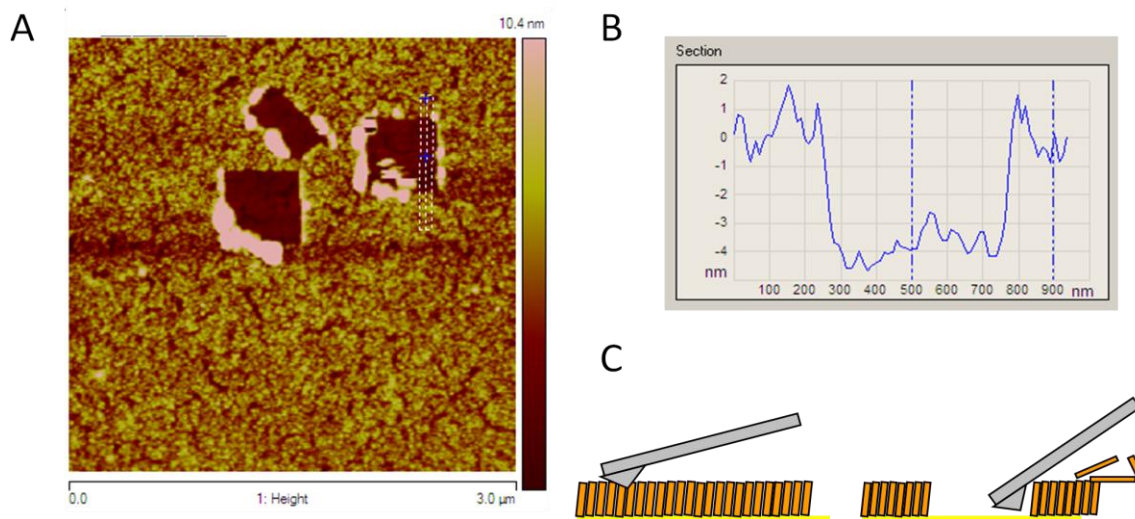


Figure 3.9: (a) AFM image relative to a nanoshaving assay on a DPTL layer; the three dark rectangles correspond to a removal of DPTL from the surface; (b) thickness variation measured at the two blue points indicated in the AFM image on the left; (c) Schematic of nanoshaving.

Figure 3.9b shows the variation of the thickness of the DPTL layer between the blue points indicated in figure 3.9a. The height of the DPTL layer corresponds to 4-5 nm, consistent with the theoretical length of a DPTL molecule (theoretical length of 4.7 nm^[94]).

Characterization with SPR

The protocol used for the preparation of tBLM in a microfluidic chamber was proposed by Terrettaz and colleagues^[116], and the process was monitored by SPR.

The formation of a monolayer of pure DPTL (figure 3.10) was performed to compare the density of molecules bound to the surface with the theoretical value of lipids which should cover the surface.

A first injection of an aqueous solution of SDS 0.5% cleans the gold surface from any impurities, which may be present on the chip (SIA kit Au, GE Healthcare).

Given the chemical resistance of the microfluidic system, it is impossible to use an ethanolic solution of DPTL, so a detergent, octyl-POE, was used. Octyl-POE form micelles containing the thiolipids; so in this condition DPTL is water-soluble and can be injected into the SPR instrument. With the final injection of SDS 0.5% any molecules non-specifically bound to the surface were removed.

RU responses are collected with the flow cells filled with PBS 0.1 M KCl, in order to remove the bulk effect.

During the first injection the signal increases very rapidly, from the level of the baseline up to 3900 RU, and after an initial peak, the signal stabilizes. With the following nine injections of DPTL the signal increases of about 100 RU each injection, although after a rinsing step with

SDS, it drops till 3800 RU; this indicates that the observed increase during the nine injections is due to hydrophobic interactions between non-polar tails of DPTL immobilized on the surface and the molecules of DPTL injected.

There is a correlation between the RU response and how much mass is bound to the surface: it is accepted by the majority of the groups who works with SPR that the best conversion factor is $1 \text{ RU} = 1 \text{ pg/mm}^2$ ^[117]. Using this conversion factor we calculated that, at the end of the experiment, on the surface there are 2.36×10^{14} DPTL molecules/cm².

Considering a flow cell area of 1.05 mm^2 , the theoretical density of lipids that should cover the whole surface was calculated: considering an area of 69 \AA^2 for a single phospholipid^[118], the flow cell should contain 1.52×10^{12} lipids (about 1.52×10^{14} molecules/cm²).

It is interesting to note that this value practically coincides with the one obtained performing the reductive stripping assay described previously (see pag. 60).

Data obtained from reductive stripping and SPR, together with the values of capacitance and resistance obtained by EIS, are consistent with the formation of a single layer of compact DPTL.

3.3.3 *tBLM formation on DPTL layer*

After the formation of DPTL layers on gold surfaces, several experiments to form lipid membranes anchored on the surface were performed^{[94][98]}.

Lipid membranes anchored to the surface obtained from compacted layers of DPTL have several drawbacks for biosensor applications: first of all the anchored lipid membrane shows a low fluidity, since the innermost layer of the membrane is composed almost entirely of lipid tails from

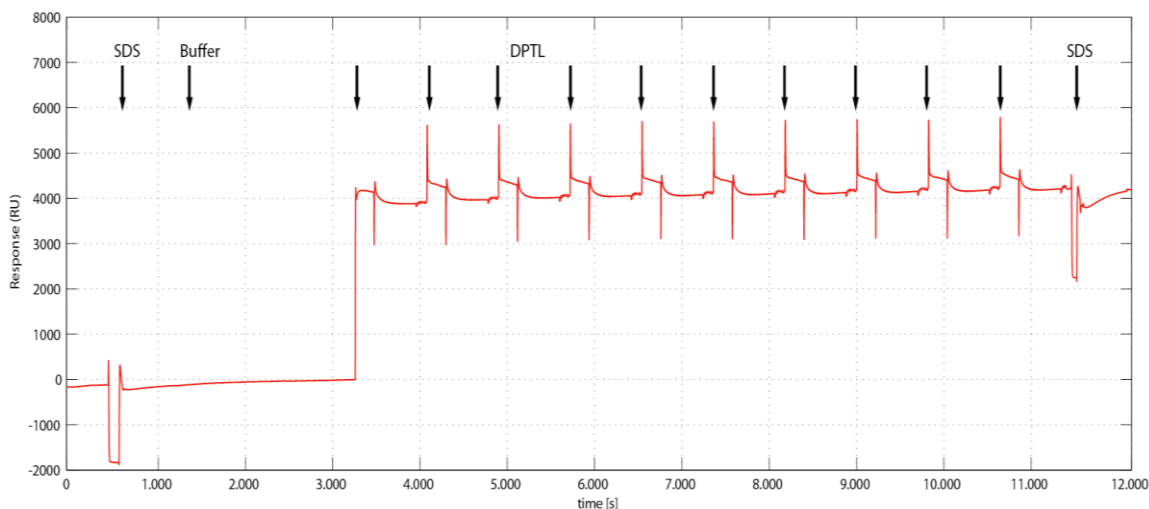


Figure 3.10: Sensorgram of the formation of a pure DPTL monolayer. The gold surface was initially cleaned with SDS 0.5%. A sequence of 10 injections of DPTL was performed in order to form a pure monolayer. The rinsing step with SDS 0.5% flows away the non-specific bound molecules from the flow cell. A final value of 3800 RU is obtained, corresponding to 2.25×10^{14} molecules/cm². Arrows indicate the injections performed during the experiment.

DPTL molecules, that are anchored to the surface. In addition the submembrane space will be very limited, as most of the space is occupied by the hydrophilic chains of DPTL.

The advantage of working on these types of membrane however is that, as mentioned previously, there are numerous examples in literature of lipid membranes anchored on this kind of surface, even if their use, for the disadvantages listed above, is in fact limited to the detection of interactions with small molecules. So, given the greater number of information that could be obtained from the literature about this kind of membrane model, the preparation of these layers was attempted.

Preparation and characterization of lipid vesicles

In literature, the most common approach to form lipid membranes on a DPTL layer involves unilamellar lipid vesicles.

In literature there are numerous protocols about the preparation of lipid vesicles, that differ about some parameters, such as the buffer used, the applied timing and the instrumentation used for the formation of vesicles.

The protocol used in the following experiments requires the preparation of a chloroform solution containing the lipid of interest. Then chloroform is evaporated under vacuum, and subsequently the pellet is hydrated by the addition of buffer (50 mM CaCl₂, 10 mM HEPES, pH 7.2) for about one hour; during this phase the solution is maintained stirred, allowing lipids to go in suspension as multilamellar lipid vesicles. Finally, to obtain unilamellar vesicles the solution was sonicated for about 20-30 minutes, until a clear solution is obtained.

Phosphatidylcholine lipids, especially 1-palmitoyl-2-oleoyl-sn-glycero-3-phosphocholine (POPC) or 1,2-dioleoyl-sn-glycero-3-phosphocholine (DOPC) were used (figure 3.11), as these types of lipid appears to be predominant in nature, and also because these two lipids have very low transition temperatures (for instance -2°C for POPC), so at room temperature they ensure high fluidity to the lipid membrane.

The solution of unilamellar vesicles was then analyzed with light scattering, to determine their size (figure 3.12). This analysis, carried out after about 30-40 minutes from the sonication step, shows the presence of three different populations of vesicles with different size. The majority of the vesicles have a diameter of about 100 nm, but at the same time vesicles of smaller diameter are observed, around 50 nm, and other vesicles much bigger, of several hundred nanometers. In several papers unilamellar vesicles sizes between 50 and 100 nm were reported; so the vesicles obtained performing the protocol described previously turn out to be larger than expected.

One possible explanation may be related to the choice of using the sonication to prepare vesicles; in fact sonication has the advantage of being simple and relatively quick to realize, but at the same time results can change using different sonicators.

Another aspect to take into consideration, especially as regards to the vesicles of big dimensions, is that light scattering measures were not carried out immediately but after several minutes, and during this period fusion processes between vesicles might have occurred. In fact, due to the high

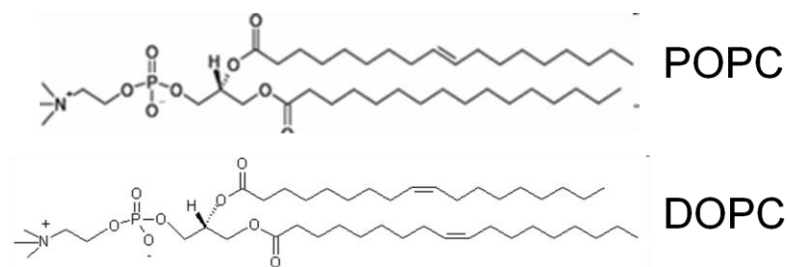


Figure 3.11: molecular structures of the two lipids used in the experiments described later.

degree of curvature of these membranes, SUV are inherently unstable and will spontaneously fuse to form larger vesicles, especially when stored below their phase transition temperature.

However, performing several readings of different samples prepared with the same protocol, the size of the vesicles resulted to be repeatable, so these vesicles were used to form tethered lipid bilayers on DPTL layers.

tBLM characterization with EIS

The protocol for the formation of tBLM is relatively simple. In fact, it requires the preparation of the solution containing vesicles and the formation of a DPTL monolayer on the working electrode surface. Then the solution containing vesicles was injected in the measuring cell, performing an incubation for at least 4-5 hours.

During the incubation period, lipid vesicles spontaneously interact with the DPTL layer, merging with each other, thus allowing the formation of a uniform lipid membrane over the entire surface.

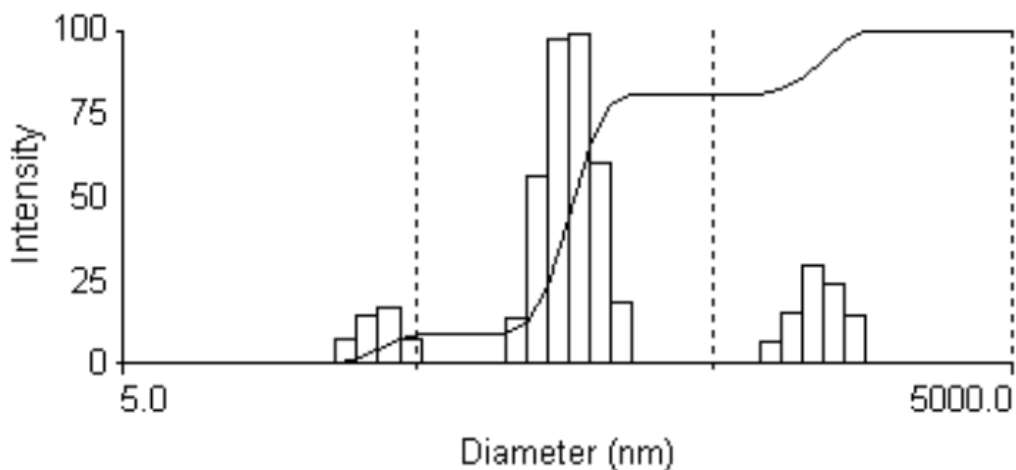


Figure 3.12: light scattering measure of a POPC vesicles solution. The graph shows the presence of a majority of vesicles with a diameter of about 100 nm, and two populations of vesicles less numerous, with a diameter of about 50 nm and the other of larger than 1 μm .

Figure 3.13 shows impedance spectra corresponding to a DPTL monolayer (blue lines) and to the resulting lipid bilayer (red lines) obtained after 4 hours of incubation in the solution containing vesicles. It is possible to observe how the impedance increases over the whole range of frequencies, and in particular at the lowest frequencies, which results in a slight decrease of capacitance and a significant increase in resistance (from 5 to 8 $M\Omega \cdot cm^2$, see figure 3.14).

Experiments with SDS to remove lipid bilayers

To be sure that the changes in capacitance and resistance are actually correlated with the formation of a lipid bilayer on the electrode surface, the removal of the membrane using sodium dodecylsulfate (SDS) was carried out.

SDS is a detergent which should be able to remove the lipids of tBLM, but which should leave intact the DPTL layer covalently bound to the surface.

After preparing the lipid bilayer on DPTL as described above, a brief washing was performed, fluxing in the measuring cell 300 μL of a solution of SDS 0.5% in H_2O at 100 $\mu L/min$. Immediately after, 300 μL of buffer (100 mM NaCl, 10 mM HEPES, pH 7.2) at 50 $\mu L/min$ was injected. Figure 3.16 show the variation obtained after the addition of SDS; as expected, the resistance and capacitance values measured after this treatment are comparable to those of the starting DPTL monolayer.

Then the lipid membrane was reconstructed directly on the surface obtained after SDS treatment, in order to understand if the previously experiments were influenced by side effects resulting from the addition of SDS. So a solution containing lipid vesicles was injected again and at the end of this treatment, another EIS measure was performed, confirming the formation of a new tBLM on the surface, as can be seen in figure 3.15 (blue spectrum).

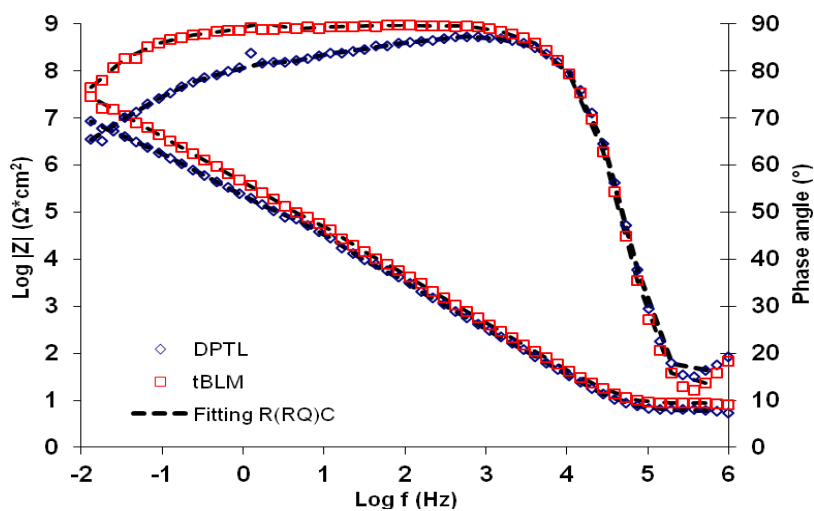


Figure 3.13: Bode plot of a DPTL layer (blue points) and of a tBLM (green triangles) formed using POPC vesicles. Red dashed lines correspond to the fitting of the tBLM spectrum with the equivalent circuit $R_{\Omega}(R_m Q_m)C_s$.

	R_{Ω}	R_m	Q_m	n	C_s
	Ω/cm^2	$\text{M}\Omega/\text{cm}^2$	nF/cm^2		$\mu\text{F}/\text{cm}^2$
1	8.377	10.28	855	0.98	0.588
2	5.9	6.29	711	0.97	3.04
3	7.7	8.1	634	0.95	4.5
4	7.05	9.76	688	0.97	1.78
Mean	7.26	8.61	722.00	0.97	2.48
d. s.	1.05	1.80	94.36	0.01	1.68

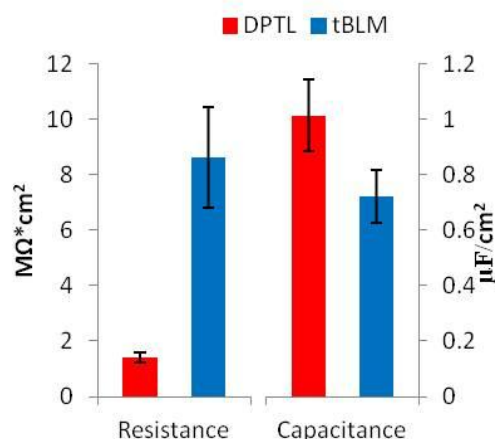


Figure 3.14: in this table were reported the values of R_{Ω} , R_m , Q_m , and C_s relative to 4 different tBLM, obtained fitting the experimental data with the equivalent circuit $R_{\Omega}(R_mQ_m)C_s$. On the right, the histogram shows the resistance and the capacitance variation after the formation of a tBLM.

It is easy to see how the spectrum obtained after the addition of the lipid vesicles, upon treatment with SDS, is practically superimposed to the one corresponding to the tBLM prior to treatment. Further tests with SDS showed that longer treatment with SDS or using higher concentrations of SDS, determine the dissolution of the lipid portion of the tBLM, but also an alteration of the DPTL layer (data not shown), suggested especially from the capacitance values, which result much higher than the capacitance of the starting DPTL layer. A possible explanation of this phenomenon may be that in these conditions SDS alter also the hydrophobic portion of the DPTL monolayer, changing its electrical parameters.

Formation and characterization of tBLM using SPR

In collaboration with the Laboratory of Life Science Electronics at EPFL in Lausanne, the formation of tBLMs on a compact layer of DPTL was checked using SPR.

As discussed before, DPTL layers were obtained in aqueous solution using a detergent. Then a solution containing POPC vesicles was prepared as described above, with a final concentration of 2 mg/mL.

In the experiments one of the two channels (channel 1) was used as a reference, while the other channel (channel 2) was used to perform the actual experiment. So in channel 2 the solution containing vesicles of POPC was fluxed for 2250 seconds, followed by a washing step in buffer (PBS 0.1 M KCl) for 120 seconds and finally by three washes with 0.5% SDS of 180 seconds each (in both channels); the passage in SDS take the system back to the initial conditions.

SUVs injections in the analysis chamber determine a steep peak in the RU response that might correspond to the interactions between vesicles and the hydrophobic tails of the DPTL molecules (see figure 3.16).

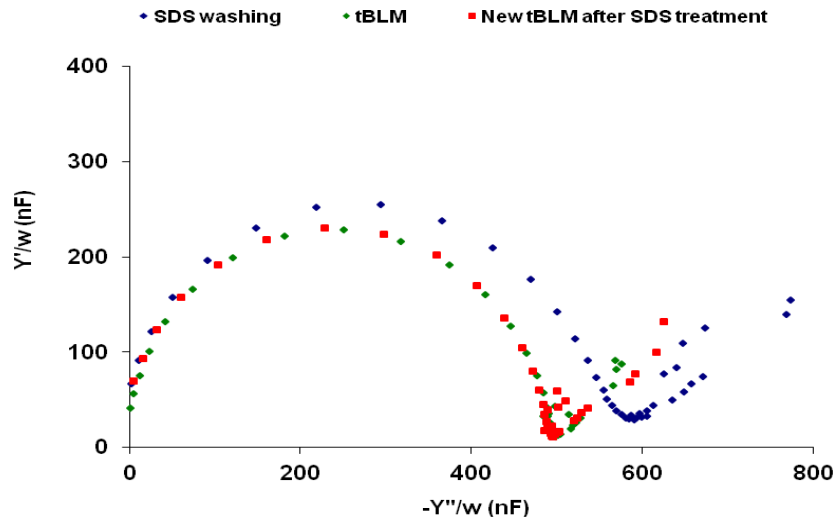


Figure 3.15: spectra corresponding to the formation of the lipid bilayer (green), after washing with SDS (blue) and the new formation of the membrane after treatment with SDS (red).

This initial phase is quick and is followed by a slower phase in which it is plausible that vesicles organize themselves in a more ordinate and defined structure.

From figure 3.16, the variation of the signal after the formation of the lipid layer for each lipid was estimated to ~ 6000 R.U. This value allows to determine how many molecules were on the surface; in fact, knowing that 1 R.U. correspond to ~ 1 pg/mm², the lipid density on the surface turns out to be 4.7×10^{14} POPC molecules/cm².

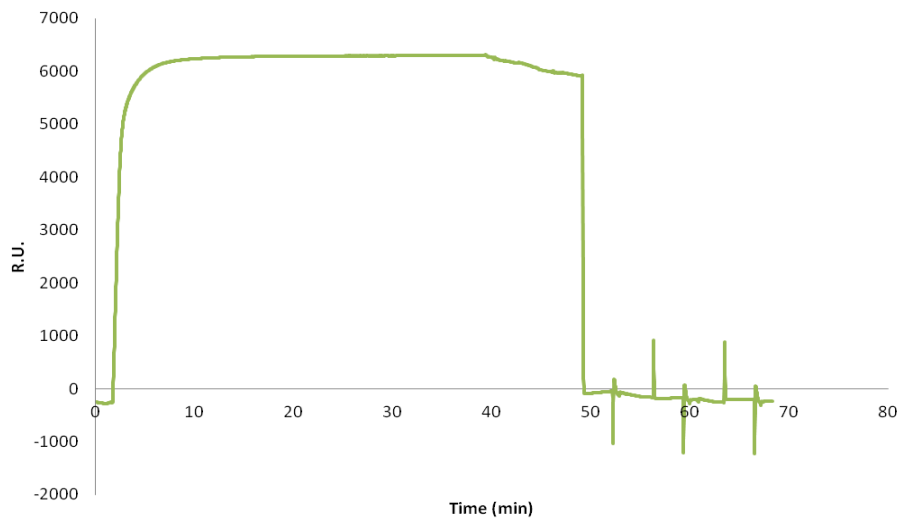


Figure 3.16: Sensorgram of the formation of tBLM on a pure DPTL monolayer. A sequence of 10 injections of DPTL was performed in order to form a pure monolayer. The rinsing step with SDS 0.5% flows away the non-specific bound molecules from the flow cell. A final value of 3800 RU is obtained, corresponding to 2.25×10^{14} molecules/cm². Arrows indicate the injections performed during the experiment.

From the reductive stripping assay, the density for a pure DPTL monolayer is $1.52 \cdot 10^{14}$ molecules/cm², therefore for a lipid bilayer it is plausible to obtain a similar density.

This value was also compared with data reported in literature, which said that the area occupied by a phosphocoline molecule in a lipid bilayer is between 50-70 Å²[119].

The theoretical density of lipid molecules in a phospholipid bilayer was calculated, and the resulting value ($3-4 \cdot 10^{14}$ molecules/cm²) is in agreement with the ones obtained in SPR experiments.

As we can see from figure 3.16, the injections of SDS 0.5% at the end of the experiment take the signal back to the starting value, indicating that only lipids that compose the tBLM are taken away after SDS treatment, without changing the amount of DPTL molecules on the surface. Even in this case the resulting DPTL can be used to form a new tBLM by the injection of lipid vesicles.

3.3.4 Formation of diluted DPTL monolayers

tBLMs described so far have dense DPTL layers and show a good passivation of the surface (the resistance of the bilayer well over 5 MΩ*cm²) and a good stability (at least in the first 7-8 hours, data not shown). Despite this, they are not suitable for the goal of this project, that is the development of an electrochemical biosensor based on model membranes, in order to study the interactions between these membranes and biomolecules of various nature.

In order to obtain a biosensor that can detect a broad spectrum of interactions, it is important that the model membranes have three basic characteristics:

- ◆ high resistance values;
- ◆ high fluidity;
- ◆ presence of a sub membrane space.

As already observed, the first feature is already present in the tBLMs described so far, while the other two parameters are practically absent.

A good hydration of both faces of the membrane is another aspect to be taken in account. Practically the presence of a submembrane space between the gold surface is required, so that the inner face of the membrane can remain hydrated. It is important also because determines a space where ions can flow, for example through pores formed in the membrane. Furthermore, the hydration of both sides of the lipid membrane determines a condition more similar to cell membranes. Finally, the presence of this submembrane space should facilitate the insertion into the lipid bilayer of transmembrane proteins with extramembrane domains, thereby making the protein-membrane interaction much more similar to what occurs *in vivo*.

The structure of DPTL molecules tends to favor the presence of this space, thanks to its hydrophilic portion, but the high density of DPTL on the surface reduces the hydration space. At the same time the high density of DPTL is responsible for the low fluidity of the lipid membrane anchored to the surface.

To overcome the drawbacks outlined above, some researchers^{[100],[101]} proposed to “dilute” the DPTL layer with smaller thiolated molecules; in this way, the lipid membrane will be anchored to the surface, but the submembrane space will be wider and with a greater hydration.

Choice of the diluent

To dilute a layer of tethering molecules, several molecules have been proposed in the literature. One of these molecules is called tetraethylene glycol-D, L- α -lipoic acid ester (TEGL) and has been employed by He and collaborators^[100] as a diluent for DPTL layers. TEGL is interesting because its structure is identical to that of DPTL, except for the lipid tails, which in this case are completely absent (see figure 3.17). DPTL layers diluted with TEGL show resistance values similar to resistance values of layers consisting only of DPTL, and the resulting tBLMs should show a greater fluidity because only a small portion of the lipids in the lower layer will be anchored to the surface. The main drawback of using TEGL as diluent concerns the submembrane region of the resulting tBLM that, in fact, continues to be almost completely occupied by the hydrophilic portions of the DPTL and TEGL.

Another dilution strategy, more suitable for the aims of this project, is based on small thiolated molecules (see figure 3.17), such as mercaptohexanol (MCH) and β -mercaptoethanol (β ME).

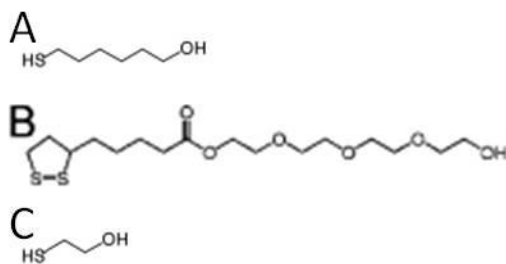


Figure 3.17: chemical structure of (A) mercaptohexanol, (B) DPTL and (C) β -mercaptoethanol.

Among these molecules, the biggest advantages should be provided by β ME, since its small dimensions should allow to maximize the submembrane volume, ensuring at the same time a good level of fluidity of the lipid bilayer. These mixed layers were proposed by McGillivray and his collaborators^[102] which, however, have used a tethering molecule different from DPTL, even if structurally they are very similar. These authors have characterized these layers also performing EIS measurements, and these data will be considered as a reference in the following pages.

Dilution experiments

Based on the results and the protocol described by McGillivray^[102], a mixed monolayer consisting of DPTL and β ME was prepared, with solutions containing DPTL and β ME in different molar ratios dissolved in ethanol and maintaining always 1 μ M as the total concentration of thiols in the

solution. After the incubation, lasting 18-19 hours in an ethanol-saturated-chamber, the surface was washed with 1 mL of ethanol and then dried with nitrogen.

Different molar ratio of DPTL and β ME were tested, containing respectively 90, 80, 70, 50 and 30% of DPTL, and they were characterized using EIS measurements. The aim of this experiments was to verify what was stated by McGillivray and colleagues, that using decreasing amounts of DPTL during the incubation, the resulting layers should show a decreasing amount of DPTL.

Figure 3.18 shows a complex admittance plot in which the impedance spectra obtained for each DPTL/ β ME molar ratio were compared. This kind of representation is useful to appreciate the capacitance variation of each layers. As can be seen, the capacitance values are distributed between two limit values: at the lower end there is the layer formed exclusively by DPTL (green curve), while at the other end we find the layer that consists only of β ME (blue curve).

Furthermore, the capacitance variation of each the mixed layers seems to be somewhat correlated with the percentage of DPTL present in the solutions used to functionalize the gold surfaces (see figure 3.19 and table 3.2).

In fact, decreasing the amount of DPTL in these solutions, the capacitance tends to increase, because the amount of DPTL will decrease also on the surface, resulting in less compact layers. This behavior is consistent with the data reported by McGillivray and colleagues. This suggests that there is a direct correspondence between the ratios of DPTL and β ME used during the functionalization and the amounts of DPTL and β ME actually present on the surface.

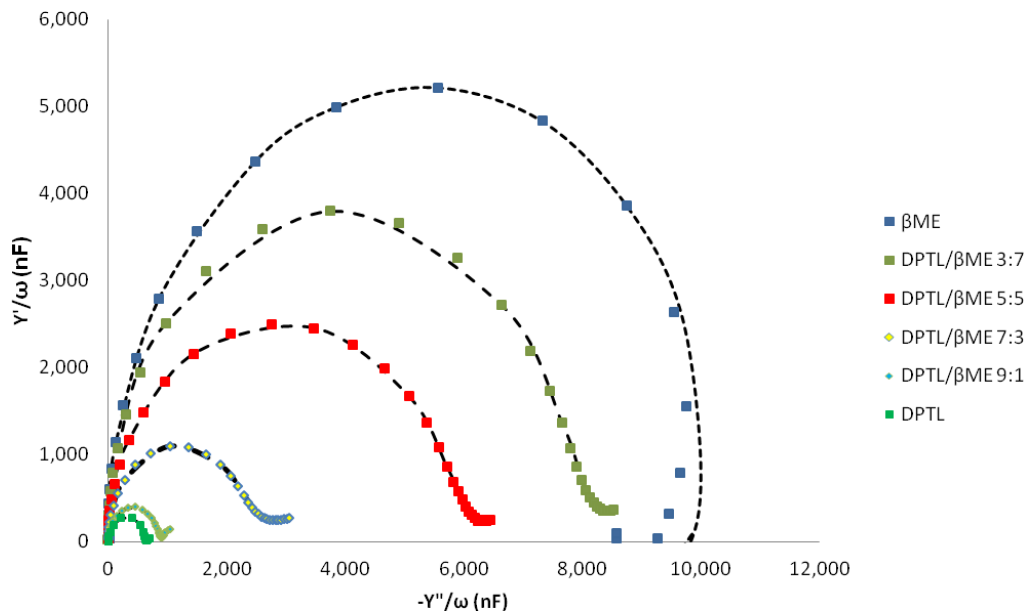


Figure 3.18: Complex admittance with several spectra of different layer of DPTL diluted with β ME. In this plot, the diameter of the semicircle corresponds to the capacitance of the layer. Black dashed lines correspond to the fitting with the equivalent circuit $R_{\Omega}(R_m Q_m)C_s$.

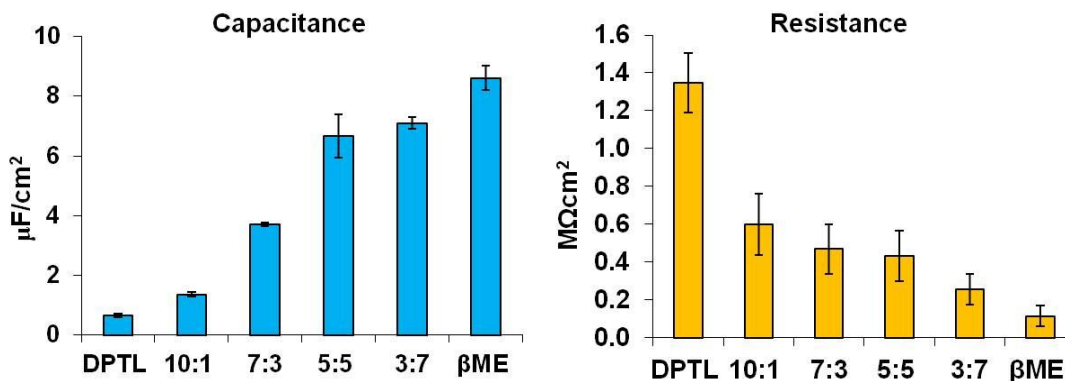


Figure 3.19: variation of capacitance (left) and resistance (right) values as a function of the change in molar ratios of DPTL:βME.

	DPTL	9:1	7:3	5:5	3:7	βME
Capacitance (μF/cm²)	0.655	1.366	3.720	6.667	7.100	8.600
d.s	0.067	0.088	0.059	0.714	0.201	0.409
Resistance (MΩ*cm²)	1.347	0.599	0.470	0.432	0.256	0.115
d. s.	0.158	0.163	0.131	0.133	0.082	0.055

Table 3.2: capacitance and resistance values as a function of the change in molar ratios of DPTL:βME

The impedance spectra were analyzed as described before, but using the following equivalent circuit: $R_{\Omega}(R_m Q_m)$, the same used in the article that we chose as reference.

From the fitting analysis (see figure 3.19), the values of capacitance and resistance for each DPTL diluted SAM with βME can be estimated (see table 3.2).

These values are consistent with the capacitance and the resistance values reported by McGillivray and colleagues, especially regarding the capacitance.

As expected, the resistance values tend to decrease with the reduction of DPTL in the incubation solutions and therefore also, presumably, with the reduction of DPTL on the surface. Actually the resistance values are lower than those reported by McGillivray, especially at higher percentages of DPTL. A possible explanation of this phenomenon may lie on difference in the quality of the gold surfaces; it is possible that the surfaces used in these experiments are rougher than those of the article, thereby with negative influence on the formation of the mixed SAM.

Furthermore, McGillivray and colleagues used a different thiolipid, although very similar to DPTL, and it can determine the formation of a layer with slightly different electrochemical characteristics compared to those measured using the DPTL.

3.3.5 Formation of tBLM on diluted DPTL monolayers

The formation of tBLM adding unilamellar lipid vesicles to different layers of DPTL diluted with β ME was evaluated. The goal is to obtain lipid membranes anchored to the surface with characteristics similar to the physiological membranes: a fluid lipid bilayer physically separate from the surface, with a submembrane space that allows the insertion of large size proteins.

McGillivray and colleagues^[102] used a different approach to complete the formation of tBLM on diluted thiolipid layers, called "rapid solvent exchange". Using this protocol they can form the lipid bilayer on all the diluted thiolipid layers, even those with very low amounts of thiolipid (obtained with 30% of thiolipid and 70% of β ME).

Unfortunately, every attempt to implement this protocol on diluted DPTL layers described above did not give positive result; in fact at the end of these tests, no changes compared to the starting resistance and capacitance values were observed. These negative results were observed also in tests performed on undiluted DPTL layers. One possible explanation is that the technique of rapid solvent exchange requires the use of a particular fluidic system, which probably can ensure a certain kind of flow during the washing step, which prevents the formation of bubbles always during the washing step, etc..

In alternative, the same protocol used previously to form tBLM on DPTL layers, that consists in flushing unilamellar lipid vesicles on diluted DPTL layers, can be applied.

To verify the formation of the lipid membrane on diluted DPTL layers, impedance measurements (from 1 MHz to 5 mHz, amplitude potential 10 mV in buffer NaCl 100 mM, HEPES 10 mM, pH 7.4) were performed. The electrical characteristics of the layers were obtained fitting the impedance spectra with the equivalent circuit described in figure 3.4.

Actually, the formation of tBLM on diluted DPTL layers can also be evaluated by a qualitative analysis of the EIS spectra represented through complex admittance plots (see figure 3.20).

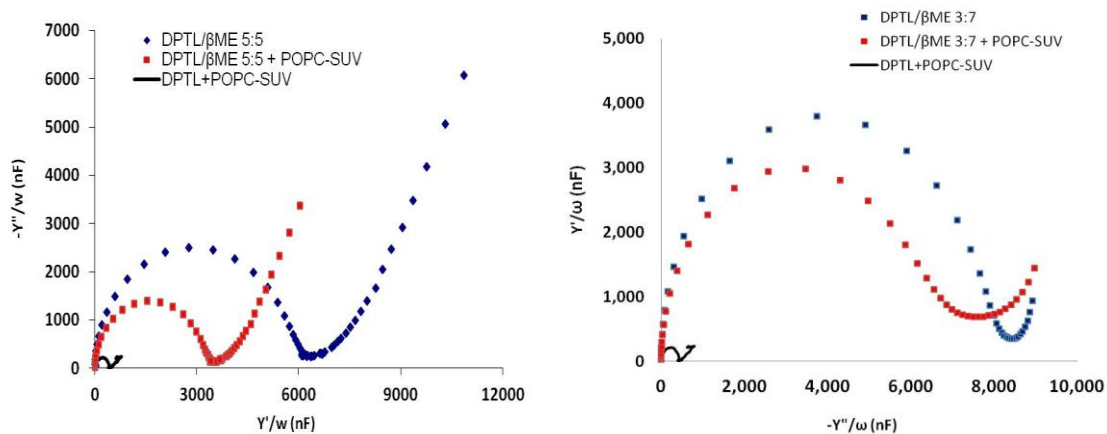


Figure 3.20: complex admittance plots relative to experiments of tBLM formation on mixed SAM of DPTL/ β ME 3:7 (on the left) and 5:5 (on the right) molar ratio.

In fact, diluted DPTL layers are characterized by high capacitance values, certainly higher than $1 \mu\text{F}/\text{cm}^2$ and thus the formation of tBLM should determine a wide decrease of capacitance, especially as regards to the higher dilutions.

The formation of tBLM on diluted DPTL layers, such as DPTL/ β ME 3:7 and DPTL/ β ME 5:5 were checked (figure 3.20). In both cases the respective complex admittance plots show a very limited decrease of capacitance, also by carrying out incubations with lipid vesicles for longer times (even after over-night incubation, data not shown).

As seen in figure 3.20, the capacitance variation obtained using vesicles (red spectrum), turns out to be much lower compared to the expected variation. The small reduction of capacitance (and a corresponding small increase in resistance, see table 3.3) can be explained considering that on these diluted DPTL layers vesicles have had the opportunity to adsorb and possibly breaking down on the surface, but probably they cannot merge to form a uniform and passivating tBLM.

Though McGillivray and colleagues state that in their diluted layers there is no phase segregation, the experiments show in figure 3.20 might be influenced by a phenomenon of phase segregation; in fact if the DPTL molecules are not distributed uniformly on the surface, then there could be large areas without DPTL in which the vesicles may have problems to adsorb and merge with each other.

Using diluted layers composed by DPTL and β ME in a molar ratio of 8:2, better results were obtained; in fact after the injection of lipid vesicles, a reduction of capacitance up to values that are consistent with the formation of a tBLM was observed (see figure 3.21).

The subsequent analysis of the impedance spectra with the equivalent circuit $R_{\Omega}(R_m Q_m)C_s$ confirmed the capacitance value indicated in the complex admittance plot (see table 3.3) and indicated a resistance value consistent with the one measured for tBLM formed of layers of dense DPTL.

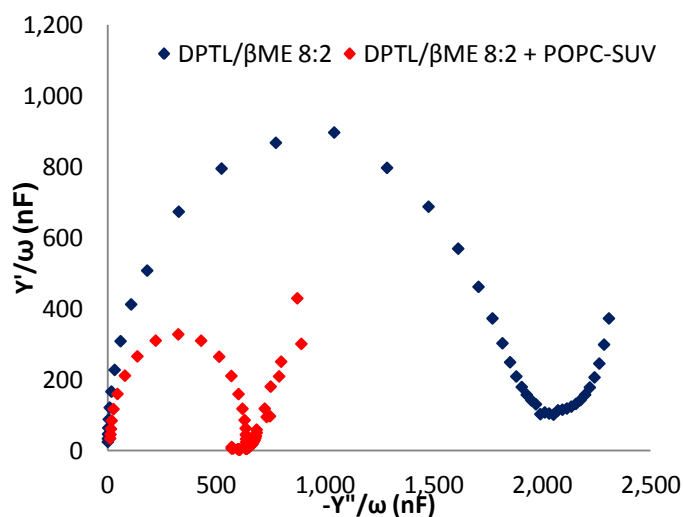


Figure 3.21: complex admittance plot relative to an experiment of tBLM formation on mixed SAM of DPTL/ β ME 8:2 molar ratio.

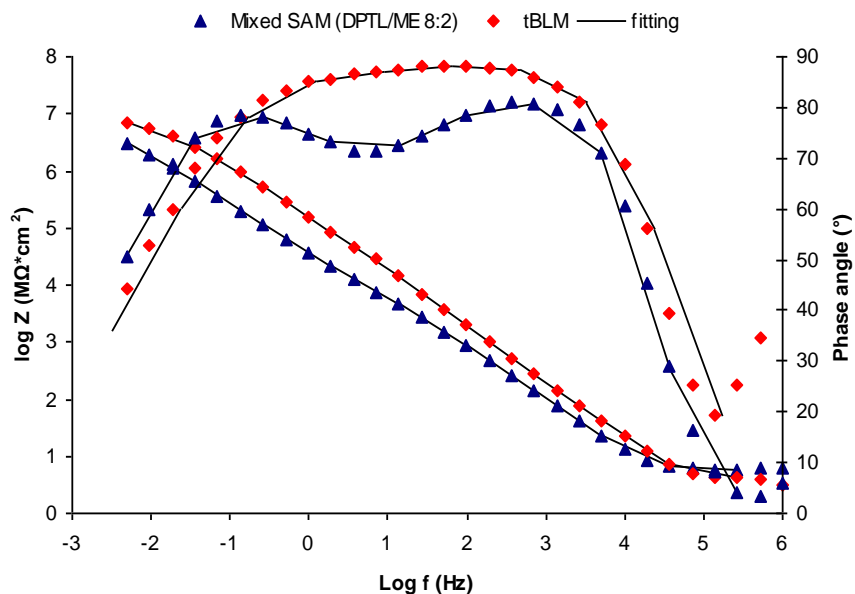


Figure: 3.22: Bode plot relative to an experiment of tBLM formation on mixed SAM of DPTL/βME 8:2 molar ratio. Black lines correspond to fitting with the equivalent circuit $R_{\Omega}(R_m Q_m)C_s$.

		9:1	8:2	5:5	3:7
$C_{DPTL/\beta ME}$	($\mu F/cm^2$)	1.206	2.07	7.55	7.82
C_{tBLM}	($\mu F/cm^2$)	0.841	0.701	6.8	7.01
$R_{DPTL/\beta ME}$	($M\Omega \cdot cm^2$)	0.712	0.492	0.538	0.226
R_{tBLM}	($M\Omega \cdot cm^2$)	7.4	6.42	0.645	0.285

Table 3.3: capacitance and resistance values before and after the tBLM formation as a function of the change in molar ratios of DPTL:βME.

With EIS measurements, the stability of these tBLM was assessed. tBLM was left in the measuring buffer (100 mM NaCl, 10 mM HEPES, pH 7.2) for the whole duration of the measures (about 7-8 hours), and every 60 minutes a full impedance spectrum was collected and analyzed as described previously. Figures 3.23 shows the trend of the capacitance and the resistance values in this range of time. Both of these parameters tend to remain constant, especially during the first hours after the tBLM formation. In the following hours the variability increases but no significant drifts were observed.

3.3.6 Conclusions and perspective

In this chapter, the development of an effective protocol for the preparation of stable and passivating tBLMs was described.

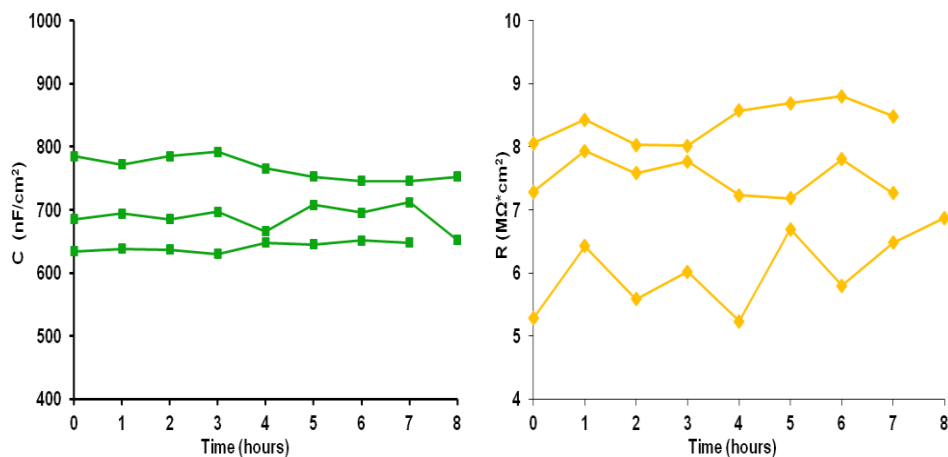


Figure 3.23: capacitance (green lines) and resistance (orange lines) variations as a function of time of three different tBLM formed using POPC vesicles on DPTL layer.

In particular, two different types of tBLM were prepared and characterized mainly with impedance measurements, but also through AFM measurements and SPR.

The simplest tBLM that was prepared is characterized by a sublayer consisting of DPTL molecules, and completed by the addition of POPC vesicles. EIS measurements carried out on these tBLM indicate the formation of a single lipid bilayer with a good passivation of the surface, with resistance values between 5 and 10 $M\Omega \cdot cm^2$. These values are lower than the ones reported in literature for tBLM prepared using DPTL as tethering molecule, where resistance of tens of $M\Omega \cdot cm^2$ are measured^[93]. One possible explanation rely on the quality of the gold surfaces used in our experiments; specifically the roughness of our gold surfaces is higher than 1 nm, so it could have negatively effects on the quality of tBLM.

The DPTL layer formation and the subsequent tBLM formation were also monitored by SPR, obtaining results consistent with those observed by EIS measurements. Unfortunately this type of tBLM is characterized by a very reduced fluidity of the lipid bilayer, as also reported by several papers in literature, making it unsuitable for a future application as a sensing element in a biosensor.

For this reason, a second type of tBLM was prepared and characterized. In this case, the sublayer is composed by DPTL and β ME, in order to obtain, at the end, a lipid bilayer anchored to the surface with a good fluidity.

Specifically it has been possible to prepare with success stable and passivating tBLM (also in this case from 5 and 10 $M\Omega \cdot cm^2$, that remains stable for at least 7-8 hours) using a mixture of DPTL and β ME with a molar ratio of 8:2 to prepare the sublayer, and POPC vesicles to complete the tBLM formation. Unfortunately, it was not possible to prepare uniform and passivating tBLM on more diluted DPTL layers, as has been reported in the literature^[101], so further efforts are required to prepare tBLM on more diluted DPTL layers.

However, the next goal is to verify the possibility of using these tBLMs as sensing elements in a biosensor for the detection of interactions between the lipid membrane and different types of macromolecules. Specifically, in the next chapter will be described numerous experiments that involves different kinds of molecules, such as gramicidin (a pore-forming peptide), melittin (a toxin), cyclohexane and dinitrophenol (pollutants) and α -synuclein (an amyloid protein).

Section III:
Biosensors based on lipid
membranes

Applications of biosensors based on lipid membranes

4.1 Introduction

Model membranes, briefly described in the previous chapter, have been mainly used to study and characterize the structure and the biophysical properties of lipid membranes, particularly with regard to their composition and the required physical and chemical conditions.

It is also known that cell membranes interact with a very large number of molecules, through its protein components, but also with the lipid bilayer. Many of these interactions are crucial for the proper functioning of the cell, but other interactions can determine disorders at the cell level, often resulting in negative effects for the whole organism.

The following pages report an overview of the applications of model membranes, and their potential applications as biosensors.

4.1.1 Studies about the biophysical properties of lipid bilayers

The functionality of any biological membrane is determined mostly by the membrane proteins embedded in it, and also by the peripheral proteins attached to the membrane surface. However, at the same time the activity of these proteins is influenced by the composition and the structure of the lipid membrane^[119].

The study of these processes *in vivo* is difficult because membrane proteins are associated with each other in a complex mixture of other protein^[120]. Furthermore it is still difficult to extract *in vivo* information regarding specific issues in the function of the cell membrane.

For this reason the reconstitution of membrane proteins in model membranes allows the investigation of features and individual activities about a given component of the membrane. To do this, various properties of model membrane must be optimized: for example the length of the fatty acid chains can influence the hydrophobicity of the membrane, which in turn can influence the activity of proteins.

The principal model systems for these studies are supported lipid bilayers, liposomes and lipid nanodisc^[121], and they have been used for instance to study membrane fusion, a key process in the cells, since it allows the transport of molecules within cells but also between cells. Much has already been understood regarding the membranes fusion, especially about the lipid components required and the proteins involved in these processes, but the exact mechanisms and the fundamental requirements of fusion are still unknown^[122].

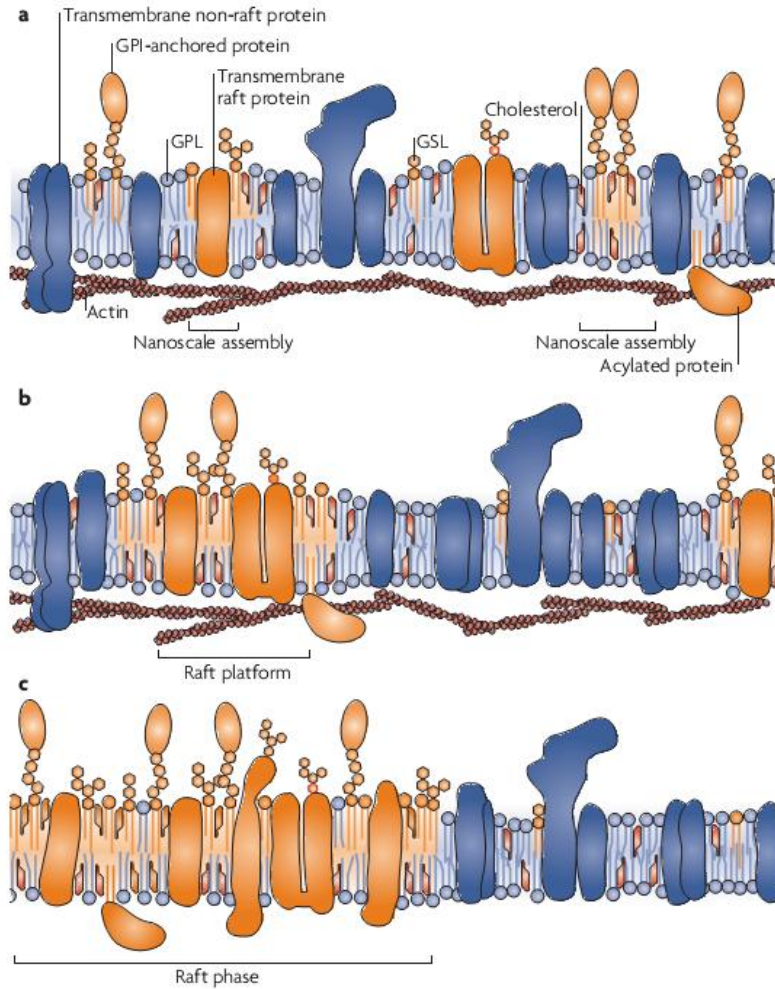


Figure 4.1: (a) Nanoscale assemblies of sterols such as cholesterol, sphingolipids such as sphingomyelin and glycosphingolipids (GSLs), and proteins in the plasma membrane fluctuate in composition. (b) In response to external signals or the initiation of membrane trafficking events, raft platforms are formed from fluctuating assemblies through lipid–lipid, lipid–protein and protein–protein oligomerizing interactions. (c) Micrometre-sized raft ‘phases’ can be induced at equilibrium. Figure reproduced from [123].

The principal model systems for the study of membrane fusion are liposomes, whose composition, size and surface charge can be easily controlled. In addition, liposomes may be just as easily functionalized with ligands of different nature in order to determine specific kind of interactions with other liposomes.

The most common approach to study events of lipid mixing^[124], content mixing^[125] and leakage is based on fluorescence technique, and among them the main one is the fluorescence resonance energy transfer (FRET).

In 1997 the concept of lipid raft was introduced. This term refers to a dynamic, nanoscale, sterol–sphingolipid-enriched, ordered assemblies of proteins and lipids (especially with saturated hydrocarbon chains), in which the metastable raft resting state can be stimulated to coalesce into larger, more stable raft domains by specific lipid–lipid, protein–lipid and protein–protein

oligomerizing interactions (see figure 4.1). Lipid rafts function as a membrane organizing structure with important roles in cellular processes such as T cell signalling, viral infection (including HIV and influenza) and membrane trafficking. Giant unilamellar vesicles (GUVs) and supported bilayers were used as simple model systems to study lipid rafts^[123].

4.1.2 Interaction with drugs

The structural complexity of the cell membrane, and the highly dynamic nature of the lipid-lipid and lipid-protein interactions, make the study of interactions with drugs and of drug delivery systems very complex. For this reason, model membranes can be very useful. In fact, these artificial structures provide insight into the role of membrane lipids in cellular uptake, to predict drug toxicity and to optimize drug delivery systems^[126].

Generally three different kinds of interaction are possible between drugs and lipids^[126]:

- a) interaction with the headgroups of lipids;
- b) interactions with the hydrophobic portion;
- c) interaction with both headgroups and hydrophobic acyl chains.

All of these possibility can be explored to identify the basis for these interactions using model membranes.

Many drugs have intracellular targets, and are therefore forced to cross one or more lipid bilayers to reach their intracellular target and perform their function. In particular, it is increasingly clear that the drug-lipid interactions have a very important role regarding the transport of the drug, its distribution and accumulation inside the cell, and in particular the effectiveness of the drug. In recent years a large number of drugs, including antibiotics^[127], antihypertensive drugs^[128], antifungal drugs^[129], antipsychotic drugs^[130] and anticancer agents^[131], have been studied in relation to their interaction with the membrane lipids, using different biophysical techniques.

For example, liposomes have been widely used to evaluate the efficacy of the drugs. In general drug effectiveness is measured determining the partition coefficient of drugs, which essentially measures the amount of drug able to enter into or through the lipid membrane in the biological system. In this case, liposomes are good systems that mimic the hydrophobic part and the outer surface of polar charged phospholipids which constitute a cell membrane^[132].

Model membranes can also be used to estimate the amount of drugs transported into the cell, their transport mechanism, but also their mechanism of toxicity, since it is possible to work at high concentrations of drugs that are known to be toxic *in vivo*^[133].

Interfacial properties of polymeric coatings used on drug delivery systems can influence the interactions with the cellular environment, and therefore the efficiency of drug delivery system of therapeutic agents for cells and tissue. So a better understanding of the interactions between lipids polymers is necessary in order to develop effective drug delivery systems, limiting their toxicity^[126].

4.1.3 Neurodegenerative diseases

Several neurodegenerative diseases (for example Alzheimer's disease, Parkinson's disease, type II diabetes mellitus, etc.) are characterized by the accumulation of insoluble protein deposits composed of fibrillar aggregates rich in β -sheets (amyloids). Amyloid fibrils are developed from single-soluble proteins that undergo a process of aggregation characterized by the misfolding of proteins and their aggregation first into prefibrillar aggregates and finally into mature amyloid fibrils^[83].

Recent studies suggest that the toxic effects of these aggregates are not due only by the presence of the high molecular weight aggregates, but rather to the simultaneous presence of fibers and prefibrillar aggregates^[134].

Furthermore, it is increasingly clear that in this process cell membranes play a crucial role; on one hand the membrane can work as a catalyst that promotes the misfolding of the proteins and their aggregation into fibers, while, at the same time, the interaction with proteins may alter the structural integrity of the membrane, causing the toxic effects^[83].

The mechanisms that determine the permeabilization of the membrane have not yet been completely clarified; however different models have been proposed, involving the formation of oligomeric pore structures that span the lipid membrane, the formation of non-specific binding between amyloid proteins and the membrane surface, or the detergent-like dissolution of the membrane caused by the growth of amyloid fibers on the surface of the cell membrane^[83].

Membrane models ensures the ability to manipulate the chemical composition and the fluidity of the membrane and are therefore of significant help in observing the changes in protein binding and permeabilization activity.

Vesicles are the most efficient model membrane in mimic natural cell membranes, because of their spherical structure and water-filled interior. Moreover, the possibility of introducing fluorophores or dyes inside them, has made the vesicles a good model in the study of membrane permeabilization, for example through dye-leakage assays^[135].

In alternative planar lipid bilayer, also called black lipid membranes, have been used to determine the ion-channel activities of α -synuclein, A- β , and some prion-derived polypeptides^[136]. There is also a growing interest in supported or tethered lipid bilayer to study these interactions, the effects on membrane permeabilization and the fibrillation of the protein.

In recent years lipid alterations has been reported in cancer^[137], diabetes^[138], and various cardiovascular diseases^[138] such as hypertension, atherosclerosis, coronary heart disease, aneurysm and thrombosis.

It has been suggested that tumor cells can in some cases acquire resistance to chemotherapy, also thanks to changes in their lipid composition; actually it is not entirely clear whether this variation in the lipid composition is the cause or the result of cancer^[138].

4.1.4 Studies about bacterial toxins and pollutants

Many pathogens act at distance producing virulence factors that are called ‘toxins’. Toxins usually are synthesized as soluble proteins that need to interact with cell lipid membranes (plasma membrane, endosomal membrane, etc.) in order to express their biological activity.

Toxins can be divided into two different categories^[84]:

- the pore forming toxins form a pore or a channel through the membrane. This channel is directly responsible for the toxicity either by disrupting the membrane permeability or by activating signal transductions pathways (α -toxin of *Staphylococcus aureus*, the aerolysin from *Aeromonas hydrophila*, the *E. coli* hemolysin);
- the translocation toxins, which need to translocate across a lipid membrane to exert their biological activity (diphtheria toxin, cholera toxin).

In many cases it has been demonstrated the utility of model membranes to characterize the interaction between toxins and lipid membranes. For instance Terrettaz and colleagues^[108] used supported lipid bilayer to investigate the interaction between cholera enterotoxin and the lipid membrane receptors monosialoganglioside. Instead tethered lipid bilayer was used by Jadhav and colleagues to functional characterized the PorB class II toxin of *Neisseria meningitides*, of which is known the ability of forming pores in lipid membranes^[139]. Also Tun and Jenkins used tethered lipid bilayer as a sensing platform for the detection of α -toxin of *Staphylococcus aureus* and exotoxin A of *Pseudomonas aeruginosa*^[140].

Model membranes can also be used to study the interaction of pollutants with lipid membranes. In fact it has been observed that many molecules classified as pollutants can interact with lipid membranes, often with negative effects for the living beings.

For example substituted phenols are widely used in the production of many and different products such as plastics, explosives, medicines, paints, detergents, pesticides and anti-oxidants, among others. Despite their general use, substituted phenols are contaminants of considerable environmental concern^[85]. In fact, they are responsible of severe environmental contamination of soil, ground water and air. Toxicity also affects many organisms by interfering with basic cell functions; in fact by simple accumulating in the membrane, some phenols can non-specifically perturb the membrane functions, causing a so-called “narcotic effect”^[141]. Moreover, substituted phenols act as uncouplers that destroy the electrochemical proton gradient by transporting protons across the membrane and/or by inhibiting the electron flow^[142]. Labelled liposomes were used to study how substituted phenols affect membrane fluidity^[85].

Another example of pollutant is represented by triazine herbicides, that are extensively used in modern agriculture. Triazines are widely distributed in aquatic environments, and triazine pollution in rivers, lakes, and seas has become a serious problem. Siontorou and colleagues developed a triazine herbicide minisensor based on surface-stabilized bilayer lipid membranes^[143].

Cyclic hydrocarbons (such as cycloalkane and terpenes) are another group of molecules classified as pollutants. The impact of cyclic hydrocarbons on microorganisms and the environmental and economical consequences are clear. However, the mechanism of the toxicity induced by these compounds has been poorly documented. The available data show that as a result of the lipophilic character of these compounds, interactions with hydrophobic parts of the cell play an important role in the mechanism of their toxic action^[144].

4.1.5 Biosensors based on model membranes

Artificial model membranes can be used as a sensitive component in biosensors, to directly detect interactions between target molecules and the lipid membrane, or using them as an environmental matrix to accommodate ion channels or membrane receptors, in order to detect specifically the molecules that can interact with these membrane components.

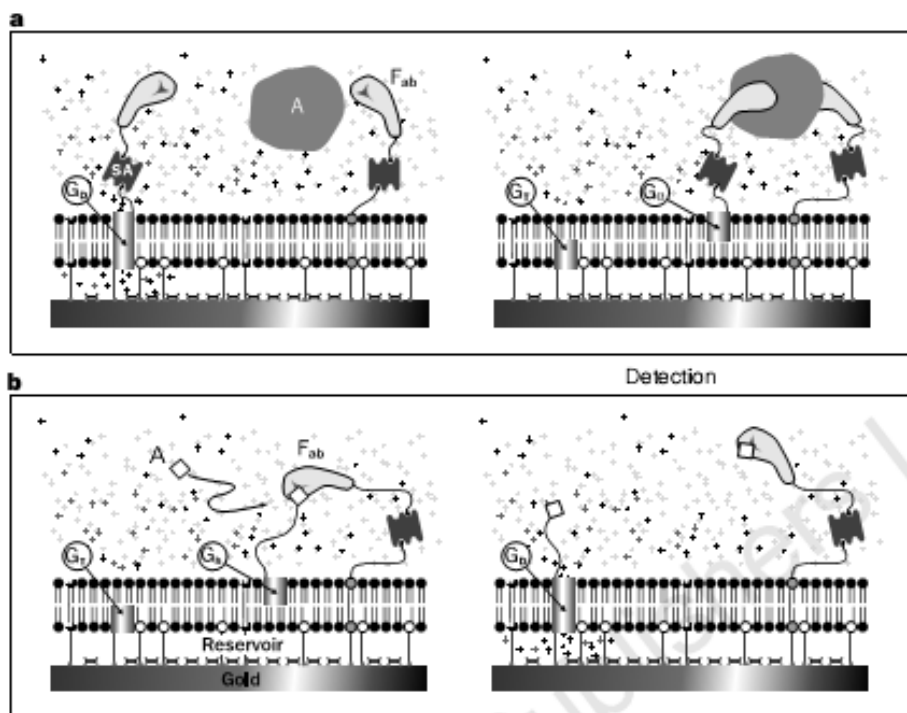


Figure 4.2: (a) Two-site sandwich assay. The mobile ion channels (MIC) are coupled to antibody fragments, as well as some of the membrane spanning lipids (MSL). In the absence of analyte (A), MIC diffuse within the outer monolayer, intermittently forming conducting dimers. The addition of the targeted analyte crosslinks the Fabs on MIC and MSL and forms complexes that tether MIC distant from their immobilized inner-layer partners. This prevents the formation of channel dimers and lowers the electrical conductivity of the membrane. (b) Competitive assay: A similar membrane is formed except that it contains hapten-linked gramicidin (Gh). Gh is thus tethered distant from its immobilized inner-layer partners (GT), preventing the formation of dimers and lowering the electrical conductance of the membrane. The sensor is stored in this state until the addition of analyte competes with the hapten for the Fab9, liberating the channel and resulting in an increase in the membrane conductance. Picture reproduced from [114].

At the first category of biosensors based on model membranes belong all those sensing platforms composed only by lipid membranes; in the case of electrochemical biosensors, the model membranes most commonly used are the supported^[143] or the tethered lipid bilayer^[139], as they can be easily prepared on metal surfaces that can serve as working electrodes. In these cases the biosensor hardly allow to specifically identify the molecule that has interacted with the lipid membrane; on the other hand this kind of biosensor would have the advantage of being able to detect the presence of a wide range of molecules present in the sample that are capable to alter the electrical characteristics of the membrane. Generally the most sensitive parameter in this kind of interactions is the resistance of the lipid bilayer, since this model membranes are characterized by a high surface passivation; therefore each interaction that can alter the integrity of the membrane will be detected as a resistance decrease. Obviously, the identification of the target molecule will require further analysis, but this type of biosensor may be useful for preliminary screening, for example in environmental monitoring. A particular that still has to be taken into consideration concerns the fact that the composition of the membrane has a high influence in the interactions between target molecules and the membrane itself, so it is important to carefully select the lipids to be used in the preparation of the model membranes.

As previously mentioned, model membranes can be used to create an environmental matrix that can accommodate transmembrane proteins as sensing elements in electrochemical biosensors. An example was describe by Stora et al.; they used the receptor protein OmpF from *E. coli* to detect the antibacterial toxin colicin N^[112]. Terrettaz et al. described a biosensor based on a synthetic ligand-gated ion channel (SLIC) integrated in a lipid bilayer, both tethered to a gold surface, to detect antibodies in blood serum and whole blood^[145].

Ion channel (ICS) biosensors represent the most advanced example of biosensors based on model membranes^[146]. Cornell and colleagues used the low-molecular-weight bacterial ion-channel gramicidin as the basis of a biosensor platform with a wide range of applications for the detection of low-molecular-weight drugs, large proteins and microorganisms^[114]. An example of ion channel biosensors was described in figure 4.2. Briefly, gramicidin was embedded in a tethered lipid membrane; in particular gramicidin monomers in the inner leaflet and membrane spanning lipids are tethered to the gold surface. At the same time gramicidin and membrane spanning lipids in the outer layer were free to move in the layer and were functionalized with antibodies.

The arrival of analyte cross-links antibodies attached to the mobile gramicidin monomers to those attached to membrane spanning lipids. This prevented the formation of gramicidin dimers, and the admittance decreases.

ICS biosensors provides a rapid detection for specific target molecules, and can be fabricated and used for multianalyte detection.

In the next paragraphs several experiments will be described, to verify the possibility of using the model membrane described in the previous chapter for the development of a biosensor based on model membranes.

4.2 Materials and methods

Reagents

All reagents are from Sigma-Aldrich unless noted otherwise, and have been used as such without further purification.

tBLM preparation

The following experiments were performed using tethered lipid bilayer prepared on a mixed SAM formed using DPTL and β ME with a molar ratio of 8:2. The protocol to prepared this tethered lipid bilayer was widely described and discussed in the previous chapter.

For the experiments that involves α -synuclein, tethered lipid bilayers prepared with vesicles containing 30% of POPG and 70% of POPC were used. Solutions containing α -synuclein were injected in the electrochemical cell, then the cell was washed with PBS buffer (50 mM, pH 7.4) with 0.05% sodium azide, and a final EIS measurements was performed.

Electrochemical measurements

Electrochemical impedance spectroscopy measurements were performed with μ Autolab Type III/FRA2. The data analysis was performed using the software FRA (Frequency Response Analyzer System) provided by the manufacturer of the instrument, and Zview (Scribner Associated Inc.) for the fitting analysis. All measurements were carried out in a 3-electrode cell in polydimethylsiloxane (PDMS), a non-toxic polymer material, transparent, and which behaves as an excellent electrical insulator. The cell is equipped with a microfluidic system, and presents a volume of 20 μ L and a working area of 15 mm².

EIS measurements were conducted in the frequencies ranges 1 MHz-5 mHz with an excitation amplitude of 10 mV and a bias potential of 0 V vs Ag/AgCl reference electrode and a platinum counter electrode. All the measurements were conducted in the following buffer: NaCl 100 mM, HEPES 10 mM, pH 7.3.

Real-time analysis were performed measured the in-phase admittance at 100 Hz every 30 seconds, using the same experimental setup and in the same buffer described above.

Pore-forming peptides and pollutants

Gramicidin was dissolved in ethanol to a final concentration of 100 μ M. Before the injection in the measuring cell, gramicidin was diluted with the following buffer (NaCl 100 mM, HEPES 10 mM, pH 7.3) to obtain a final concentration of 5 μ M (with 1% ethanol).

Melittin was dissolved directly in NaCl 100 mM, HEPES 10 mM, pH 7.3, at a concentration of 5 μ M.

Just before performing the measurement, several solutions of cyclohexane in NaCl 100 mM, HEPES 10 mM (pH 7.3) were prepared: specifically 0.05%, 0.1% and 1%.

2, 4 dinitrophenol was dissolved in NaCl 100 mM, HEPES 10 mM (pH 7.3), with the following final concentrations: 15 μ M and 50 μ M.

In all these experiments at least 30 minutes of incubation inside the cell were performed; after that 200 μ L of buffer at 30 μ L/min was injected to wash the cell, and finally EIS measurements were performed.

α -synuclein oligomers and fibers preparation

First α -synuclein monomers were incubated in PBS buffer for 6 hours at 37°C; then the solution was centrifuged with a 100 kDa filter for 15 minutes at 8000 RCF, and finally the concentration of α -synuclein monomers was measured using a spectrophotometer.

α -synuclein aggregates were generated by incubating α -synuclein (between 40-80 μ M) in 200 μ l of PBS buffer (50 mM, pH 7.4) with 0.05% sodium azide to avoid bacterial growth during protein aggregation at 37 °C for 2–15 days with continuous shaking at 1000 rpm.

α -synuclein at different stages of aggregation was diluted in PBS buffer (50 mM, pH 7.4) with 0.05% sodium azide to a final concentration of 1 μ M.

Sample preparation and AFM imaging

The samples for AFM imaging were initiated by depositing 10 μ l of α -synuclein aggregates on the freshly cleaved mica (RubyRed Mica Sheets, Electron Microscopy Sciences, Fort Washington, USA) at room temperature (\sim 25 °C). After adsorption for 5 min, the mica surface was gently washed with the 20–30 drops (1–1.5 ml) of double distilled water (Milli-Q H₂O), to remove excess salts and unbounded proteins from the surface. The sample was dried by condensed nitrogen gas by blowing over the mica surface and stored at room temperature (\sim 25°C) for imaging.

All the images for characterizing α -synuclein aggregates were obtained by Multimode AFM facility (Nanoscope III, Veeco/Digital Instruments, Santa Barbara, CA) with scanner 2795E in a tapping mode. Slandered etched silicon cantilevers (Ultra sharp NSC15/AIBS silicon probes with tip apex radius of \sim 10 nm, resonant frequency range of AFM cantilever 325 Hz, and number of pixels (512 \times 512) were used for imaging in air. All the images were taken at room temperature (\sim 25 °C)

In most experiments, the samples were diluted \sim 10 times with PBS then equilibrated at RT for 10 minutes prior to deposition in an attempt to minimize overlap of individual α -synuclein aggregates.

4.3 Results and discussion

4.3.1 Model pore-forming peptides and toxins

As explained in the introduction to this chapter, many peptides or proteins, such as bacterial toxins or amyloid proteins, can interact with lipid membranes forming pores or channels that cross the bilayer, altering the electrical properties of the membrane. It is possible to detect and study these effects using peptides of which is known the ability to form pores in lipid membranes, such as gramicidin.

Moreover, when biomembrane models consisting of a hydrophilic spacer interposed between the electrode surface and a lipid bilayer, it is important to verify whether the hydrophilic spacer may act as a satisfactory reservoir of inorganic ions. A simple but extremely useful test consists in incorporating in the lipid bilayer the pore-forming peptide gramicidin, verifying the extent in the conductance increases of biomembrane models.

4.3.1.1 Gramicidin

Gramicidin is a channel-forming peptide produced by *Bacillus brevis* and it is composed by 15 alternating L- and D-amino acid residues organized in a α -helix. Due to its small size and its well-defined function, gramicidin has become a model for the study of membrane-protein interactions. It can insert within membranes either as a monomer or as a dimer. Only the dimeric form can span through the membrane and, hence, allows the passage of ions from one side to the other one of the bilayer^[147].

Gramicidin channels allow the passage of monovalent cations, flowing down their electrochemical gradients. Gramicidin conductance is dependent on the dimerization constant and on the species and the concentration of ions in the bathing solution; whereas the K^+ and Na^+ ions

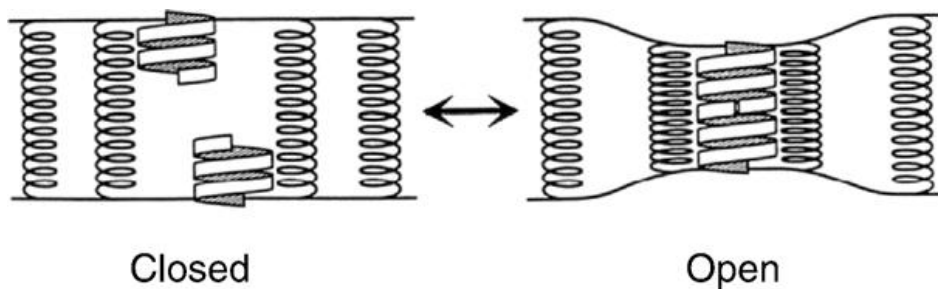


Figure 4.3: Schematic representation of the monomeric (left) and the dimeric (right) configuration of the gramicidin insert within membranes. Figure taken from [147]

penetrate the channel, other ions like the bigger tetramethylammonium $((\text{CH}_3)_4\text{N}^+)$ or ammonium (NH_4^+) ions are excluded.

Interaction of gramicidin with tBLM

Several EIS measurements were performed to check the ability of the tBLM prepared as described in the previous chapter to detect the presence of gramicidin in solution.

Gramicidin is not soluble in aqueous solutions so it is necessary to dilute the stock solution prepared in pure ethanol with the following buffer, 100 mM NaCl, 10 mM HEPES, (pH 7.3), to a final concentration of 5 μM of gramicidin (and 1% of ethanol). 200 μL of gramicidin solution was immediately injected in the measuring cell, where a gold surface modified with a tBLM (with a sublayer of DPTL and βME with 8:2 molar ratio) was used as working electrode. After 1 hour the cell was washed with 200 μL of buffer, and an EIS measurement was performed, in order to verify the effect of gramicidin on tBLM.

Observing the impedance spectra in a prototypical experiment shown in figure 4.4, after the treatment with gramicidin there is a large decrease of impedance, especially at low frequencies, as indicated by the deflection point that can be observed around 10 Hz.

Fitting these data with the following equivalent circuit, $R_\Omega(R_m Q_m)C_s$, the capacitance and the resistance variations can be quantified. Figure 4.5 shows the corresponding results: a large decrease of resistance (from 6.64 to 0.34 $\text{M}\Omega \cdot \text{cm}^2$), while the capacitance remains almost the same (from 0.808 to 0.803 $\mu\text{F}/\text{cm}^2$). The large decrease of resistance is consistent with values reported in literature^[99] and it was due by the presence of gramicidin that permeabilize the membrane, and not by a destruction of the lipid bilayer, because otherwise the increase of capacitance would have been much more pronounced.

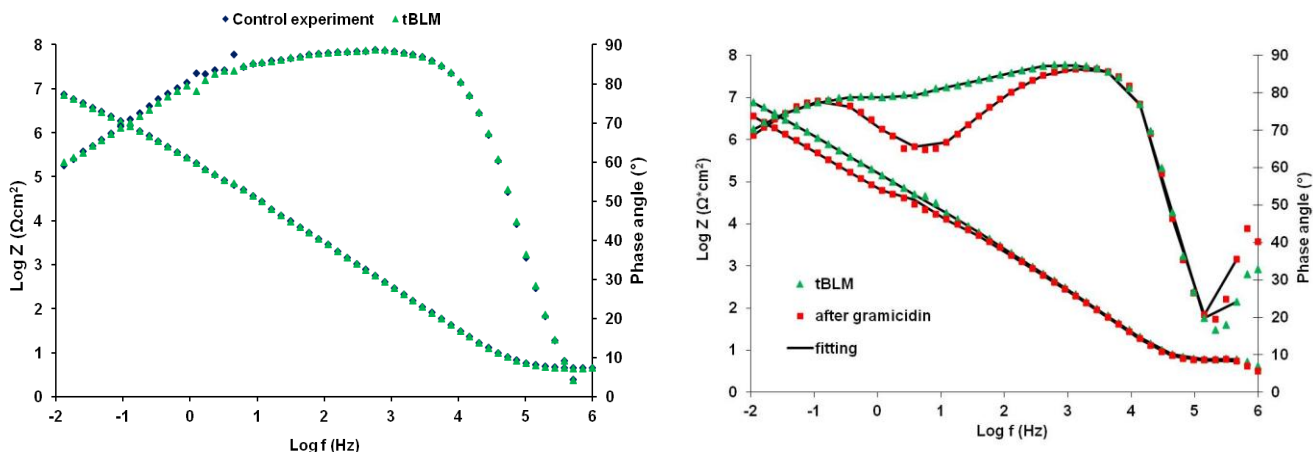


Figure 4.4: on the left impedance spectra of control experiment were shown. On the right were reported impedance spectra before and after a 1 hour treatment with gramicidin 5 μM . All the tBLMs used in these experiments have been prepared with 8:2 molar ratio of DPTL and βME , respectively. All the spectra were fitted with the equivalent circuit $R_\Omega(R_m Q_m)C_s$ and the values obtained are shown in the table of figure 4.6.

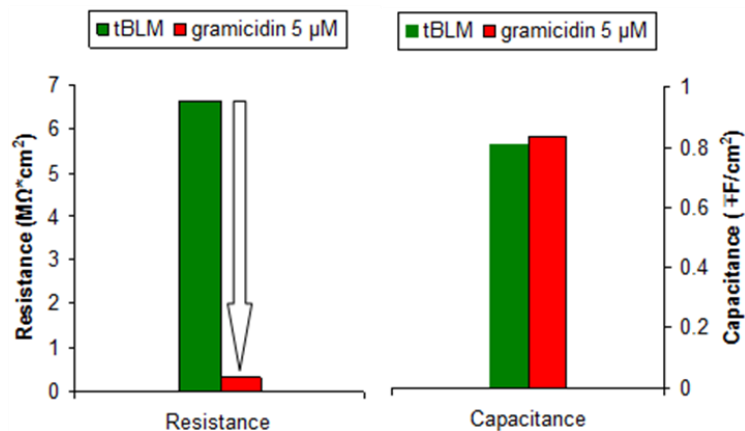


Figure 4.5: resistance and the impedance variation after 1 hour treatment with gramicidin 5 μM .

Control experiments carried out by injecting the same solutions in the absence of gramicidin lead to no change of signal; one example of control experiment is shown in figure 4.4, and the corresponding values of capacitance and resistance were reported in the table in figure 4.6.

To assess the importance of using membranes with a good fluidity in the recognition of gramicidin, an experiment on a tBLM obtained from a DPTL-only sublayer was performed by applying the same protocol described above.

The obtained spectrum was reported in figure 4.6 and the capacitance and resistance values are collected in the attached table. It is possible to observe also in this case an inflection point of $\log |Z|$ around 10 Hz after the treatment with gramicidin, but the impedance decrease observed at lower frequencies is much more limited than what observed using a tBLM prepared on a diluted DPTL layer. This in fact results in a lower decrease of resistance (from 4.49 to 1.84 $\text{M}\Omega \cdot \text{cm}^2$ in

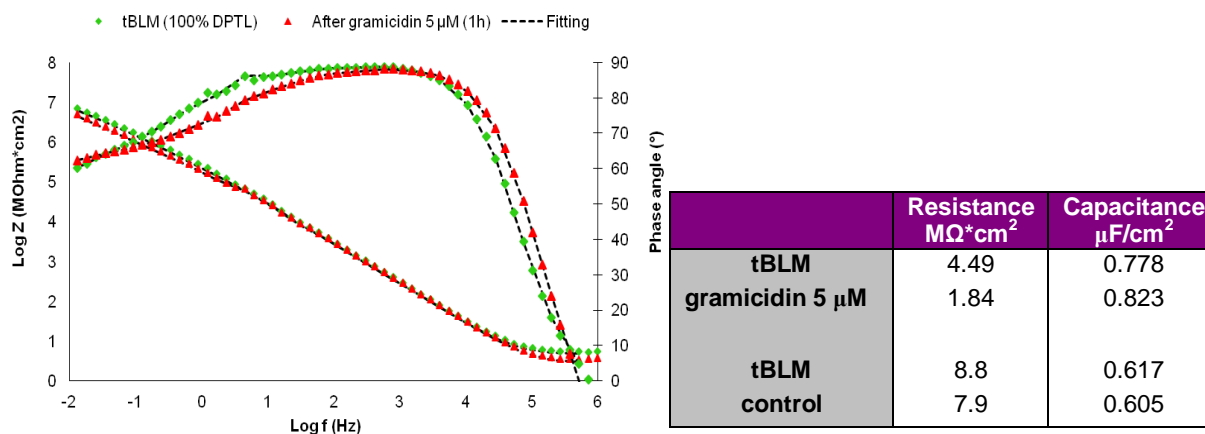


Figure 4.6: impedance spectra before and after a 1 hour treatment with gramicidin 5 μM , using a tBLM prepared with 100% DPTL. In the table on the right, resistance and capacitance values of different experiments with gramicidin were reported.

this example). It is therefore plausible that the dilution of the DPTL layer with β ME determines a greater fluidity of the lipid membrane that allows peptides such as gramicidin to insert in the double layer.

Real-time detection of gramicidin

The impedance spectra described so far were obtained performing a measurement before and another one after the treatment with gramicidin. Actually a strategy that allow to observe what happen during the treatment with gramicidin could be more useful, but it's difficult to do performing the measurements described above, because they required several minutes to be done. So the impedance variation at a single frequency was checked, choosing it in the range of frequencies where the wider impedance variations was observed.

More precisely the in-phase admittance, a measure of the permeability of the membrane, at 100 Hz was checked. This method has already been described in the literature; more precisely Cornell and colleagues monitored the in-phase admittance at 10 Hz using ion channel biosensor to detect thyroid-stimulating hormone^[114]. The choice of the frequency used in the real-time measurements has been carried out analyzing the impedance spectra reported in figure 4.4, that show the effect of gramicidin on tBLM. In particular it was assessed the frequency range in which the effect of gramicidin is more marked, and 100 Hz was considered the best frequency for this analysis.

Control experiments were performed and an example is shown in figure 4.7; it is evident that the injection of buffer does not determine any variation of signal.

Figure 4.8 shows a prototypical experiment with gramicidin. Before the injection of gramicidin, the in-phase admittance at 100 Hz of the tBLM in the measuring buffer was monitored for some minutes, until a stable baseline was obtained.

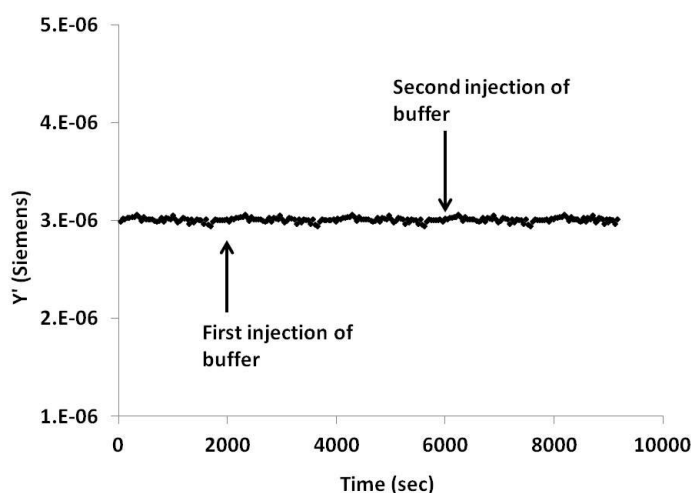


Figura 4.7: response of tBLM biosensor to two different buffer injection. The admittance is measured at 100 Hz using an excitation amplitude of 10 mV and an offset potential of 0 mV at the gold electrode relative to the test solution.

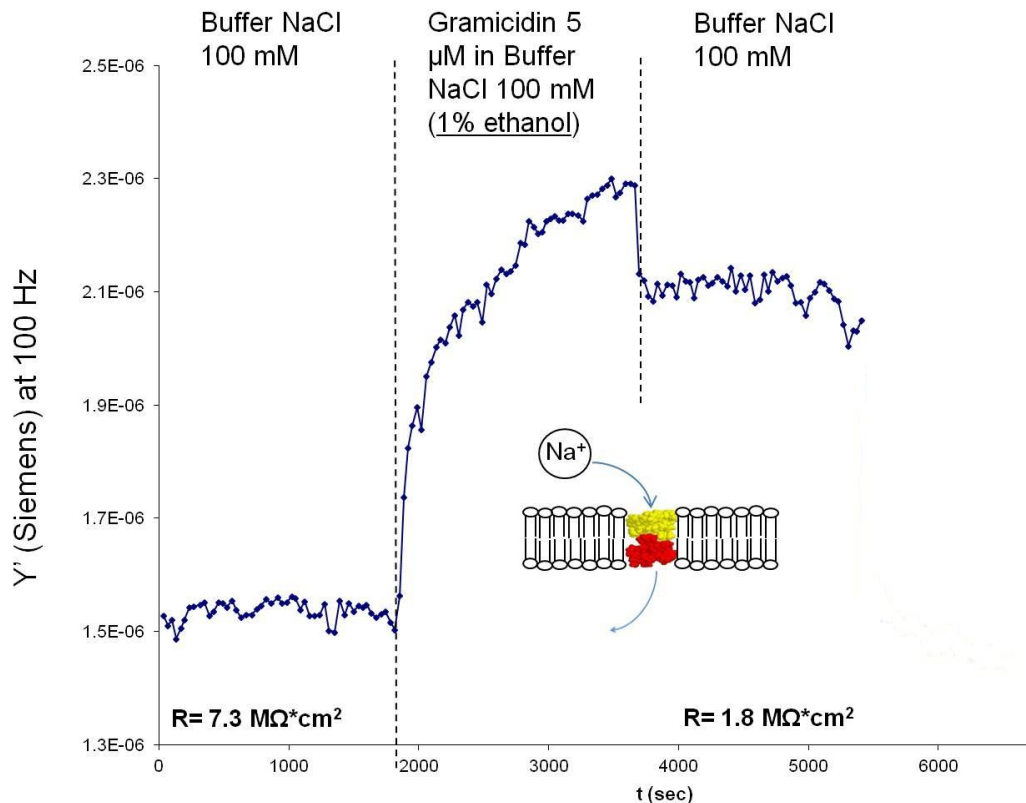


Figure 4.8: response of tBLM biosensor to gramicidin. The admittance is measured at 100 Hz using an excitation amplitude of 10 mV and an offset potential of 0 mV at the gold electrode relative to the test solution. In the picture were also reported the resistance values before and after the treatment calculated from EIS spectra.

Then 200 μL of gramicidin 5 μM in 1% ethanol was injected, and we observed an increase of conductivity just a few minutes after the injection.

The signal enhancement at the beginning of the injection is almost instantaneous, and it is probably due by the presence of ethanol in the injected solution. The signal continues to increase even after the end of the injection of gramicidin, and is monitored for about 30 minutes (in this case with an admittance variation of 0.8 μS), after which a washing step with the measuring buffer is carried out, to eliminate the gramicidin in solution and the ones that has not been interacted steadily on the membrane. The effect is an instantaneous signal drop (of about 0.2 μS), probably due to the elimination of ethanol from the solution within the measuring cell.

In the absence of gramicidin the signal is stable, even if the admittance results higher than the starting one, indicating that gramicidin has formed pores in the lipid membrane.

4.3.1.2 Melittin

Melittin is a cationic and hemolytic α -helical peptide and it is present in the venom of the European honey bee *Apis mellifera*^[148, 149]. It is composed by 26 amino acid residues with a total molecular weight of 2850 Da and it has an amphiphilic nature: the amino-terminal region is

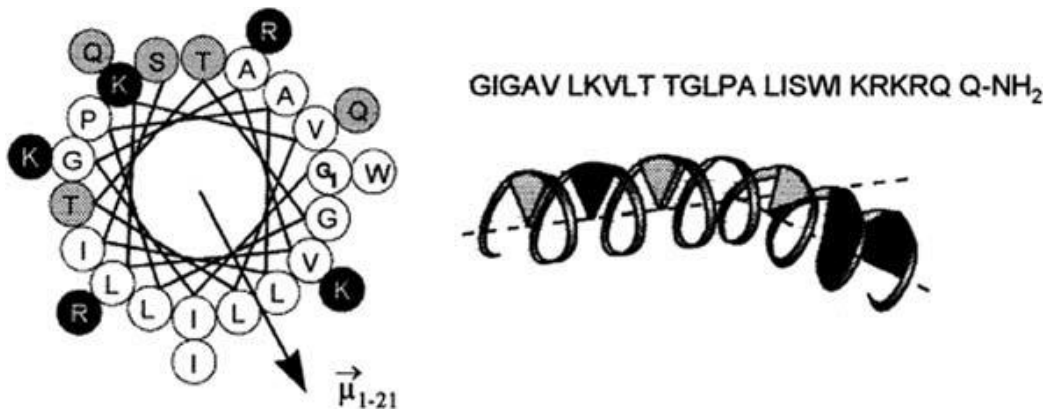


Figure 4.9: Schematic representation of the top-side (left) and the front-side (right) configuration of a monomer of melittin. Figure taken from [150].

mostly hydrophobic, while the carboxy-terminal region is hydrophilic due to the presence of a sequence of charged amino acids. Thanks to the amphiphilic properties, melittin is water soluble^[149, 151]. Its molecular structure (Figure 4.9), determined from crystals grown in aqueous solution, is a bent α -helical rod. Depending on experimental conditions such as pH, ionic strength and peptide concentration, melittin is either monomeric α -helices in the membrane interface arranged parallel to the bilayer plane, or tends to form tetramers in solution. Once the melittin bound to the cell surface, it induces lysis of the cell by forming defects in the lipid bilayer.

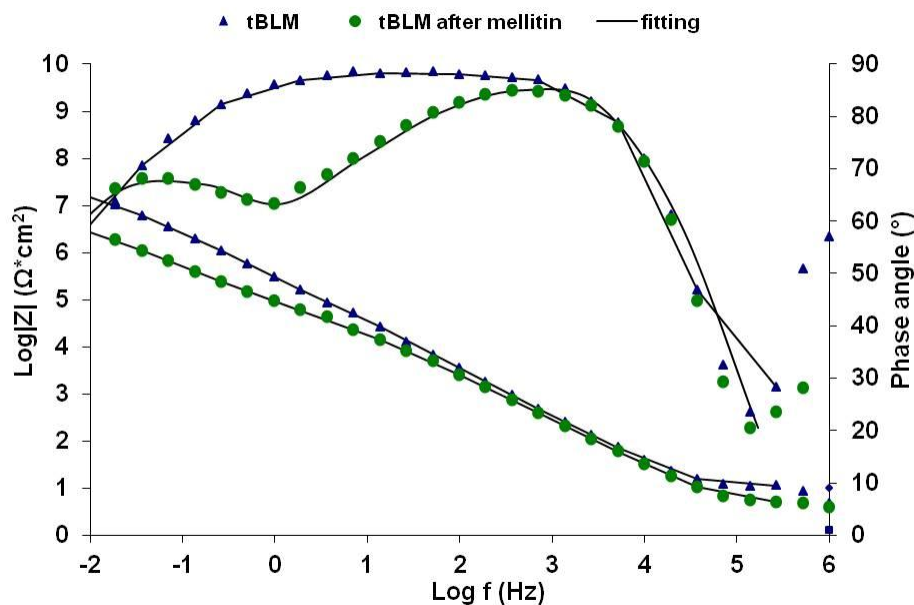


Figure 4.10: impedance spectra before and after a 1 hour treatment with melittin 5 μ M, using a tBLM prepared with 8:2 molar ratio of DPTL and β ME, respectively.

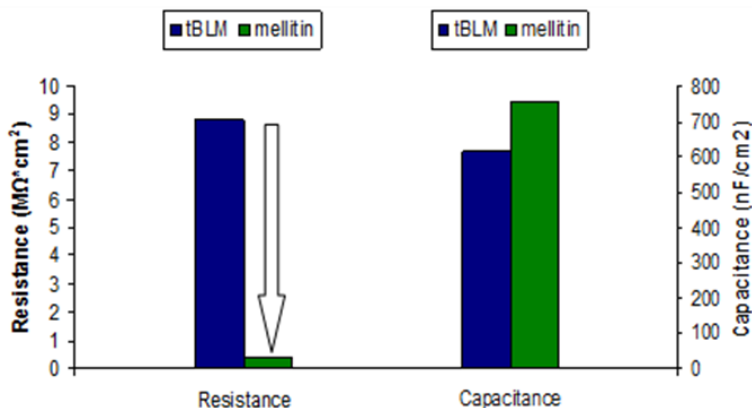


Figure 4.11: resistance and the impedance variation after 1 hour treatment with melittin 5 μ M.

Interaction of melittin on tBLM

A prototypical experiment is shown in figure 4.10; more precisely, impedance spectra obtained before and after a melittin treatment were reported.

tBLMs (with a mixed layer of DPTL and β ME 8:2 in molar ratio) were prepared on a gold working electrode and characterized with EIS.

Then 200 μ L of a solution containing 5 μ M of melittin in the measuring buffer was injected in the cell; after one hour of incubation the cell was washed with 200 μ L of measuring buffer and another EIS measure was performed, in order to evaluate the effects of melittin on the lipid bilayer.

A large decrease of impedance at low frequencies can be observed, especially at frequencies lower than 10 Hz.

The impedance spectra were analyzed with the following equivalent circuit, $R_{\Omega}(R_m Q_m)C_s$, and the corresponding data were reported in figure 4.11. In this particular experiment, melittin treatment results in a large decrease of membrane resistance (from 8.8 to 0.39 $M\Omega \cdot cm^2$) and a slight increase of capacitance (from 617 to 719 nF/cm^2). These results are consistent with data reported in literature^[99] suggesting that melittin has interacted with the lipid membrane causing the formation of defects in the bilayer which remain stable even after the washing step.

Real-time measurements

Also in this case the in-phase admittance at 100 Hz was checked; an example of what was observed is reported in figure 4.12. First of all, the in-phase admittance of a tBLM was checked until a stable signals was measured. Then 200 μ M of melittin 5 μ M was injected in the measuring cell.

The conductivity of the membrane begins to increase almost immediately (maximum variation corresponding to 5.5 μ S), and after about an hour the measuring cell was washed with measuring buffer and also in this case the permeability of the tBLM remains higher than the starting permeability, suggesting the formation of stable and permanent defect on the lipid bilayers.

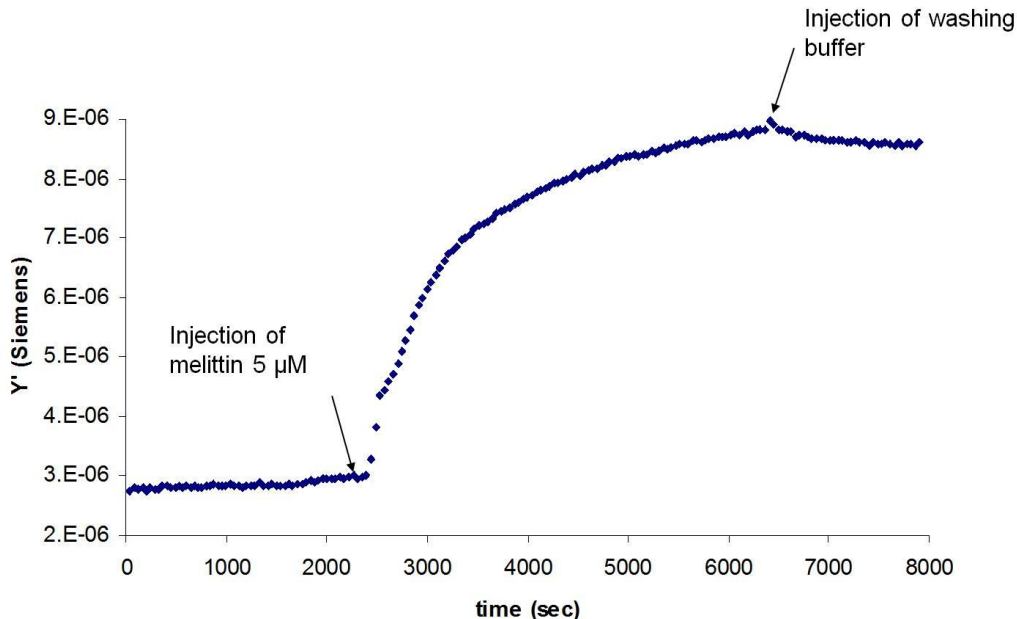


Figure 4.12: response of tBLM biosensor to gramicidin. The admittance is measured at 100 Hz using an excitation amplitude of 10 mV and an offset potential of 0 mV at the gold electrode relative to the test solution.

4.3.1.3 Conclusions

Model membranes anchored on the solid surface developed in the experiments reported so far, can detect the presence of model pore-forming peptides such as gramicidin and melittin. EIS measurements allow to characterize by an electrochemical point of view the interactions between these molecules and the lipid membrane, while performing impedance measurements at a single frequency, specifically at 100 Hz, a real time detection of these interactions is allowed.

At this stage real-time measurements is used primarily on a qualitative level, while for more quantitative determinations EIS measurements over a wide range of frequencies remains the best solution.

As expected, the treatments with both of these peptides result in a large decrease in resistance of the interface, since they determine the formation of pores or other defects in the lipid bilayer through which the passage of ions from the solution to the electrode surface is allowed. Instead capacitance values undergo minor variations, indicating that the lipid bilayers were not removed from the surface during the treatments with gramicidin and melittin.

Experiments conducted with gramicidin made it possible also to demonstrate the effective presence of a lipid bilayer on the surface and of a satisfactory reservoir of inorganic ions between the surface and the membrane. Moreover the fluidity of the tBLM used in these experiments seem to be sufficient to allow the insertion of peptides within the lipid membrane.

4.3.2 Pollutants molecules

Many substances classified as pollutants can interact with lipid membranes, causing harmful effects at the cellular level and, in some cases, causing negative effects also in whole organisms. For this reason detecting their presence in the environment may be of fundamental importance. In the following sections will be describe the experiments conducted with two molecules classified as pollutants, cyclohexane and 2,4 dinitrophenol.

4.3.2.1 Cyclohexane

Cyclohexane is mainly used as solvent in industrial chemistry, for example in the production of polyethylene. Cyclohexane is used also as raw material in the production of nylon 6.6. In particular, cyclohexane is becoming increasingly important as an industrial solvent replacing benzene, which is known to be carcinogenic.

Cyclohexane is released into the environment primarily as an air pollutant from industrial sources. Cyclohexane evaporates from water and soil exposed to air; once in air, it is expected to break down to other chemicals. Because it is a liquid that does not bind well to soil, cyclohexane that makes its way into the ground can enter groundwater.

Plants and animals living in environments contaminated with cyclohexane can store small amounts of the chemical. Uribe et al. reported the toxic effects of cyclohexane on the energy transduction in *S. cerevisiae*^[152]. Moreover cyclohexane inhibited oxygen uptake in intact cells and isolated mitochondria. Studies on isolated mitochondria showed that ATP synthesis was impaired whereas ATP hydrolysis was slightly increased. Uptake of potassium ions was also impaired, and dissipation of the mitochondrial membrane potential was observed^[152]. These studies indicate that the permeability barrier of the inner mitochondrial membrane was disrupted by cyclohexane.

Cyclohexane is mildly irritating to the eyes and can cause nervous system impairments such as headaches, anesthesia, tremors, and convulsions if inhaled in large quantities. However, its long term toxicity is considered very low. It has moderate acute toxicity to aquatic life and it has caused membrane damage in an ornamental crop species.

Results and discussion

For these experiments tBLM based on DPTL layer diluted with β ME in a molar ratio of 8:2 was prepared.

The cyclohexane is very slightly soluble in aqueous buffer, and the more concentrated solution that has been possible to prepare is a 1% solution of cyclohexane in buffer 100 mM NaCl, 10 mM HEPES, pH 7.3. After the injection of the solution (at 200 μ L/min), an almost instantaneous increase of the in-phase admittance at 100 Hz was observed, up to reach a very high value (about 28 μ S in the prototypical experiment shown in figure 4.13).

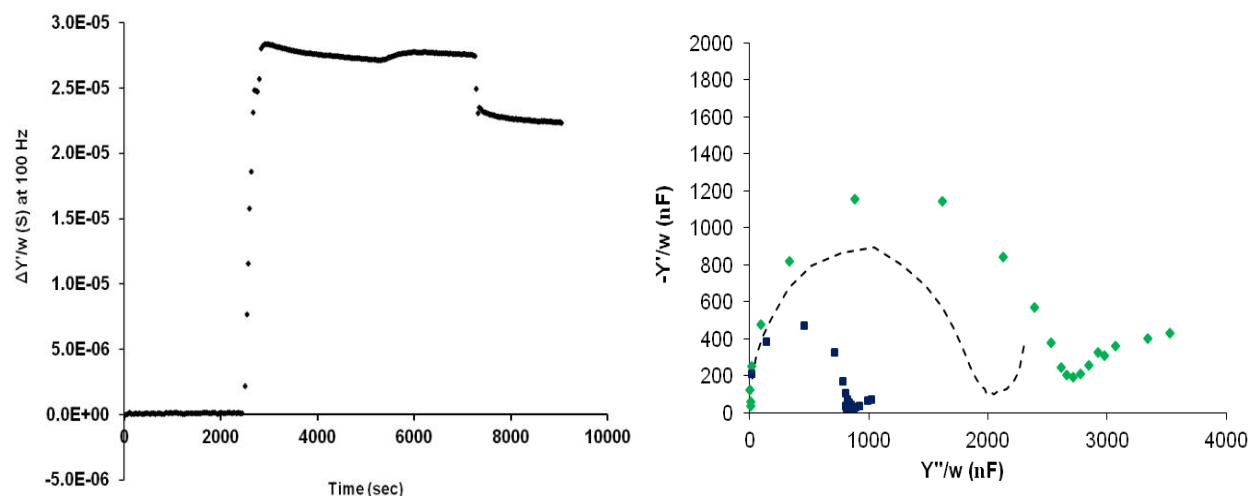


Figure 4.13: On the left: response of tBLM biosensor to cyclohexane 1%. The admittance is measured at 100 Hz using an excitation amplitude of 10 mV and an offset potential of 0 mV at the gold electrode relative to the test solution. On the right: complex admittance plot of tBLM (blue spectrum), DPTL+ β ME (dotted spectrum) and after treatment with cyclohexane 1% (green spectrum).

After about 5000 seconds a washing step with measuring buffer was carried out and a slight decrease of admittance was observed, and then it stabilized immediately. An EIS measurement from 1 MHz to 1 Hz (figure 4.13) shows how the capacitance at the electrode interface ($2.92 \mu\text{F}/\text{cm}^2$) has been substantially increased compared to that of the starting tBLM ($0.818 \mu\text{F}/\text{cm}^2$), but also with respect to the mixed SAM of DPTL and β ME ($2.12 \mu\text{F}/\text{cm}^2$). This suggests that at this concentration cyclohexane behaves as a detergent, destroying the lipid bilayer, but also alters the diluted DPTL layer below.

Two solutions of more dilute cyclohexane, respectively 0.05% and 0.1% were prepared and injected into the cell in two different experiments (figure 4.14). The effect on the in-phase admittance is always an increase in permeability, but much more limited than what observed before. Moreover both the measures were affected by high noise. The measurements made with the cyclohexane solution of 0.05% shows a very limited increase of permeability, about $0.5 \mu\text{S}$ in the best case, while doubling the concentration the admittance increase to about $1.5 \mu\text{S}$.

So it seems that lower concentrations of cyclohexane destabilizes the lipid bilayer, as expected considering the apolar nature of this molecule, but they cannot remove the lipid membrane from the surface.

4.3.2.2 2,4 dinitrophenol

2,4 dinitrophenol (DNP) is a molecule that belongs to the larger category named as phenolic compounds or substituted phenols.

Phenolic compounds exert their toxic activity at the level of the lipid membrane, considering the high correlation between toxicity and the hydrophobicity of various phenolic compounds. This

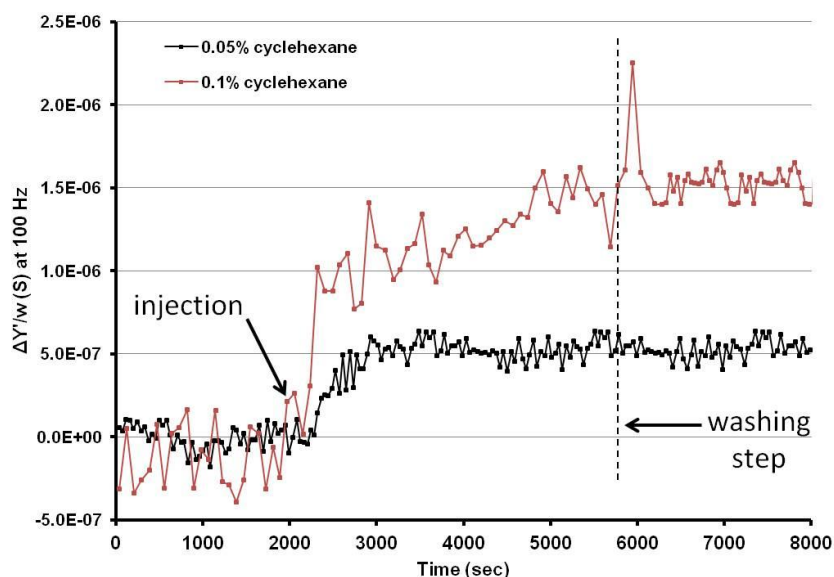


Figure 4.14: response of tBLM biosensor to cyclohexane 0.05% (black curve) and 0.1% (red curve). The admittance is measured at 100 Hz using an excitation amplitude of 10 mV and an offset potential of 0 mV at the gold electrode relative to the test solution.

conclusion is based on observations that phenol changes membrane functioning and influences protein-to-lipid ratios in the membrane^[144]. Heipieper et al. demonstrated that addition of phenol and 4-chlorophenol to suspensions of *E. coli* induced efflux of potassium ions^[153]. Moreover, substituted phenols can act as uncouplers that destroy the electrochemical proton gradient by transporting protons across the membrane and/or by inhibiting the electron flow^[153].

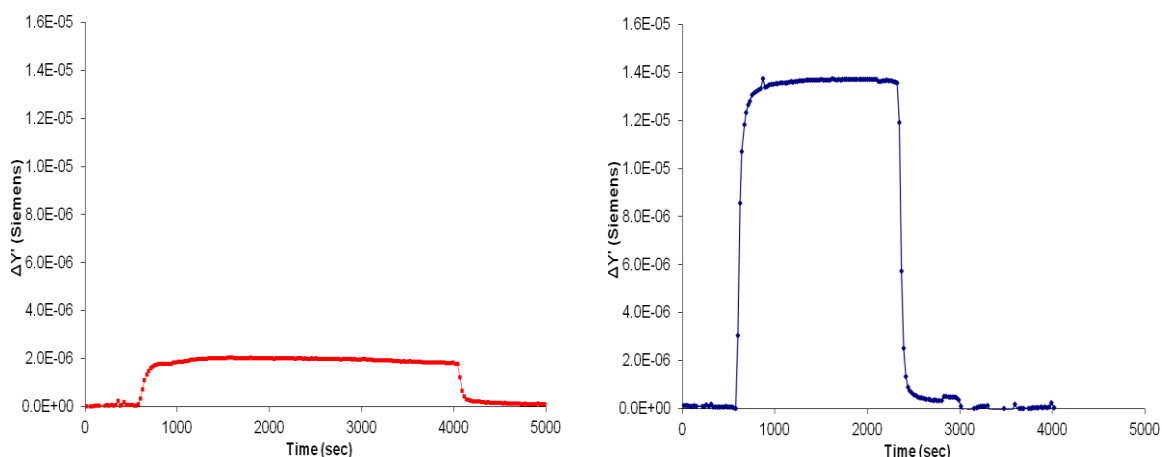


Figure 4.15: response of tBLM biosensor to 2, 4 DNP 15 μM (red curve) and 50 μM (blue curve). The admittance is measured at 100 Hz using an excitation amplitude of 10 mV and an offset potential of 0 mV at the gold electrode relative to the test solution.

Results and discussion

As in the experiments described previously, tBLMs prepared on DPTL diluted with β ME in a 8:2 molar ratio, were mounted in the measuring cell and characterized by EIS measurements using the following buffer: NaCl 100 mM, HEPES 10 mM, pH 7.3.

Immediately after a solution containing DNP 15 or 50 μ M in the measuring buffer (NaCl 100 mM, HEPES 10 mM, pH 7.3) was injected in the electrochemical cell (at 20 μ L/min) and the in-phase admittance at 100 Hz was measured as described before; figure 4.15 shows prototypical experiments conducted with these concentrations.

With a concentration of 15 μ M an increase of admittance just few seconds after the injection (about 2 μ S) was observed, indicating an increase of permeability of the lipid bilayer. The injection of DNP was followed by the injection of measuring buffer, at the same flow rate, and we observed that the starting permeability was restored, suggesting that dinitrophenol can interact with lipid membranes, but through weak interactions.

As shown in figure 4.14, increasing the concentration of DNP injected in the cell to 50 μ M, a higher increase of admittance was observed (about 13.5 μ S in the best case), but also in this case the following washing step seemed to restore the starting permeability.

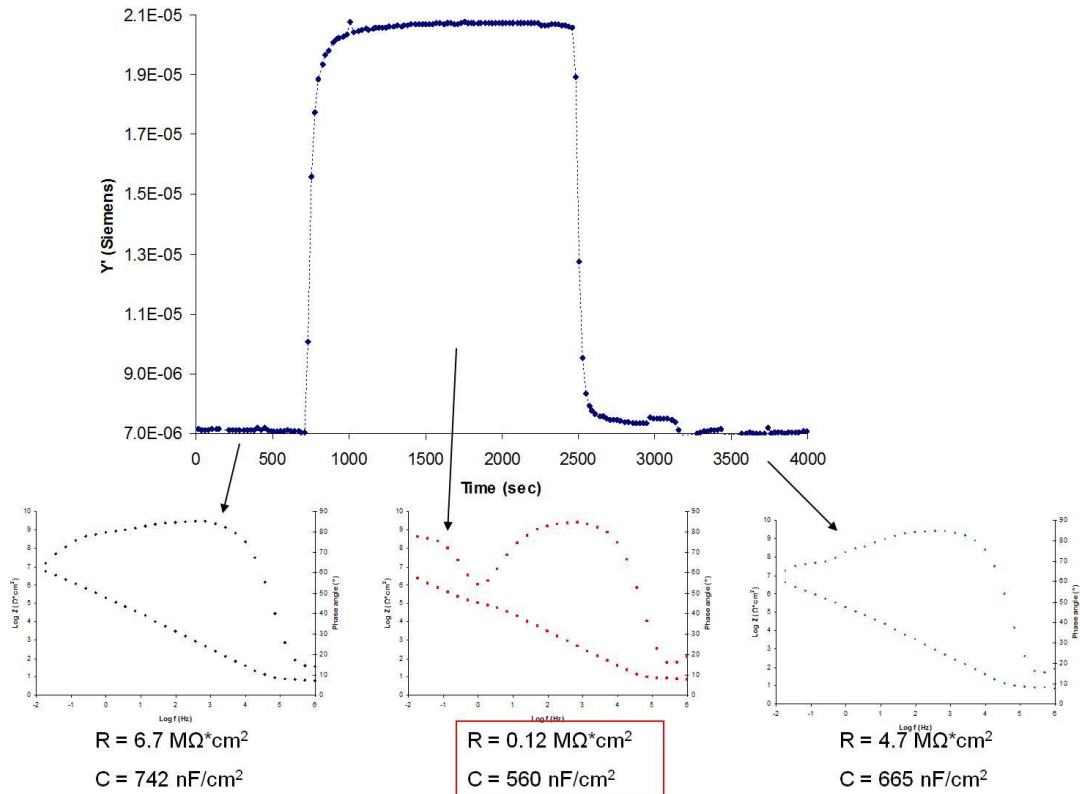


Figure 4.16: response of tBLM biosensor to 2, 4 DNP 50 μ M. The admittance is measured at 100 Hz using an excitation amplitude of 10 mV and an offset potential of 0 mV at the gold electrode relative to the test solution. For every stage of the experiment EIS spectra were collected and fitted with the equivalent circuit $R_{\Omega}(R_m Q_m)C_s$.

To verify if this increasing signal correspond actually to a greater permeabilization, EIS measurements at every stage of this experiment were performed and in fact the increase in permeability corresponds to a large drop of resistance before the washing step (see figure 4.16). Instead after the washing step the starting permeability was restored as observed before, and in fact also the starting resistance was almost restored.

4.3.2.3 Conclusions

Both the analyzed molecules, respectively cyclohexane and 2,4 dinitrophenol, have shown the ability to interact with tBLM. Some of the results were expected, given the lipophilicity of these two molecules, and show that the model membrane used for these experiments is potentially capable to detect the presence of these substances in solution.

The particular behavior of DNP suggests the possibility of more advanced analysis using our model membrane; in fact, we have seen how it is possible to distinguish stable interactions, such as those involving the cyclohexane, but also gramicidin and melittin, from interactions mediated by weak interactions, as in the case of DNP. It is therefore possible to think that this biosensor based on model membrane, although it is not specific to a particular molecule, may allow to distinguish between groups of molecules, characterized by specific interactions with the lipid membrane.

However, it is important to note that a fundamental role is played by the lipid composition of the membrane used as the sensing element in this biosensor. An example is represented by experiments carried out with another molecule called atrazine (data not shown). In these experiments no signal was detected following the injection of atrazine in the measuring cell, and this suggests that this molecule does not interact with our model membrane. At the same time, in literature is reported that triazine herbicides can interact with a particular lipid called dipalmitoylphosphatidic acid^[143]. So it is possible that the negative results of the experiments with atrazine are due to the lipid composition of the membrane used, and at the same time indicates that the lipid composition is a very important feature that has to be taken in account in the following experiments.

4.3.3 α -synuclein

An increasing fraction of the population is affected by neurodegenerative diseases such as Alzheimer's disease and Parkinson's disease (PD).

PD is characterized by the appearance of large intracellular protein aggregates called Lewy bodies, that are rich in amyloid fibrils formed by the protein α -synuclein. In addition, it is known that mutated forms of α -synuclein are associated with hereditary forms of PD^[154]. These observations suggest that α -synuclein is one of the key players in PD progression.

Alpha-synuclein is a 143-amino acid long neuron-specific protein, and it is extremely well conserved among distantly related species.

The sequence of α -synuclein can be divided into three main regions^[83]:

- ◆ N terminus: interacts with the surfaces of the cellular membranes, assuming an α -helix structure;
- ◆ the intermediate region: also known as non-amyloid component, is purely hydrophobic;
- ◆ C-terminus: region very rich of acidic residues, which is highly negatively charged and unstructured.

Depending on the surface curvature of the model membrane, usually liposomes, membrane-bound α -synuclein can adopt different conformation^[83]:

- ◆ α -synuclein on SDS micelles with high surface curvature adopts an antiparallel helix-turn-helix conformation;
- ◆ bent α -helical structures were observed when α -synuclein interacts with vesicles;
- ◆ a fully extended α -helix was observed when α -synuclein interacts with large vesicles.

Extended α -helical structures of membrane-bound α -synuclein more likely represent the situation *in vivo*, in which membrane surfaces have relatively low curvature.

Membrane binding probably mediate the enrichment of α -synuclein at presynaptic terminals where it can regulate the stabilization and release of synaptic vesicles.

α -synuclein oligomers have been shown to permeabilize lipid membranes both in cellular and membrane model systems^[155], so membrane permeabilization can be feasible mechanism by which α -synuclein could lead to neuronal death. Mitochondrial dysfunction has also been highlighted as an important contributor to PD pathogenesis; in fact mitochondria are rich in the negatively charged lipid cardiolipin and α -synuclein associates with this and other anionic lipids.

There are many ways in which proteins can destabilize the membrane integrity^[83] and the mechanisms by which oligomers cause membrane permeabilization have not been unambiguously determined. To identify the mechanism through which membrane permeabilization is promoted, it is crucial to understand the interaction between α -synuclein and lipids.

Preparation α -synuclein aggregates and AFM images

α -synuclein monomers were incubated in PBS buffer for 6 hours at 37°C; then the solution was filtrated using 100 kDa centrifugal filter for 15 minutes at 8000 RCF and the concentration of the monomers was measured with spectrophotometer. It is very difficult to see α -synuclein monomers by AFM, being their end radius of curvature of the order of 10 nm.

α -synuclein oligomers were prepared incubating α -synuclein monomers (with a concentration between 20 and 40 μ M) in 100 μ L of PBS buffer 50 mM, pH 7.4 at 37°C with continuous shacking at 1000 rpm.

Images were taken in tapping mode AFM, as shown in figure 4.17. The heights of the oligomers were measured between 3-5 nm, which is compatible with the expected height of early formed oligomers¹⁵⁶.

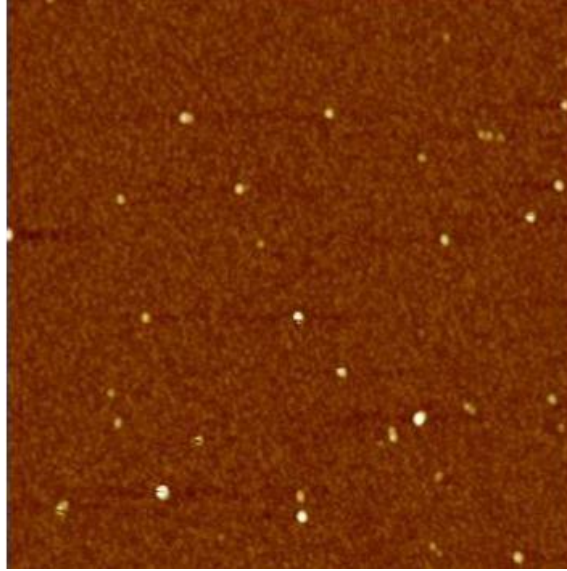


Figure 4.17: AFM image analysis of early-formed α -synuclein oligomers ($2\mu\text{m} \times 2\mu\text{m}$, data scale 10 nm).

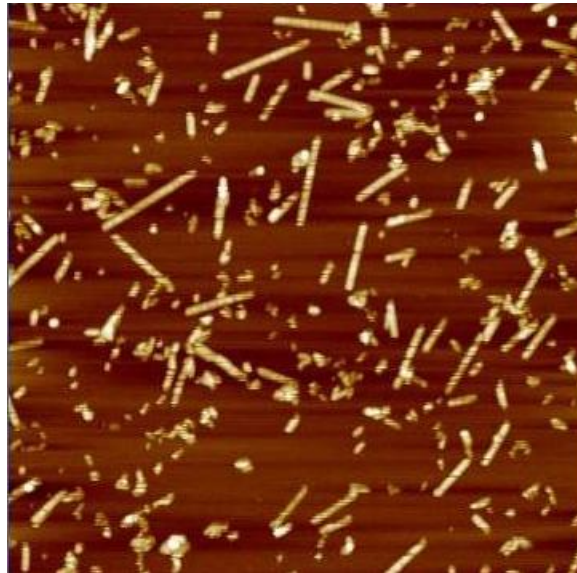


Figure4.18: AFM image analysis of early-formed α -synuclein mature fibrils ($2\mu\text{m} \times 2\mu\text{m}$, data scale 10 nm).

Mature fibrils were prepared after incubating α -synuclein monomers (also in this case with concentration between 20 and 40 μM) in 100 μL of PBS buffer 50 mM, pH 7.4 at 37°C for 3-6 days with continuous shaking at 1000 rpm. Images were taken in tapping mode AFM as shown in figure 4.18.

The height of α -synuclein mature fibrils was measured around 8 nm.

Electrochemical recognition of α -synuclein

The goal of the following experiments was to verify the possibility of detecting the interaction between the lipid membrane and the α -synuclein in its various stages of aggregation using the tBLM described in the previous chapter.

The main aspect to take into consideration before starting these experiments, as noted above, concerns what is the best lipid composition for this type of measures.

In literature, several experiments relating to the various stages of aggregation of α -synuclein and the type of interaction that occurs with lipid membranes have already been reported^{[155],[156],[157]}. In these experiments vesicles are the most used model membranes; in particular the experiments have been conducted using LUV (diameters between 100 and 150 nm) consist of POPG, a lipid characterized by a negatively charged polar head.

In fact the authors of these articles reported that the interaction between α -synuclein and lipid membranes is favored by a high content of negatively charged phospholipids and a pronounced curvature of the membrane. Through leakage experiments it was possible to observe that especially α -synuclein oligomers can interact with the vesicles, increasing their permeability. Since the permeabilization of the membrane is influenced by the size of the dye trapped inside the vesicles, the authors suggest that this type of interaction leads to the formation of pores in the lipid bilayer of the vesicles, which allow the release from the vesicle of dyes under a certain molecular weight.

Thus as regards the composition of tBLM used in these experiments, the first choice was to use the same sublayer of DPTL and β ME (8:2 molar ratio) and POPG as phospholipid for the completion of the lipid membrane.

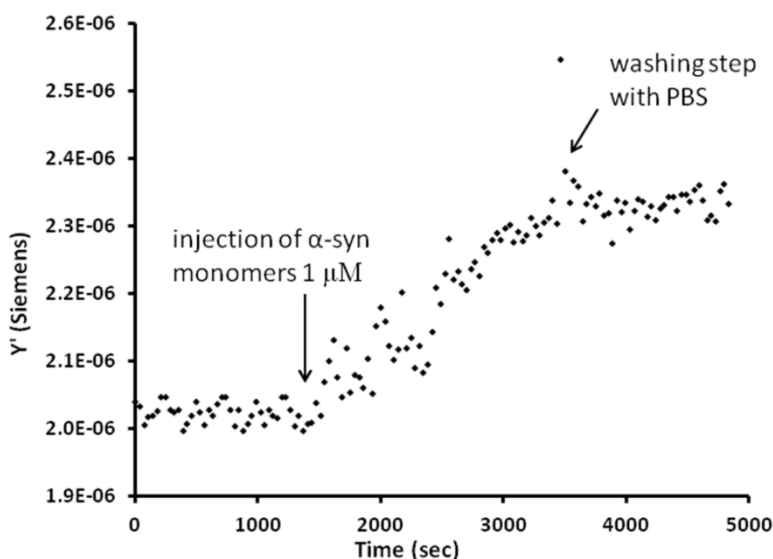


Figure 4.19: response of tBLM biosensor to α -synuclein monomers 1 μ M. The in-phase admittance is measured at 100 Hz using an excitation amplitude of 10 mV and an offset potential of 0 mV at the gold electrode relative to the test solution.

Unfortunately, the tests carried out to prepare this tBLM gave negative results (data not shown); in particular the main issue involved the vesicles fusion on the sublayer, which seems to be more difficult, leading to the formation of tBLM with low passivation (resistance just over $2 \text{ M}\Omega\cdot\text{cm}^2$) and also unstable.

So tBLMs prepared with a mixture of 70% POPC and 30% POPG, always on a sublayer formed by DPTL and β ME, were prepared; a tBLM very similar has been described by He and colleagues^[99], and shows a good stability in time and also a good passivation.

As described in the previous paragraph, a protocol to prepare the various stages of aggregation from monomers of α -synuclein was applied.

The electrochemical measurements can be divided into two phases: in a first phase the interaction between α -synuclein and the lipid membrane was monitored measuring admittance variations at a single frequency, as described in the previous paragraphs. Instead in a second step the interaction was characterized by impedance measurements, but over a wide range of frequencies.

The first tests were carried out using a monomer solution of α -synuclein $1 \mu\text{M}$ in 50 mM PBS, pH 7.4 and a prototypical result is shown in figure 4.19.

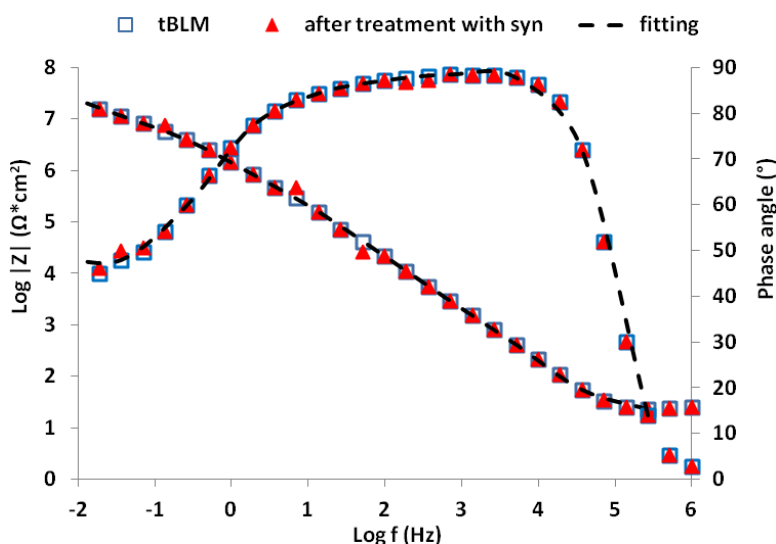


Figure 4.20: impedance spectra before and after a 1 hour treatment with α -synuclein monomers $1 \mu\text{M}$, using a tBLM prepared with 8:2 molar ratio of DPTL and β ME, respectively.

α-synuclein monomers $1 \mu\text{M}$ in PBS			
		tBLM	after α-syn
R_{Ω}	$(\Omega\cdot\text{cm}^2)$	6.51	7.89
Q_m	(nF/cm^2)	717.5	731.4
n		0.97	0.97
R_m	$(\text{M}\Omega/\text{cm}^2)$	6.9	5.7
C_s	$(\mu\text{F}/\text{cm}^2)$	3.9	3.5

Table 4.1: in this table were reported the values of R_{Ω} , R_m , Q_m , and C_s , obtained fitting the experimental data reported in figure 4.19, using the equivalent circuit $R_{\Omega}(R_m Q_m)C_s$.

After a first step in which PBS (50 mM) was injected in the measuring cell and the in-phase admittance at 100 Hz was monitored to assess the stability of the tBLM, 200 μL of α -synuclein monomers 1 μM at 20 $\mu\text{L}/\text{min}$ were injected into the measuring cell.

The signal begins to increase suggesting an increase in the permeability of the lipid membrane, although after about an hour from the injection of the monomers, the admittance increase is very limited, about 0.3 μS in the best case. However, the subsequent injection of buffer (200 μL of 50 mM PBS at 20 $\mu\text{L}/\text{min}$) determines a signal stabilization of the admittance; this suggests that the increase of permeability observed can be attributed to the presence of the monomers in the measuring cell, and then to their possible interaction with the tBLM.

Just before the beginning of this experiment, and immediately after, two EIS measurements with a frequency range from 6 MHz to 5 mHz were performed, to see the overall effect of this interaction. Both measurements were carried out in 50 mM PBS, pH 7.4; the resulting spectra are shown in figure 4.20, and the values of capacitance and resistance resulting from the fitting with the equivalent circuit $R_{\Omega}(R_m Q_m)C_s$ are shown in Table 4.1.

The two impedance spectra are practically superimposed, and also the values of R_m and Q_m (relative to the lipid bilayer) do not show a significant change after the treatment with α -synuclein monomers (for instance in this particular example the resistance slightly decreases from 6.9 to 5.9 $\text{M}\Omega\cdot\text{cm}^2$), suggesting that, despite the high concentration, the monomers in the time taken into consideration do not affect the permeability of the membrane model.

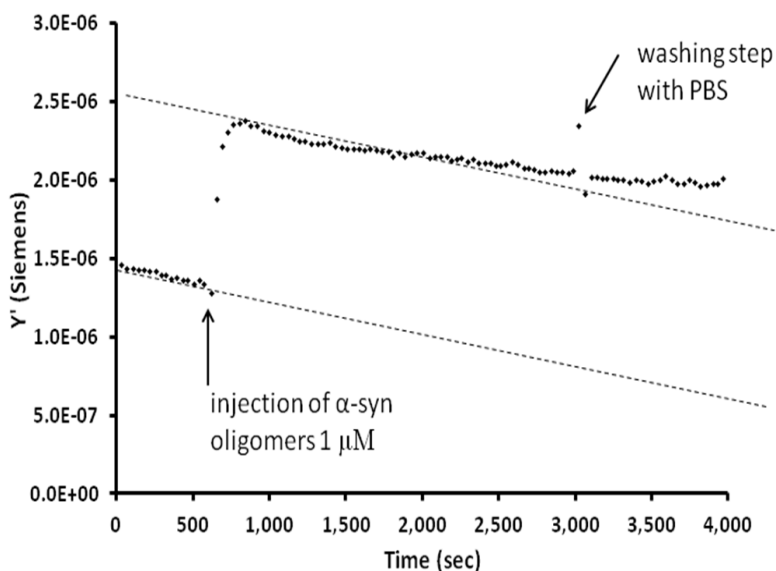


Figure 4.21: response of tBLM biosensor to α -synuclein oligomers 1 μM . The in-phase admittance is measured at 100 Hz using an excitation amplitude of 10 mV and an offset potential of 0 mV at the gold electrode relative to the test solution.

For α -synuclein oligomers the experiments were carried out with the same protocol, performing both real-time monitoring of the interaction with lipid membranes, and impedance measurements of a wide spectrum of frequencies. The prototypical experiment in figure 4.21 shows a drift in the in-phase admittance at 100 Hz after the injection of PBS 50mM, pH 7.4 in the measuring cell (figure 4.21).

Despite this, the in-phase admittance measured in this step was used as baseline. After about 500 seconds, 200 μ L of the solution containing α -synuclein oligomers 1 μ M was injected into the measuring cell at 20 μ L/min. In this case a very rapid increase of the admittance was observed, and after about a minute from the injection the signal becomes stable, maintaining a drift similar to that observed in the baseline with PBS only.

After about 40 minutes from the injection of the oligomers, 200 μ l of PBS 50 mM at 20 μ L/min were injected into the measuring cell, with no changes in the admittance signal; the overall change of admittance due to the injection of α -synuclein oligomers is about 1 μ S.

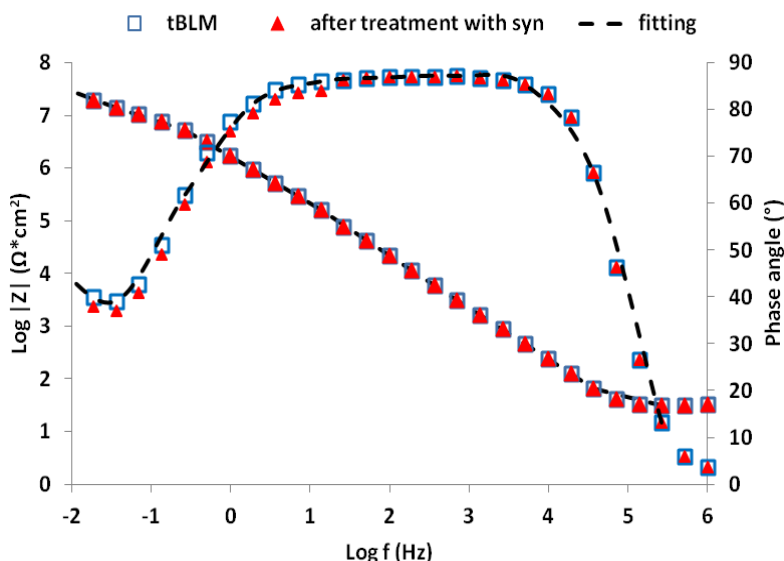


Figure 4.22: impedance spectra before and after a 1 hour treatment α -synuclein oligomers 1 μ M, using a tBLM prepared with 8:2 molar ratio of DPTL and β ME, respectively.

α -synuclein oligomers 1 μ M in PBS			
		tBLM	after α -syn
R_{Ω}	$\Omega \cdot \text{cm}^2$	8.13	7.89
Q_m	nF/cm^2	742	751.5
n		0.97	0.97
R_m	$\text{M}\Omega/\text{cm}^2$	4.2	3.5
C_s	$\mu\text{F}/\text{cm}^2$	3.3	2.8

Table 4.2: in this table were reported the values of R_{Ω} , R_m , Q_m , and C_s , obtained fitting the experimental data reported in figure 4.21, using the equivalent circuit $R_{\Omega}(R_m Q_m)C_s$.

Also in this case the EIS measurements before and after the real-time assay do not show any significant variation, as can be seen comparing the impedance spectra in figure 4.22 and the data corresponding to the fitting of these spectra reported in table 4.2. Although the admittance variation is greater than what observed with the monomers, also in this case it seems that the permeability of the tBLM has not been affected by the interaction with α -synuclein.

Figure 4.23 shows a prototypical experiment in which the real-time variation of the in-phase admittance at 100 Hz was monitored, after the injection of α -synuclein fibers 1 μ M in the measuring cell. As in previous experiments, the in-phase admittance before this injection was checked in PBS buffer 50 mM, pH 7.4 to determine the baseline. After about 1800 seconds 200 μ L of α -synuclein mature fibers 1 μ M were injected at 20 μ L/min. Even in this case the maximum variation (about 0.3 μ S) was reached after about three minutes from the injection, then the signal tends to stabilize, and also after an injection of 200 μ L of PBS 50 mM to 20 μ L/min (about 3000 seconds from the injection of the fibers) the signal remains stable.

As also observed in the previous experiments, the impedance spectra measured before and after the real-time experiment (figure 4.24) do not show significant differences, as well as from the values obtained from the fitting of these spectra (table 4.3).

All this results suggest that also the fibers do not lead to a significant variation of permeability of the membrane model.

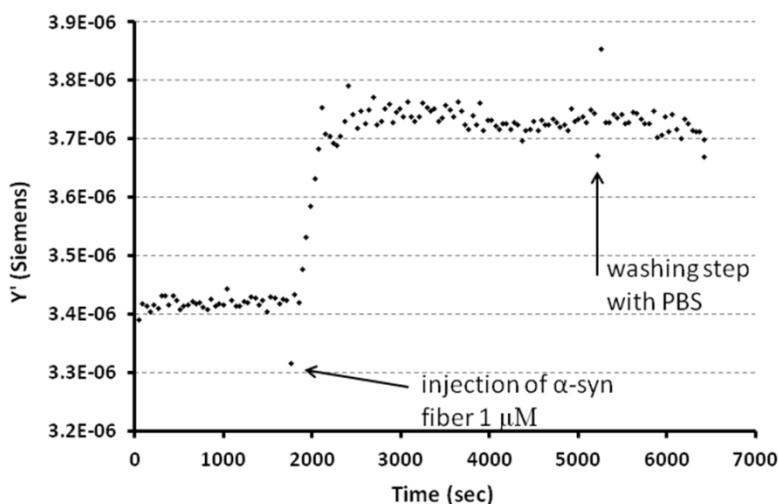


Figure 4.23: response of tBLM biosensor to α -synuclein oligomers 1 μ M. The in-phase admittance is measured at 100 Hz using an excitation amplitude of 10 mV and an offset potential of 0 mV at the gold electrode relative to the test solution.

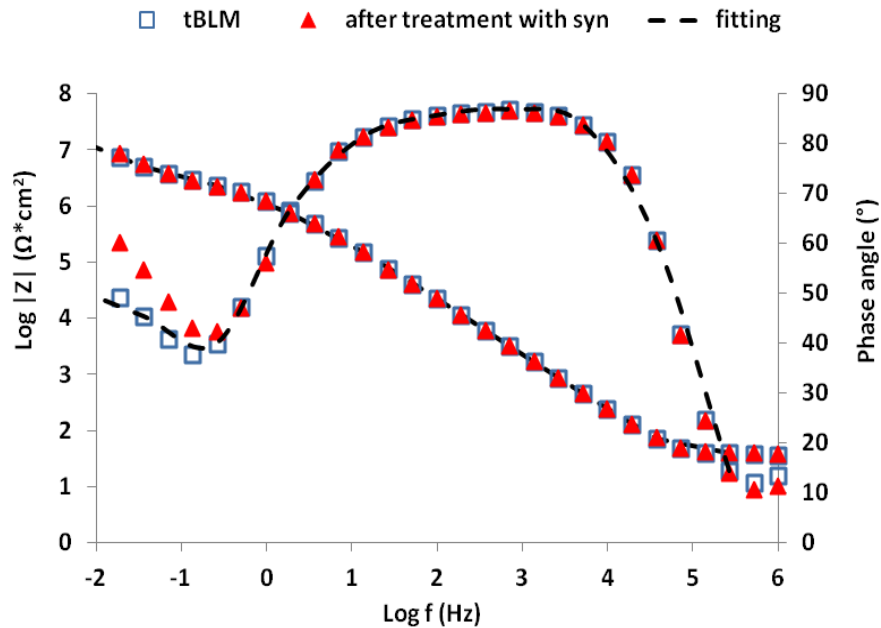


Figure 4.24: impedance spectra before and after a 1 hour treatment of α -synuclein mature fiber 1 μ M, using a tBLM prepared with 8:2 molar ratio of DPTL and β ME, respectively.

α -synuclein fibers 1 μ M in PBS			
		tBLM	after α -syn
R_{Ω}	Ω^*cm^2	6.94	7.12
Q_m	nF/cm ²	805	791
n		0.97	0.97
R_m	M Ω /cm ²	3.1	2.58
C_s	μ F/cm ²	5.1	3.54

Table 4.3: in this table were reported the values of R_{Ω} , R_m , Q_m , and C_s , obtained fitting the experimental data reported in figure 4.23, using the equivalent circuit $R_{\Omega}(R_mQ_m)C_s$.

Conclusions

The experiments performed with α -synuclein in its various stages of aggregation seem to indicate a possible interaction with the tBLMs used in these experiments, although the effects on the permeability apparently are not very high.

Obviously these data are not conclusive since, as said at the beginning of this paragraph, it is very likely that these tBLMs can be improve for this type of analysis. In particular, additional efforts are required to obtain the tBLMs consisting exclusively of POPG and at the same time with a good stability.

Several modifications have to be made also to the measurement protocol, for example, lengthening the incubation time of α -synuclein in the measuring cell, trying to use different buffers that may further facilitate the interaction with the model membrane, or by carrying out the real-time measures at other frequencies.

Certainly also the protocol for the preparation of α -synuclein aggregates must be improved; in particular it would be necessary to prepare solutions containing only one type of aggregate, and not a mixture of them, as were presumably the solutions used for these experiments. Another variation to the protocol that could be interesting regards the possibility to perform these experiments at physiological temperature (37°C).

SPR experiments based on these model membranes to detect any interaction with-synuclein in the different stages of aggregation are planned.

4.3.4 Conclusions and perspective

The experiments described in this chapter concerning model pore-forming peptides (gramicidin), toxins (melittin), pollutants, (cyclohexane and 2.4 DNP) and α -synuclein show how the model membrane described in the previous chapter is potentially capable of operating as sensing element for biosensor.

Experiments conducted with gramicidin demonstrate the effective presence of a lipid bilayer on the surface and of a satisfactory reservoir of inorganic ions between the surface and the membrane. Gramicidin, melittin, cyclohexane and 2.4 DNP determine a large decrease in the interface resistance, since they determine the formation of pores or other defects in the lipid bilayer that allow the passage of ions from the solution to the electrode surface. Instead capacitance values undergo minor variations, indicating that the lipid bilayer was not removed from the surface during the treatment with these molecules. The preliminary measurements with α -synuclein in its various stages of aggregation seem to indicate a possible interaction with the tBLMs used in these experiments, although the effects on the permeability apparently are very low.

In general, the possibility of monitor in real time the interactions between the lipid membrane and the target molecules is very interesting because it allows to have useful results in a few minutes. At the same time EIS measurements on a wide range of frequencies allow a better characterization of the interactions.

As already noted in the introduction of this chapter, this particular type of biosensor was not designed to be specific to a particular target molecule, and therefore has the advantage of being able to detect the presence of a wide range of molecules (obviously without recognize them) that can interact with the lipid membrane and then alter its electrical characteristics. For this reason this type of biosensor may be applied in preliminary screening analysis, for example in environmental monitoring.

Section IV: conclusions

Conclusions

Electrochemical biosensors represent a subclass of biosensors that combine the sensitivity of electrochemical sensors with the high specificity of recognition processes of biological molecules used as sensing elements. The interest around this class of biosensors is also due to several advantages, including simple and low cost instrumentation and the possibility to develop miniaturized, multiplexing and portable devices, allowing *in situ* analysis of different compounds simultaneously.

Nanobiotechnology is drastically revolutionizing the biosensors development and different transduction strategies exploit concepts developed in these field to simplify the analysis operations for operators and end users, offering higher specificity, higher sensitivity, higher operational stability, integrated sample treatments and shorter analysis time.

The aim of this PhD work has been the application of nanobiotechnological strategies to electrochemical biosensors for the detection of biological macromolecules.

In the first project a DNA nanotechnological strategy called hybridization chain reaction (HCR) was applied as an amplification strategy to enhance hybridization signals in a DNA biosensor. HCR is an interesting enzyme-free reaction based on DNA nano-assembly. It requires two hairpin species which are stable in this conformation; then the binding event between probe and target triggers a cascade of hybridization events and leads to the accumulation of mass on the surface which can be easily detected. Specifically, HCR products have been detected using two different electrochemical techniques: through linear sweep voltammetry measurements, using a minor groove binder called Hoechst 33258 in a label-based biosensor, and through capacitive measurements in a label-free biosensor. In addition SPR was employed as another label-free detection strategy to recognize HCR products after hybridization events.

Sequences belonging to different waterborne pathogen organisms as *C. parvum*, *G. lamblia* and HEV were chosen as the target of these biosensors. We found that HCR can be implemented on a solid surface and used as a signal amplification strategy in DNA biosensors. SPR results confirm the molecular mechanism proposed for the HCR and in particular HCR results particularly promising for multiplexed detections on array systems.

Employing HCR with the label-based biosensor, a decrease in the limit of detection by about 2 orders of magnitude is observed ($\sim 10^{-10}$ M). HCR also seems to improve the ability of the biosensor to discriminate between perfect matched and mismatched DNA targets; in addition the particular mechanism of HCR allows to discriminate the position of the mismatch in the target sequence.

Then application of HCR as a label-free strategy to amplify the hybridization signal was evaluated. HCR has proved capable to amplify the hybridization signal in SPR and capacitive assays, even though low amplification factors were observed. Specifically, the maximum amplification factor measured in SPR experiments was approximately 5-fold and a decreasing of limit of detection of about one order of magnitude is observed. The preliminary results obtained with the capacitive label-free sensor indicate the possibility of applying HCR to parallelized, automated and point-of-care biosensors.

Considering the low signal enhancing (with amplification factor of 5-7), HCR looks far from what could be required for biosensing applications. This signal enhancing is much lower comparing with the amplification ratio obtained in experiments performed on magnetic beads with HCR hairpin labeled with fluorophores^[60] (up to 20-fold). This discrepancy could be due to possible limitations in the electron exchange of Hoechst 33258 with the surface, especially regarding Hoechst 33258 molecules that are at a certain distance from the surface. Moreover the detection limit of 100 pM obtained with HCR is higher compared to other signal amplification strategies for electrochemical DNA sensors (usually in the order of magnitude of 10^{-12} M or lower).

The second project concerned the application of another nanobiotechnological strategy based on a biological model lipid membrane used as the sensing element in an electrochemical biosensor, for the recognition of interactions between the lipid membrane and different types of target molecules.

The biological model lipid membranes were anchored to the surface using a tethering molecule called 2,3-di-*O*-phytanyl-*sn*-glycerol-1-tetraethylene glycol-D,L- α -lipoic acid ester (DPTL), diluted with β -mercaptoethanol (β ME). Phosphatidylcholines (POPC and DOPC) were used to complete the lipid bilayer, to obtain lipid membranes with an electrical resistance in the M Ω range (specifically between 5 and 10 M Ω *cm²), measured through electrochemical impedance spectroscopy. So the membrane is physically separated from the surface, with the formation of a hydrophilic space between the surface and the lipid membrane. An advantage of these model membranes is that they can accommodate integral membrane proteins, thanks to this submembrane space and, at the same time, the anchoring to the solid surface makes them particularly resistant and stable and therefore it is possible to apply on them numerous surface-sensitive techniques, such as SPR, AFM and electrochemical measures.

To verify whether the hydrophilic spacer interposed between the electrode surface and the lipid bilayer act as a satisfactory reservoir of inorganic ions, experiments with gramicidin, a model pore-forming peptide, were performed. These experiments demonstrate the effective presence of a lipid bilayer on the surface and also the presence of a satisfactory reservoir of inorganic ions between the surface and the membrane.

This particular kind of biosensor was not designed to be specific to a particular target molecule, and therefore has the advantage of being able to detect the presence of a wide range of molecules

(without to recognize them) that can interact with the lipid membrane and then alter its electrical characteristics. For this reason this type of biosensor can be applied in the analysis of preliminary screening, for example in environmental monitoring.

Experiments concerning model pore-forming peptides (gramicidin), toxins (melittin), pollutants, (cyclohexane and 2.4 DNP) and amyloid proteins (α -synuclein) show how the model membrane prepared in our laboratory is potentially capable of operating as sensing element for biosensor.

Gramicidin, melittin, cyclohexane and 2.4 DNP determine a large decrease in the interface resistance, since they determine the formation of pores or other defects in the lipid bilayer that allow the passage of ions from the solution to the electrode surface. At the same time, capacitance values undergo minor variations, indicating that the lipid bilayer was not removed from the surface during the treatment with these molecules. The preliminary measurements with α -synuclein in its various stages of aggregation seem to indicate a possible interaction with the tBLMs used in these experiments, although the effects on the permeability are apparently very low.

In conclusion, nanobiotechnological strategies were applied with some success as an amplification strategy in a DNA biosensors (HCR) and as the sensing element in a label-free electrochemical biosensor.

For HCR applications, some optimization steps are surely required in order to improve the amplification ratios, for example reducing the steric hindrance on the surface to obtain the maximum overall yield on the surface. As mentioned before, it is possible that some electroactive molecules interacting with the ds-DNA are too far from the surface and so cannot be detected, determining the low amplification ratio. An improvement could be achieved in the case where the electroactive molecules were free to diffuse in solution. For example Shimron and colleague used two hairpin structures that determine, after the HCR, the formation of numerous G-quadruplex. Hemin/G-quadruplex complex has catalytic properties and it can convert a specific substrate into an electroactive product free to diffuse in solution, and thus probably easier to detect, allowing to improve the sensitivity of this strategy.

The experiments obtained with tBLM as sensing element are just preliminary results and further analysis are required, both to confirm the obtained results, and to improve the quality of the measurements.

In particular, it will be necessary to move toward a parallelization of the measure, and also toward a greater automation. This not only allows less time-consuming analysis, but it will also improve the quality of the analysis, because through the parallelization the biosensor will be able to analyze the same sample with different model membranes, each with a particular lipid composition. This is a crucial factor for the efficiency of the biosensor, because the composition of the lipid membrane greatly influence the interactions with the target molecules, as indicated by the experiments with α -synuclein.

Acknowledgments

First, I want to thank Prof. Bruno Samorì and Dr. Giampaolo Zuccheri for allowing me to carry out my PhD project in their group and supporting me in every situation.

I would like to thank the people who have worked with me in my PhD work, in particular Dr. Alessandra Vinelli, for the work done in HCR experiments, and also Silvia Dalba and Diletta Quarta Colosso, who worked on experiments about model membranes. I want also to thank Prof. Carlotta Guiducci and her colleagues at the Laboratory of Electronics Life Sciences at EPFL in Lausanne, in particular Dr. Fabio Spiga for SPR measurements with HCR and Samuel Kilchenmann and Marco Spinsanti for SPR measurements performed on model membranes. Similarly I thank Dr. Attila Bonyàr and all his colleagues who worked with him at Budapest University of Technology and Economics (BME) in carrying out the SPR imaging measurements on HCR.

A big thanks goes to all the colleagues that I have had in these years, for the discussions and support offered to me: Simone, Federica, Francesca, Daniel, Rosita, Mark, Lisa, Andrea Raspadori and Andrea Zauli and others.

I want to thank especially Dr. Daniele Gazzola for the crucial help given in the develop of the electrochemical cells and for the many useful discussions on electrochemistry.

Finally, a big thank goes to my family who has always supported me in all these years.

References

1. Lowe, C.R., *Biosensors*. Trends in biotechnology, 1984. **2**(3): p. 59-65.
2. Grieshaber, D., et al., *Electrochemical Biosensors - Sensor Principles and Architectures*. 2008. p. 1400-1458.
3. Chaubey, A. and B.D. Malhotra, *Mediated biosensors*. Biosensors and Bioelectronics, 2002. **17**: p. 441-456.
4. Kasemo, B., *Biological surface science*. Surface Science, 2002. **500**(1&3): p. 656-677.
5. Wang, J., ed. *Analytical Electrochemistry*. 2006, John Wiley & Sons VCH: Hoboken, New Jersey, USA.
6. Campas, M., D. Garibo, and B. Prieto-Simon, *Novel nanobiotechnological concepts in electrochemical biosensors for the analysis of toxins*. Analyst, 2012. **137**(5): p. 1055-1067.
7. Ahmed, M.U., et al., *Electrochemical DNA biosensor using a disposable electrochemical printed (DEP) chip for the detection of SNPs from unpurified PCR amplicons*. Analyst, 2007. **132**(5): p. 431-438.
8. Wang, J., et al., *DNA electrochemical biosensors for environmental monitoring. A review*. Analytica Chimica Acta, 1997. **347**: p. 1-8.
9. Wang, J., *SURVEY AND SUMMARY: From DNA biosensors to gene chips*. Nucleic Acid Research, 2000. **28**(16): p. 3011-3016.
10. Erdem, A. and M. Ozsoz, *Electrochemical DNA Biosensors Based on DNA-Drug Interactions*. Electroanalysis, 2002. **14**(14): p. 965-974.
11. Pellegrini, G.E., G. Carpico, and E. Coni, *Electrochemical sensor for the detection and presumptive identification of quinolone and tetracycline residues in milk*. Analytica Chimica Acta, 2004. **520**: p. 13-18.
12. Volpe, G., et al., *Development of an Immunomagnetic Electrochemical Sensor for Detection of BT&• CRYIAB/CRYIAC Proteins in Genetically Modified Corn Samples*. Analytical Letters, 2006. **39**(8): p. 1599-1609.
13. Winqvist, F., P. Wide, and I. Lundström, *An electronic tongue based on voltammetry*. Analytica Chimica Acta, 1997. **357**: p. 21-31.

14. Maynard, C., et al., *Waterborne Pathogen Detection by Use of Oligonucleotide-Based Microarrays*. Applied and Environmental Microbiology, 2005. **71**(12): p. 8548-8557.
15. Straub, T.M. and D.P. Chandler, *Towards a unified system for detecting waterborne pathogens*. Journal of Microbiological Methods, 2003. **53**: p. 185-197.
16. Tegnell, A., et al., *The European Commission's Task Force on Bioterrorism*. Emerging Infectious Diseases, 2003. **9**(10): p. 1330-1332.
17. Bartlett, P.N., ed. *Bioelectrochemistry Fundamentals, Experimental Techniques and Applications*. 2008, John Wiley & Sons: West Sussex, England.
18. Ronkainen, N.J., H.B. Halsall, and W.R. Heineman, *Electrochemical biosensors*. Chemical Society Reviews, 2010. **39**: p. 1747-1763.
19. Thevenot, D.R., et al., *Electrochemical biosensors: recommended definitions and classifications*. Biosensors and Bioelectronics, 2001. **16**((1-2)): p. 121-131.
20. Bakker, E. and E. Pretsch, *Potentiometric sensors for trace-level analysis*. Trac-Trends in Analytical Chemistry, 2005. **24**(3): p. 199-207.
21. Bard, A.J. and L.R. Faulkner, *Electrochemical methods. Fundamentals and applications*. 2 ed. 2001: Wiley.
22. Wang, J., *Glucose Biosensors: 40 Years of Advances and Challenges*. Electroanalysis, 2001. **13**(12): p. 983-988.
23. Updyke, S.J. and G.P. Hicks, *The Enzyme Electrode*. Nature, 1967. **214**: p. 986-988.
24. Gregg, B.A. and A. Heller, *Cross-linked redox gels containing glucose oxidase for amperometric biosensor applications*. Analytical Chemistry, 1990. **62**(3): p. 258-263.
25. Nakatani, H.S., et al., *Biosensor based on Xanthine Oxidase for monitoring Hypoxanthine in fish meat*. American Journal of Biochemistry and Biotechnology, 2005. **1**(2): p. 85-89.
26. Mo, J.-W. and W. Smart, *Lactate biosensors for continuous monitoring*. Front. Biosci., 2004. **9**(2): p. 3384-3391.
27. Palleschi, G., et al., *Lactate and glucose electrochemical biosensors for the evaluation of the aerobic and anaerobic threshold in runners*. Medical & Biological Engineering & Computing, 1990. **28**(3): p. 25-28.

28. Karube, I. and M. Suzuki, *Microbial Biosensors in Biosensors: A Practical Approach*, E.G. Cass, Editor. 1990, Oxford University Press: Oxford, England.
29. Kuang, H., et al., *Fabricated aptamer-based electrochemical signal-off• sensor of ochratoxin A*. *Biosensors and Bioelectronics*. **26**(2): p. 710-716.
30. Jianyun, L., et al., *Application of Quantum Dots Based Electrochemical Biosensors*. *Progress in Chemistry*, 2010. **22**(11): p. 2179-2190.
31. Hashimoto, K., K. Ito, and Y. Ishimori, *Sequence-Specific Gene Detection with a Gold Electrode Modified with DNA Probes and an Electrochemically Active Dye*. *Analytical Chemistry*, 1994. **66**: p. 3830-3833.
32. Ronkainen, N.J., et al., *Electrochemical immunoassay moving into the fast lane*. *Trends in Analytical Chemistry*, 2002. **21**(4): p. 213-225.
33. van Emon, J.M., ed. *Immunoassay and Other Bioanalytical Methods*. 2007, CRC Press: Boca Raton, FL, USA.
34. Dequaire, M., C. Degrand, and B. Limoges, *An Electrochemical Metalloimmunoassay Based on Colloidal Gold label*. *Analytical Chemistry*, 2000. **72**: p. 5521-5528.
35. Guo, H., et al., *MCM-41 Mesoporous Material Modified Carbon Paste Electrode for the Determination of Cardiac Troponin I by Anodic Stripping Voltammetry*. *Talanta*, 2005. **68**: p. 61-66.
36. Park, S.J., T.A. Taton, and C.A. Mirkin, *Array-Based Electrical Detection of DNA with Nanoparticle Probes*. *Science*, 2002. **295**: p. 1503-1506.
37. Richter, M.M., *Electrochemiluminescence (ECL)*. *Chemical Review*, 2004. **104**: p. 3003-3036.
38. Yan, G., et al., *Rapid and Sensitive Immunomagnetic-Electrochemiluminescent Detection of p53 Antibodies in Human Serum*. *Journal of Immunology Methods*, 2004. **288**: p. 47-54.
39. Xu, X., et al., *Novel Solution-Phase Immunoassays for Molecular Analysis of Tumor Markers*. *Analyst*, 2001. **126**: p. 1285-1292.
40. Namba, Y., M. Usami, and O. Suzuki, *Highly Sensitive Electrochemiluminescence Immunoassay Using the Ruthenium Chelate-Labeled Antibody Bound to the Magnetic Micro Beads*. *Analytical Chemistry*, 1999. **15**: p. 1087-1093
41. Sassolas, A., B.D. Leca-Bouvier, and L.J. Blum, *DNA biosensors and microarrays*. *Chem. Rev.*, 2008. **108**: p. 109-139.

42. Palacek, E., *From Polarography of DNA to Microanalysis with nucleic acid-modified electrodes*. *Electroanalysis*, 1996. **8**(1): p. 7-14.
43. Gooding, J.J., *Electrochemical DNA Hybridization Biosensors*. *Electroanalysis*, 2002. **14**(17): p. 1149-1156.
44. Mearns, F.J., et al., *DNA Biosensor Concepts Based on a Change in the DNA Persistence Length upon Hybridization*. *Electroanalysis*, 2006. **18**(19): p. 1971-1981.
45. Zhang, Y., H.-H. Kim, and A. Heller, *Enzyme-Amplified Amperometric Detection of 3000 Copies of DNA in a 10- μ L Droplet at 0.5 fM Concentration*. *Analytical Chemistry*, 2003. **75**: p. 3267- 3269.
46. Wang, J., et al., *Metal Nanoparticle-Based Electrochemical Stripping Potentiometric Detection of DNA Hybridization*. *analytical Chemistry*, 2001. **71**(22).
47. Patolsky, F., A. Lichtenstein, and I. Willner, *Electronic Transduction of DNA Sensing Processes on Surfaces: Amplification of DNA Detection and Analysis of Single-Base Mismatches by Tagged Liposomes*. *Journal of American Chemical Society*, 2001. **123**(22): p. 5194-5205.
48. Xie, H., et al., *Highly Sensitive Amperometric Detection of Genomic DNA in Animal Tissues*. *Nucleic Acid Research*, 2004. **32**: p. e15.
49. Umek, R.M., et al., *Electronic Detection of Nucleic Acids: a Versatile Platform for Molecular Diagnostics*. *Journal of Molecular Diagnostic*, 2001. **3**(2): p. 74-84.
50. Mearns, F.J., et al., *DNA Biosensor Concepts Based on a Change in the DNA Persistence Length upon Hybridization*. *Electroanalysis*, 2006. **18**(19-20): p. 1971-1981.
51. Ah, C.S., et al., *Electric detection of DNA hybridization by nanoparticle nanoswitch*. *Curr. Appl. Phys.*, 2006. **6s1**: p. e157–e160.
52. Wang, J., *Nanoparticle-based electrochemical DNA detection*. *Anal. Chim. Acta*, 2003. **500**(1-2): p. 247-257.
53. Cai, H., et al., *Electrochemical detection of DNA hybridization based on silver-enhanced gold nanoparticle label*. *Anal. Chim. Acta*, 2002. **469**(2): p. 165-172.
54. Holmlin, R.E., P.J. Dandliker, and J.K. Barton, *Charge Transfer through the DNA Base Stack*. *Angew. Chem., Int. Ed. Engl.*, 1997. **36**(24): p. 2715–2730.

55. Kelley, S.O., E.M. Boon, and J.K. Barton, *Single-base mismatch detection based on charge transduction through DNA*. *Nucleic Acid Res.*, 1999. **27**(24): p. 4830-4837.
56. Millan, K.M. and S.R. Mikkelsen, *Sequence-selective biosensor for DNA Based on electroactive hybridization indicators*. *Anal. Chem.*, 1993. **65**(17): p. 2317-2323.
57. Hashimoto, K., K. Ito, and Y. Ishimori, *Sequence-Specific Gene Detection with a Gold Electrode Modified with DNA Probes and an Electrochemically Active Dye*. *Anal. Chem.*, 1994. **66**(21): p. 3839-3833.
58. Choi, Y.-S., K.-S. Lee, and D.-H. Park, *Single nucleotide polymorphism (SNP) detection using microelectrode biochip array*. *J. Micromech. Microeng.*, 2005. **15**: p. 1938-1946.
59. Dirks, R.M. and N.A. Pierce, *Triggered amplification by hybridization chain reaction*. *PNAS*, 2004. **101**(43).
60. Niu, S., Y. Jiang, and S. Zhang, *Fluorescence detection for DNA using hybridization chain reaction with enzyme-amplification*. *Chemical Communications*. **46**(18): p. 3089-3091.
61. Huang, J., *Pyrene-Excimer Probes Based on the Hybridization Chain Reaction for the Detection of Nucleic Acids in Complex Biological Fluids*. *Angewandte Chemie International Edition*. **50**(2).
62. Choi, J., *Immuno-Hybridization Chain Reaction for Enhancing Detection of Individual Cytokine-Secreting Human Peripheral Mononuclear Cells*. *Analytical Chemistry*. **83**(17): p. 6890-6895.
63. Mohan, H., et al., *Quenching of nucleotide-derived radicals by bisbenzimidazole derivative Hoechst 33258 in aqueous solution*. *Proc. Indian. Acad. Sci.*, 2000. **112**(4): p. 487-496.
64. Loontjens, F.G., et al., *Binding of Hoechst 33258 and 4',6-diamidino-2-phenylindole to self-complementary decadeoxynucleotides with modified exocyclic base substituents*. *Biochemistry*, 1991. **30**(1): p. 182-189.
65. Kerman, K., M. Kobayashi, and E. Tamiya, *Recent trends in electrochemical DNA biosensor technology*. *Meas. Sci. Technol.*, 2004. **15**: p. R1-R11.
66. Sufen, W., P. Tuzhi, and C.F. Yang, *Electrochemical studies for the interaction of DNA with an irreversible redox compound - Hoechst 33258*. *Electroanalysis*, 2002. **14**(23): p. 1648-1653.

67. Besenicar, M., et al., *Surface plasmon resonance in protein-membrane interactions*. Chem Phys Lipids, 2006. **141**(1-2): p. 169-78.
68. He, L., et al., *Colloidal Au-Enhanced Surface Plasmon Resonance for Ultrasensitive Detection of DNA Hybridization*. J. Am. Chem. Soc., 2000. **122**(38): p. 9071-9077.
69. Goodrich, T.T., H.J. Lee, and R.M. Corn, *Direct Detection of Genomic DNA by Enzymatically Amplified SPR Imaging Measurements of RNA Microarrays*. J. Am. Chem. Soc., 2004. **126**(13): p. 4086-4087.
70. Lee, H.J., et al., *Enzymatically Amplified Surface Plasmon Resonance Imaging Detection of DNA by Exonuclease III Digestion of DNA Microarrays*. Anal. Chem., 2005. **77**(16): p. 5096-5100.
71. Berggren, C., B. Bjarnason, and G. Johansson, *An immunological Interleukine-6 capacitive biosensor using perturbation with a potentiostatic step* Biosensors and Bioelectronics 1998. **13**(10): p. 1061-1068.
72. Christine Berggren, P.S.J.B.G.J., *A Feasibility Study of a Capacitive Biosensor for Direct Detection of DNA Hybridization*. Electroanalysis, 1999. **11**(3): p. 156-160.
73. Berggren, C., et al., *A Feasibility Study of a Capacitive Biosensor for Direct Detection of DNA Hybridization*. Electroanalysis, 1999. **11**(3): p. 156-160.
74. Zuker, M. and P. Stiegler, *Optimal computer folding of large RNA sequences using thermodynamics and auxiliary information*. Nucleic Acid Res., 1981. **9**(1): p. 133-148.
75. Goodman, R.P., *NANEV: a program employing evolutionary methods for the design of nucleic acid nanostructures*. Biotechniques, 2005. **38**(4): p. 548-550.
76. Zadeh, J.N., et al., *NUPACK: analysis and design of nucleic acid systems*. J. Comput. Chem. , 2011. **32**: p. 170-173.
77. Yu, J.-R., S.-U. Lee, and W.-Y. Park, *Comparative Sensitivity of PCR Primer Sets for Detection of Cryptosporidium parvum*. The Korean Society for Parasitology, 2009. **47**(3): p. 5.
78. Guy, R.A., C. Xiao, and P.A. Horgen, *Real-Time PCR Assay for Detection and Genotype Differentiation of Giardia lamblia in Stool Specimens*. Journal of Clinical Microbiology, 2004. **42**(7): p. 3317-3320.

79. Orrù, G., et al., *Detection and quantitation of hepatitis E virus in human faeces by real-time quantitative PCR*. Journal of Virological Methods, 2004. **118**(2): p. 77-82.
80. Zheng, Y., et al., *Surface-initiated DNA self-assembly as an enzyme-free and nanoparticle-free strategy towards signal amplification of an electrochemical DNA sensor*. Analyst, 2011. **136**(3): p. 459-462.
81. Lubrich, D., S.J. Green, and A.J. Turberfield, *Kinetically Controlled Self-Assembly of DNA Oligomers*. Journal of the American Chemical Society, 2009. **131**(7): p. 2422-2423.
82. Guan, Y., et al., *Multiple Binding Modes for Dicationic Hoechst 33258 to DNA*. The Journal of Physical Chemistry B, 2007. **111**(25): p. 7336-7344.
83. Butterfield, S.M. and H.A. Lashuel, *Amyloidogenic protein-membrane interactions: mechanistic insight from model system*. Angew. Chem. Int. Ed., 2010. **49**: p. 5628-5654.
84. Cabiaux, V., C. Wolff, and J.-M. Ruyschaert, *Interaction with a lipid membrane: a key step in bacterial toxins virulences*. International Journal of Biological Macromolecules, 1997. **21**: p. 285-298.
85. Nunes, C., et al., *Substituted phenols as pollutants that affect membrane fluidity*. Journal of Environmental Biology, 2008. **29**(5): p. 733-738.
86. Seddon, A.M., et al., *Drug interactions with lipid membranes*. Chem. Soc. Rev., 2009. **38**: p. 2509-2519.
87. Chan, Y.-H.M. and S.G. Boxer, *Model membrane system and their applications*. Current Opinion in Chemical Biology, 2007. **11**: p. 1-7.
88. Guidelli, R., et al., *Bioelectrochemistry at metal / water interfaces*. Journal of Electroanalytical Chemistry, 2001(504): p. 1-28.
89. Jesorka, A. and O. Orwar, *Liposomes: Technologies and Analytical Applications*. Annual Review of Analytical Chemistry, 2008. **1**: p. 801-832.
90. Tanaka, M. and E. Sackmann, *Polymer-supported membranes as models of the cell surface*. Nature, 2005. **437**(7059): p. 656-663.
91. Kiessling, V. and L.K. Tamm, *Measuring Distances in Supported Bilayers by Fluorescence Interference-Contrast Microscopy: Polymer Supports and SNARE Proteins*. Biophysical Journal, 2003. **84**(1): p. 408-418.

92. Vockenroth, I.K., et al., *Formation of tethered bilayer lipid membranes probed by various surface sensitive techniques*. *Biointerphases*, 2009. **4**(2): p. 19-26.
93. Naumann, R., et al., *Tethered lipid bilayers on ultraflat gold surfaces*. *Langmuir*, 2003. **19**: p. 5435-5443.
94. Wang, X., et al., *A facile approach for assembling lipid bilayer membranes on template-stripped gold*. *Langmuir*, 2010. **26**(23): p. 18239–18245.
95. Junghans, A. and I. Koper, *Structural analysis of tethered bilayer lipid membranes*. *Langmuir*, 2010. **26**(13): p. 11035-11040.
96. Dorvel, B.R., et al., *Formation of tethered bilayer lipid membranes on gold surfaces: QCM-Z and AFM study*. *Langmuir*, 2007. **23**: p. 7344-7355.
97. Schiller, S.M., et al., *Archaea analogue thiolipids for tethered bilayer lipid membranes on ultrasmooth gold surfaces*. *Angew. Chem. Int. Ed.*, 2003. **42**(2): p. 208-211.
98. Becucci, L. and R. Guidelli, *Equilibrium distribution of K⁺ ions in the hydrophilic spacer of tethered bilayer lipid membranes*. *Soft matter*, 2009. **5**: p. 2294-2301.
99. He, L., et al., *Tethered bilayer lipid membranes based on monolayers of thiolipids mixed with a complementary dilution molecule. 1. Incorporation of channel peptides*. *Langmuir*, 2005. **21**(25): p. 11666-72.
100. Valincius, G., et al., *Enzyme Activity to Augment the Characterization of Tethered Bilayer Membranes*. *The Journal of Physical Chemistry Letters B*, 2006. **110**: p. 10213-10216.
101. McGillivray, D.J., et al., *Molecular-scale structural and functional characterization of sparsely tethered bilayer lipid membranes*. *Biointerphases*, 2007. **2**(1): p. 21-33.
102. Kwak, K.J., et al., *Formation and finite element analysis of tethered bilayer lipid membrane*. *Langmuir*, 2010. **26**(23): p. 18199-208.
103. Hong, Q., *Two-step membrane binding by Equinatoxin II, a pore-forming toxin from the sea anemone, involves an exposed aromatic cluster and a flexible helix*. *J. Biol. Chem*, 2002. **277**(44): p. 41916-24.
104. Richter, R.P., R. Berat, and A.R. Brisson, *Formation of solid-supported lipid bilayers: an integrated view*. *Langmuir*, 2006. **22**: p. 3497-3505.

105. Lei, S.B., et al., *AFM characterization of gramicidin-A in tethered lipid membrane on silicon surface*. Chemical Physics Letters, 2006. **429**: p. 244-249.
106. Vockenroth, I.K., et al., *Functional incorporation of the pore forming segment of AChR M2 into tethered bilayer lipid membranes*. Biochimica et Biophysica Acta, 2007. **1768**: p. 1114-1120.
107. Vockenroth, I.K., et al., *Stable insulating tethered bilayer lipid membranes*. Biointerphases, 2008. **3**(2): p. FA68-FA73.
108. Terrettaz, S., et al., *Protein binding to supported lipid membranes: investigation of the cholera toxin-ganglioside interaction by simultaneous impedance spectroscopy and surface plasmon resonance*. Langmuir, 1993. **9**: p. 1361-1369.
109. Cremer, P.S. and S.G. Boxer, *Formation and spreading of lipid bilayers on planar glass support*. J. Phys. Chem. B, 1999. **103**: p. 2554-2559.
110. Williams, L.M., et al., *Kinetics of formation of single phospholipid bilayers on self-assembled monolayer supports, as monitored by surface plasmon resonance*. Supramolecular science, 1997. **4**(3-4): p. 513-517.
111. Wiegand, G., et al., *Electrical properties of supported lipid bilayer membranes*. J. Phys. Chem. B, 2002. **106**: p. 4245-4254.
112. Stora, T., J.H. Lakey, and H. Vogel, *Ion-channel gating in transmembrane receptor proteins: functional activity in tethered lipid membranes*. Angew. Chem. Int. Ed., 1999. **38**(3): p. 389-392.
113. Yaron, P.N., et al., *Single wall carbon nanotubes enter cells by endocytosis and not membrane penetration*. Journal of Nanobiotechnology, 2011. **9**(45).
114. Cornell, B.A., et al., *A biosensor that uses ion-channel switches*. Nature, 1997. **387**: p. 580-583.
115. Raguse, B., et al., *Tethered lipid bilayer membranes: formation and ionic reservoir characterization*. Langmuir, 1998. **14**: p. 648-659.
116. Hong, Q., et al., *Two-step membrane binding by Equinatoxin II, a pore-forming toxin from the sea anemone, involves an exposed aromatic cluster and a flexible helix*. J Biol Chem, 2002. **277**(44): p. 41916-24.
117. Stenberg, E., et al., *Quantitative-Determination of Surface Concentration of Protein with Surface-Plasmon Resonance Using Radiolabeled Proteins*. Journal of Colloid and Interface Science, 1991. **143**(2): p. 513-526.

118. Keller, C.A. and B. Kasemo, *Surface specific kinetics of lipid vesicle adsorption measured with a quartz crystal microbalance*. Biophysical Journal, 1998. **75**(3): p. 1397-1402.
119. Frenkel, E.J., et al., *Lipid-protein interactions on human erythrocyte-membrane acetylcholinesterase*. Eur. J. Biochem., 1980. **109**: p. 377-382.
120. Kucik, D.F., E.L. Elson, and M.P. Sheetz, *Weak dependence of mobility of membrane protein aggregates on aggregate size supports a viscous model of retardation of diffusion*. Biophysical Journal, 1999. **76**: p. 324-322.
121. Shen, H.-H., T. Lithgow, and L.L. Martin, *Reconstitution of membrane proteins into model membranes: seeking better ways to retain protein activities*. Int. J. Mol. Sci., 2013. **14**: p. 1589-1607.
122. Marsden, H.R., I. Tomatsu, and A. Kros, *Model systems for membrane fusion*. Chem. Soc. Rev., 2011. **40**: p. 1572-1585.
123. Simons, K. and M.J. Gerl, *Revitalizing membrane rafts: new tools and insight*. Nature Reviews Molecular Cell Biology, 2010. **11**: p. 688-699
124. Nikolaus, J., et al., *Direct visualization of large and protein-free hemifusion diaphragms*. Biophysical Journal, 2010. **98**(7): p. 1192-1199.
125. Ravoo, B.J., W.D. Weringa, and J.B.F.N. Engberts, *Membrane fusion in vesicles of oligomerizable lipids*. Biophysical Journal, 1999. **76**: p. 374-386.
126. Peetla, C., A. Stine, and V. Labhasetwar, *Biophysical interactions with model lipid membranes: applications in drug discovery and drug delivery*. Molecular pharmaceutics, 2009. **6**(5): p. 1264-1276.
127. Bensikaddour, H., et al., *Characterization of the interactions between fluoroquinolone antibiotics and lipids: a multitechnique approach*. Biophysical Journal, 2008. **94**: p. 3035-3046.
128. Barcelo, F., et al., *The hypotensive drug 2-hydroxyoleic acid modifies the structural properties of model membranes*. Mol. Membr. Biol., 2004. **21**: p. 261-268.
129. Corvis, Y., et al., *Interactions of fungistatic antibiotic, griseofulvin, with phospholipid monolayers used as models of biological membranes*. Langmuir, 2006. **22**: p. 7701-7711.
130. Hidalgo, A.A., et al., *Interaction of two phenothiazine derivatives with phospholipid monolayers*. Biophys. Chem, 2004. **109**: p. 85-104.

131. Preetha, A., N. Huilgol, and R. Banerjee, *Effect of fluidizing agents on paclitaxel penetration in cervical cancerous monolayer membranes*. J. Membr. Biol., 2007. **219**: p. 83-91.
132. Klopman, G. and H. Zhu, *Recent methodologies for the estimation of n-octanol/water partition coefficients and their use in the prediction of membrane transport properties of drugs*. Mini-Rev. Med. Chem., 2005. **5**: p. 127-133.
133. Baginski, M., J. Czub, and K. Sternal, *Interaction of amphotericin B and its selected derivatives with membranes: molecular modeling studies*. Chem. Rec., 2006. **6**: p. 320-332.
134. Lashuel, H.A. and P.T.J. Lansbury, *Are amyloid diseases caused by protein aggregates that mimic bacterial pore-forming toxins?* Q. Rev. Biophys., 2006. **39**(2): p. 167-201.
135. Qi, W., et al., *Two disaccharides and trimethylamine N-Oxide affect AB aggregation differently, but all attenuate oligomer-induced membrane permeability*. Biochemistry, 2009. **48**(37).
136. Van Gelder, P., F. Dumas, and M. Winterhalter, *Understanding the function of bacterial outer membrane channels by reconstitution into black lipid membranes*. Biophys. Chem, 2000. **15**(86): p. 153-167.
137. Franky, D.S., et al., *Significance of alterations in plasma lipid profile levels in breast cancer*. Integr. Cancer Ther., 2008. **7**: p. 33-41.
138. Vigh, L., et al., *The significance of lipid composition for membrane activity: new concepts and ways of assessing function*. Prog. Lipid Res., 2005. **44**: p. 303-344.
139. Jadhav, S.R., et al., *Functional characterization of PorB class II porin from Neisseria meningitidis using a tethered bilayer lipid membrane*. Biosensors and Bioelectronics, 2008. **24**: p. 831-835.
140. Tun, T.N. and A.T.A. Jenkins, *An electrochemical impedance study of the effect of pathogenic bacterial toxins on tethered bilayer lipid membrane*. Electrochemistry communications, 2010. **12**: p. 1411-1415.
141. Tilak, K.S., K. Veeraiyah, and M.S. Butchiram, *Effect of phenol on haematological components of Indian major carps Catla Catla, Labeo rohita and Cirrhinus mrigala*. J. Environ. Biol., 2007. **28**: p. 177-179.
142. Escher, B.I., M. Snozzi, and R.P. Schwarzenbach, *Uptake, speciation and uncoupling activity of substituted phenols in energy transducing membranes*. Environ. Sci. Technol., 1996. **30**: p. 3071-3079.

143. Siontorou, C.G., et al., *A triazine herbicide minisensor based on surface-stabilized bilayer lipid membranes*. Anal. Chem., 1997. **69**: p. 3109-3114.
144. Sikkema, J., J.A.M. De Bont, and B. Poolman, *Mechanisms of membrane toxicity of hydrocarbons*. Microbiological reviews, 1995. **59**(2): p. 201-222.
145. Terrettaz, S., et al., *Immunosensing by synthetic ligand-gated ion channel*. Angew. Chem. Int. Ed., 2001. **40**(9): p. 1740-1743.
146. Krishnamurthy, V., S.M. Monfared, and B.A. Cornell, *Ion-channel biosensors - Part I: construction, operation, and clinical studies*. IEEE transactions on nanotechnology, 2010. **00**(00): p. 2010.
147. Kelkar, D.A. and A. Chattopadhyay, *The gramicidin ion channel: a model membrane protein*. Biochim Biophys Acta, 2007. **1768**(9): p. 2011-25.
148. Habermann, E., *Bee and wasp venoms*. Science, 1972. **177**(4046): p. 314-22.
149. Dempsey, C.E., *The actions of melittin on membranes*. Biochim Biophys Acta, 1990. **1031**(2): p. 143-61.
150. Raghuraman, H. and A. Chattopadhyay, *Melittin: a membrane-active peptide with diverse functions*. Biosci. Rep., 2007. **27**(4-5): p. 189-223.
151. Sansom, M.S., *The biophysics of peptide models of ion channels*. Prog Biophys Mol Biol, 1991. **55**(3): p. 139-235.
152. Uribe, S., et al., *Effects of cyclohexane, an industrial solvent, on the yeast S. cerevisiae and on isolated yeast mitochondria*. Applied and Environmental Microbiology, 1990. **56**(7): p. 2114-2119.
153. Heipieper, H.-J., H. Keweloh, and H.-J. Rehm, *Influence of phenols on growth and membrane permeability of free and immobilized E. coli*. Applied and Environmental Microbiology, 1991. **57**: p. 1213-1217.
154. Zarranz, J.J., et al., *The new mutation, E46K, of alpha-synuclein causes Parkinson and Lewy body dementia*. Ann. Neurol., 2004. **55**(2): p. 164-173.
155. van Rooijen, B.D., M.A.E. Claessens, and V. Subramaniam, *Lipid bilayer disruption by oligomeric alpha-synuclein depends on bilayer charge and accessibility of the hydrophobic core*. Biochimica et Biophysica Acta, 2009. **1788**: p. 1271-1278.
156. van Rooijen, B.D., M.A.E. Claessens, and V. Subramaniam, *Membrane permeabilization by oligomeric alpha-synuclein: in search of the mechanism*. Plos one, 2010. **5**(12): p. e14292.

157. Stockl, M., M.A.E. Claessens, and V. Subramaniam, *Kinetic measurements give new insights into lipid membrane permeabilization by alpha-synuclein oligomers*. *Molecular Biosystems*, 2011. **8**: p. 338-345.